

UCSF

UC San Francisco Electronic Theses and Dissertations

Title

On Generation of Variation in Craniofacial Development and Evolution

Permalink

<https://escholarship.org/uc/item/4b41w2rx>

Author

Yu, Jane

Publication Date

2012

Peer reviewed|Thesis/dissertation

On Generation of Variation in Craniofacial
Development and Evolution

by

Jane Yu

DISSERTATION

Submitted in partial satisfaction of the requirements for the degree of

DOCTOR OF PHILOSOPHY

in

Biomedical Sciences

in the

GRADUATE DIVISION

of the

UNIVERSITY OF CALIFORNIA, SAN FRANCISCO

Acknowledgements

This work could not have been completed without the support of my loving family, especially: my dearest Michael Kennedy Hall, Debra Yu & David Amusin, Patrice & Jason Yu, and Bobbie & Mark Hall.

Thank you to my committee members, Tamara Alliston, Ralph Marcucio, and Nadav Ahituv for their encouragement, support, and efforts along the way.

Parts of this dissertation project originated in the work of Andrew Jheon, Brian F. Eames, and the lab's Principal Investigator. Many of the themes and ideas embodied in this text are heavily influenced by the work of von Baer, Darwin, Fisher, Orr, and longtime lab neighbor, John Gerhart.

This work was supported by the National Science Foundation through the Graduate Research Fellowship awarded to me under Grant DGE-0648991, as well as in part by the NIDCR K99-DE NIDCR K99-DE022059 to Andrew Jheon; F32 DE016778 to Brian F. Eames; and NIDCR R01 DE016402 to the Principal Investigator.

Abstract

On Generation of Variation in Craniofacial

Development and Evolution

Jane Yu

Avian species display a remarkable diversity of facial morphologies, from the small, pointed, insect-catching beak of the common sparrow, to the long, narrow, nectar-sipping beak of a hummingbird. Using fate-mapping studies, we know that all facial skeletal elements are derived from neural crest mesenchyme (NCM), a multipotent embryonic cell population. From transplant experiments, we know that NCM plays an instructive role in patterning and growth in the face (i.e., when we transplant quail NCM into a duck host, the chimera forms a quail-like face and beak). What remains to be understood is how NCM carries out the components of what is undoubtedly a very complex task – to pattern beaks with great precision for function in established niches, but also to allow plasticity for evolution in response to changes in the natural environment.

Thus, one of the questions I address during my dissertation research is what are developmental, cellular, and molecular mechanisms underlying evolvability in avian faces? I have previously been intrigued by the rapid rate of

generation of novel beak morphologies as historically described in Darwin's finches and other models. To begin to understand these phenomena, I investigated the function, regulation, and evolution of one transcription factor, *Runx2*, as a model for understanding processes that can modulate the generation of heritable, selectable, phenotypic variation.

Runx2 is often considered a master regulator of osteogenesis. However, mechanisms by which *Runx2* might regulate timing of osteogenesis *in vivo* have not been previously described. Here, by using a unique avian chimeric experimental system, we identify *Runx2* as a critical player in both NCM-dependent timing of osteogenesis and developmental growth and patterning of the craniofacial complex. Specifically, we find that NCM controls stage- and species-specific cell cycle progression and *Runx2* expression in highly interwoven processes. Further, *Runx2* expression levels affect mandible size and correlate to species-specific sequence variation at a highly evolvable *Runx2* regulatory region. Taken together, these data suggest that NCM may be able generate a range of skeletal element sizes and morphologies in part by temporally regulating cell cycle in conjunction with cell differentiation through highly regulated, mutation-labile transcription factors such as *Runx2*.

Table of Contents

1. Introduction	1
a. Adaptation in the craniofacial complex	1
b. Ontogenetic and phylogenetic origins of the vertebrate face	3
c. When do sources of variation in facial development first appear?	6
d. Genetic and molecular regulation in facial development	9
e. The transcription factor Runx2 – a model for sources of variation	17
i. Roles of Runx2 in osteogenesis	18
ii. Interactions between Runx2 and cell cycle	21
iii. Runx2 in disease	24
iv. Molecular regulation of Runx2	26
2. Neural crest controls osteogenesis and species-specific patterning of the facial skeleton by regulating cell cycle	31
a. The avian chimeric system	31
b. NCM controls timing of osteogenesis	32
i. NCM establishes timing of mineralization	32
ii. Neural crest mesenchyme regulates spatiotemporal expression of genes involved in mineralization	33
iii. Host vasculature and blood mineral levels provide a permissive environment for donor-directed osteogenesis	33

iv. Neural crest mesenchyme controls timing of osteoid deposition	35
v. Neural crest mesenchyme controls timing of osteoblast differentiation	35
c. Neural crest mesenchyme regulates cell cycle progression	36
i. Neural crest mesenchyme regulates proliferation at the G1/S checkpoint	36
ii. Neural crest mesenchyme modulates expression of cell cycle regulators	38
d. Transient, early over-expression of D-type cyclins accelerates osteogenic differentiation	39
e. Runx2 levels affect mandible size	40
i. Continuous runx2 over-expression decreases overall mandible size	40
ii. Endogenous Runx2 levels during development correlate with species-specific mandible size	41
f. Discussion: proposed mechanisms by which NCM controls size of facial elements	41
3. Evolvability in the craniofacial complex	47
a. Debates on evolvability	47
i. What is evolvability?	47
ii. Laws of variation	48
iii. Variation in stable populations	51

iv. Population mixing	
v. Re-interpreting the framework	52
b. Biological relevance of tandem repeats	54
c. Correlations between tandem repeats in Runx2 and craniofacial proportions	56
d. Survey and implications of Runx2 tandem repeats in avians ...	58
e. Mutation-prone sequences in other transcription factors involved in craniofacial patterning	62
f. Craniofacial defects as a consequence of a genetic “shotgun approach”	69
g. Conclusion	74
4. Methods and Technique Development	79
a. Bone formation rate	80
b. Bone material properties	82
i. Tissue Diagnostic Instrument (TDI)	82
ii. Mineral content by X-ray	84
iii. Tissue mineral density by μ CT	85
iv. Biochemical inhibition of TGF β Type I Receptor	86
c. Gain- and loss-of-function techniques	89
v. Mesenchymal electroporation at HH21	89
vi. <i>Ex ovo</i> mesenchymal electroporation at HH21	91
vii. Confined mesenchymal electroporation at HH21	92
viii. Mesenchymal lipofection	93

ix.	Neural crest electroporation at HH8	94
x.	Electroporation of neural crest-specific, tetracycline-inducible constructs	95
d.	Transient gain and loss of function	97
xi.	p27 knockdown in quail and quack by shRNA	97
xii.	Electroporation of D-type cyclins <i>in ovo</i>	102
xiii.	Runx2 over-expression for <i>in vitro</i> osteogenesis	102
xiv.	Runx2 knockdown in quail and quack by siRNA	104
e.	Stable gain of function	106
xv.	Retroviral over-expression of Runx2	106
xvi.	Retroviral over-expression of RANKL and OPG	112
f.	Cell cycle analyses	117
xvii.	Wst-1 cell viability proliferation assay	117
xviii.	BrdU Injection	118
xix.	Flow cytometry	119
xx.	Analysis of genes regulating cell death and cell cycle	119
g.	Section histology, immunohistochemistry, and tissue staining	120
xxi.	Skeletal preparations	120
xxii.	Alkaline phosphatase assay	120
xxiii.	Milligan's trichrome	121
xxiv.	Antibody staining	121
h.	Protein expression analyses	123

xxv. Western blot	123
i. Vascularization analyses	126
xxvi. Calcium and phosphorus levels in blood	126
xxvii. Quantification of blood vessel volume	126
j. Cell and tissue culture	127
xxviii. Transfection of DF-1 cells	127
xxix. Production of RCAS virus	128
k. Molecular biology	129
xxx. <i>In situ</i> hybridization	129
xxxi. qRT-PCR	129
l. Generation of chimeras	130
m. Tools	131
xxxii. Pulling Needles for Injection	131
xxxiii. Tungsten needles for surgery	131
n. Statistical methods	132
o. Oligonucleotide Sequences	132
5. Figures	139
6. References	178

List of Tables

Table 1. <i>Runx2</i> Q:A ratios in avian species	62
Table 2. Mutability of genes involved in craniofacial patterning	70
Table 3. Primary antibodies for Western blot	123
Table 4. Secondary antibodies for Western blot	124
Table 5. Primers for detecting mRNA expression by qRT-PCR	132
Table 6. Primers for cloning	135
Table 7. Primers for sequencing	136
Table 8. Primers for shRNA synthesis	137

List of Figures

1. Ontogenetic and Phylogenetic Origins of the Face	139
2. Molecular and Cellular Regulation in Craniofacial Development	141
3. Avian Chimeric System	143
4. NCM Controls Timing of Mineralization	145
5. NCM Controls Expression of Mineralization Genes and Levels of Circulating Minerals	147
6. NCM Controls Timing of Osteoid Deposition	149
7. NCM Controls Timing of Osteoblast Differentiation	151
8. NCM Regulates Stage- and Species-Specific Cell Cycle Progression	153
9. Transient D-Type Cyclins and Continuous Runx2 Over-expression Analyses	155
10. Laws of Variation	157
11. Runx2 Repeats and Facial Shape	158
12. Runx2 Repeats and Rate of Growth	160
13. Relations between Avian Growth Rate and Adult Weight	162
14. Bone Tissue Properties	164
15. Gain- and Loss-of-Function Techniques	165
16. Transient Gain-and Loss-of-Function Analyses	167
17. Effects of Runx2 Over-Expression on Proliferation and <i>In Vitro</i> Mineralization	169
18. Effects of Runx2 Over-Expression on Morphology	171
19. Effects of OPG and RANKL Over-Expression on Beak Length Ratio	173

20. Western Blot and qRT-PCR	175
21. Roles for Cell Cycle and Osteogenic Regulation in Generation of Variation	177

“There is one fundamental thought that permeates all the forms and stages of animal development and governs all their relationships. It is the same thought that, in the cosmos, collects the separated masses into spheres and binds these together into a solar system; The same that allows the scattered dust on the surface of the metallic planet to develop into living forms. This thought, however, is nothing but life itself, and the words and syllables in which it expresses itself, are the different forms of the living” (Von Baer, 1828).

Chapter 1: Introduction

1A. Adaptation in the Craniofacial Complex

Evolution occurs as a result of interplay of two main parameters: variation and selection. Over generational time, phenotypic and genetic variations in the population are passively selected for or against as they impact survival and reproductive fitness; thus do animals change and adapt to seemingly limitless environments, stressors, and niches, as living legacies of their ancestors on our earth today.

One of the most historically highlighted models of adaptive change is rooted in avian facial morphology, as in Darwin’s famous finches. Part of the reason for this focus is likely practical: the face and beak are largely external structures that can be easily observed and measured. However, another reason that naturalists have been able to record instances of craniofacial adaptation time and again is that shape, size, and integration of facial components are under strong selective

forces: these traits are absolutely crucial for fitness, impacting feeding, respiration, and communication, in most avians, as well as multitude of other functions including nesting, boring, digging, and even thermoregulation, in some subsets. Added to these selective pressures are constraints of weight and balance for birds of flight, providing us with a uniquely powerful system for understanding adaptation. For this dissertation, although we shall survey adaptation in a number of organisms, the majority of our observations and experiments will focus on avians.

The study of adaptive selection in avians is necessarily done retrospectively, through rigorous observational science. However it is only in organisms with much shorter lifespans – and larger ranges of ethical experimental models – that we are able to perform studies of prospective selection and create testable hypotheses in adaptation. In general, these are non-vertebrate organisms that lack a two-part jaw (as will be distinguished from the vertebrate jaw in Introductory **Chapter 1B**, which will describe ontogenetic and phylogenetic origins of the face). However, the field has recently made great gains in understanding craniofacial adaptation by investigating genetic and molecular sources of variation in craniofacial forms. Wherever genetic differences result in variation observable during development and growth, evolutionary and developmental biologists can test the extent to which these genetic differences are necessary and/or sufficient to generate certain phenotypes by gain- and loss-of-function techniques. Several well-studied examples of such genetic sources of variation shall be discussed in Introductory **Chapter 1D**, (with a short explanation

behind the range of examples chosen in Introductory **Chapter 1C**). One transcription factor in particular, Runx2, identified in our lab to be important for craniofacial growth and patterning in conjunction with interactions with cell cycle, shall be described in further detail in Introductory **Chapter 1E**, while the data delineating the path by which we arrived at our findings will be presented in **Chapter 2**. Proposed mechanisms that may contribute to generation of variation of size and shape of facial elements, specifically based on our data shall be outlined in **Chapter 2E**, and lastly, the ways in which these mechanisms may be related to the evolvability of the craniofacial complex shall be explained in **Chapter 3**. Throughout this document, I hope to highlight the utility of an important concept I have only just touched upon: that testable, functional studies of adaptation in vertebrates necessarily rely upon understanding molecular underpinnings that regulate growth, development, and variation. In addition, through our data, I hope to show that adaptation, growth, and development have the potential to be more deeply understood when we consider timing of biological events side by side with cellular and morphological processes.

1B. Ontogenetic and Phylogenetic Origins of the Vertebrate Face

To understand how craniofacial variation arises during development, we must first address how the face is formed in our model, avians, which are a class of vertebrates. Importantly, craniates are in part distinguished from other metazoans in that they possess a multipotent embryonic cell population known as neural crest, which goes on to form all the bones and cartilage of the face and jaw.

Neural crest cells originate in the dorsolateral margins of the neuroepithelium during neurulation, undergo epithelial-mesenchymal transition, and migrate extensively to form a variety of cell and tissue types (Figure 1A). Like mesodermal mesenchyme, neural crest mesenchyme (NCM) gives rise to an enormous number of overlapping derivatives, in addition to bone and cartilage, including tendon, adipocytes, and dermis, and uniquely gives rise to many others including glia, melanocytes, and endocardium, thus, it is sometimes regarded as the “the fourth germ layer” (Hall, 2000a).

Some of what is known about NCM derivatives, historically, comes from fate-mapping studies in amphibians due to ease of manipulation – i.e., prior to migration, NCM can be surgically transplanted or extirpated as solid epithelial cell sheets at the surface of the embryo (Figure 1B). However, a limitation of using amphibians for study of craniofacial development is that much of the skeletogenesis that contributes to the facial structures occurs after metamorphosis. In our lab, we rely heavily on a cross-species avian chimeric model, which retains ease of manipulation and accessibility, while allowing us the ability to follow NCM throughout skeletal development (Schneider and Helms, 2003). This system will be described in further detail in **Chapter 2**.

Modern systems of inquiry into functions and properties of NCM also include zebrafish and mouse genetic models. By bringing together the findings from the various model systems used to study NCM, the field has generated much debate surrounding the topic of NCM autonomy in craniofacial patterning. Classic chick studies at first seemed to support a “pre-programming model”,

whereby first arch NCM that was grafted heterotopically in the place of second or third arch neural crest at the time of neurulation was able to retain its identity post-migration to produce duplicated first arch skeletal elements (Noden, 1983). However, more recent transplant studies performed in mouse and zebrafish have demonstrated a large amount of NCM plasticity, wherein NCM can take on the cell and tissue fates of its environment. As noted by Trainor et al. (2000, 2002, 2003a) the abilities of NCM to be both plastic and retain some intrinsic patterning information are not mutually exclusive, and where the balance lies between the two in developmental processes may be strongly influenced by a population effect – that is, larger numbers of cells transplanted together are more likely to support maintenance of intrinsic signaling information.

In addition to tracing the ontogenetic path of how NCM creates the two-part vertebrate jaw of mammals, avians, and all Craniates (which shall be done in more detail in **Chapter 1D.**), we can also glean information on properties of NCM by examining evolutionary processes and divergent forms through which NCM has varied. For example, by evaluating the Japanese marine lamprey (*Lampetra japonica*) we find that NCM may be as susceptible to physical forces and barriers as to genetic and molecular regulation. The Japanese marine lamprey is a jawless vertebrate, yet has cephalic neural crest cells (CNC) that originate along the neuraxis and eventually populate the mandibular arch, as in gnathostomes. A key difference however, is that in gnathostomes, a stream of neural crest cells is able to migrate and grow rostrally between Rathke's pouch and the olfactory placode to form a maxillary process, and eventually an upper jaw via medial

fusion (Figure 1E). In contrast, in lampreys, a homologous stream of cells grows rostrally beneath a nasohypophyseal plate (this large plate being a possible reflection of a primitive vertebrate organization before the separation of oral and olfactory components that we now see in gnathostomes), which acts as a physical barrier to migration and growth (Kuratani et al., 2001; Shigetani et al., 2002; Kuratani, 2005a, 2005b).

Importantly, a change in cephalic crest cell migration pathways may majorly contribute to creating the separate identities of the upper lip in lampreys versus the maxilla and upper jaw seen in gnathostomes, especially when considering the impact that local molecular signaling has been shown to have on cell fates and craniofacial structures (to be described in **Chapter 1D**). These interpretations of lamprey CNC migration have been corroborated to some extent by data from the chick *talpid* mutant, in which hypophyseal development is affected, and the maxilla is unable to develop (Ede and Kelly, 1964). In this model, it is again crucially important to practice not only comparative anatomy, but to use experimental embryology to evaluate the kinds of genetic and molecular regulation that can lead to changes in tissue interactions by shifting location (heterotopy) or timing of developmental events (heterochrony) to produce different morphologies. In the section after the next, I highlight several steps throughout craniofacial ontogeny that have theoretical or observed potential for bring about these changes.

1C. When Do Sources of Variation in Craniofacial Development First Appear?

In determining which steps of craniofacial ontogeny to detail in the next chapter for their ability to be sources of variation and adaptation, I weighed a couple of different viewpoints regarding an oft-debated topic within the field of vertebrate development, which is when differences between body (and facial) patterns first emerge. Some define a “phylotypic stage” in early development (corresponding to the tail bud stage), where it is believed that all vertebrate embryos express characters common to the vertebrate lineage, causing them to appear very similar in form, possibly due to constraints on vertebrate body plans (von Baer, 1828). In this school of thought, it is not until after this stage that species-specific body plans begin to be divergent and distinguishable as to their later functional morphologies.

Although it is indisputable that vertebrates share similarities at the tail bud stage (including pharyngeal pouches, dorsal nerve cord, and somites), a gross morphological constraint at this time point does not preclude the presence of more difficult-to-detect species-specific differences at the same moment, or in prior stages, which may have significant impact on an organism’s eventual morphology. One perspective is that the ideas of observational scientists and anatomists have always been biased by our own limits of detection. Up until the present, technology and technique has steadily improved to allow us to see divergences and distinctions where we previously could not. Where before we illustrated embryos in pen and ink, we were held back by our ability to perceive and record any details finer than gross anatomy. Now we can photograph individual tissues with sub-cellular resolution, detect molecular patterns of

expression, and much more.

This pattern of observing minute variations with increasing resolution throughout history has led us into being constantly surprised by the information contained in the embryo, and more recently, by just how very early species-specific traits can begin to direct patterning events. An very nice example from these last couple years comes from snails: their beautifully spiralled shells, which spin clockwise or counterclockwise, are created as a result of uneven deposition of external calcium. These shells generally form their first whorl before a snail even hatches. When searching for the sources of species-specific information determining chirality, scientists began investigating earlier and earlier events in snail development, ultimately finding that adult snail shell chirality is determined by pre-blastula asymmetrical expression of polarity genes *Nodal* and *Pitx*, leading to the formation of the calcium-secreting organ on one side of the body or the other. Even more surprisingly, chirality can be predicted by the very first cell cleavage events and arrangements post-fertilization. In fact, even before cleavage, under a microscope, when the zygote appears to be a single homogenous structure, there is little doubt that transferred maternal proteins are already establishing a break in symmetry (Grande and Patel, 2009).

Therefore, if only out of hope that we do not ignore that which we cannot “see” – although the bulk of the experiments I performed during my dissertation research address only species-specific variation arising during mid-development directly – it is my intention that we pay close attention to circumstances leading up to the stages of focus, as well as the growth and patterning that take place

afterward, and throughout the life of the animal. Thus, in the next paragraphs I strive to provide a comprehensive view of potential sources of species-specific variation in the face, similar to those outlined in the Palimpsest Model (Hallgrímsson et al., 2009), beginning from the first appearance of neural crest.

1D. Genetic and Molecular Regulation in Facial Development

The earliest overt identification of neural crest is made anatomically and morphologically – neural crest cells lie as bilateral strips along the dorsal neural tube, just below the surface ectoderm. During their induction, the number and location of cells that are fated to become neural crest are influenced by secreted signals from the neural plate and neural tube, including Bmps, Shh, and Notch. Next, neural crest cells undergo epithelial-mesenchymal transition (EMT) and delaminate from the neural tube, responding to signals such as Bmps, Slug, and Snail. The EMT that occurs during post-neurulation in fact has much in common with the EMT that has been studied in cell cancer models. That is, EMT in both cases likely involve integrins, cell-adhesion proteins, and tissue forces. Recently it has also been shown that applied stress and tissue mechanical properties, such as elastic modulus, can drive EMT through altering Rac1b localization and cytoskeletal changes (Lee et al., 2012; Gjorevski et al., 2012). Thus, it is conceivable that species-specific differences could arise in number of ways during these processes, with some examples being differences in:

1. Cell numbers in areas receiving signaling, pre-induction
2. Neural crest numbers post-induction, due to:

- i. Responsiveness to secreted signaling factors, or
- 3. Range, concentration, and diffusion or extinction of secreted signals, or timing of their expression or cellular release. Also,
- 4. Neural crest numbers post delamination, due to:
 - i. Cell adhesion properties
 - ii. Tissue geometry leading to unique patterns of stress-strain forces fostering EMT.

In addition, any of these differences could be propagated and reinforced by downstream signaling events.

After neural crest cells delaminate and become mesenchymal in nature, the cells migrate extensively throughout the body, to various locations depending on their identity. Necessarily then, identity is already partially specified before crest cells even leave the neural tube. One instance of pre-patterning is expression of Hox genes along the neural tube and body axis. The regions that give rise to pre-mandibular neural crest are in a Hox-free zone, (i.e. expressing no Hox family genes), while the second arch and more rostral segments express combinations of Hoxb1, Hoxa2, Hoxa3, and Hoxa4. Further, heterotopic transplantation or Hox gene misexpression can cause tissue transformations (Rijli et al., 1993; Gendron-Maguire, 1993; Creuzet et al., 2002). In this context, premandibular neural crest mesenchyme that is destined to become connective tissue migrates in streams toward the front of the embryo to form the much of the

developing face, filling the first arch. Other neural crest-derived cell types have very different paths – for example, melanocytes, which provide pigmentation to the skin, disperse widely, far from their starting points. The migration path itself is highly regulated through extracellular matrix properties and signals: proteins such as fibronectin, laminin, tenascin, and certain collagens and proteoglycans can promote migration, while ephrin signaling can inhibit migration (Krull et al., 1997; Santiago and Erickson, 2002).

During these steps, variation in eventual morphologies could arise as a result of differences in:

1. Cell/tissue identity, as specified before migration
2. Rate of migration
3. Migration paths, due to:
 - a. Extracellular matrix protein makeup or distribution
 - b. Chemoattractant and chemorepellant distribution
 - c. Signaling receptors on neural crest cell surfaces

Importantly, neural crest cells are also influenced by maintenance factors, as well as chemotactic and proliferative signals as they near their destinations. Once neural crest cells that are fated to form the face reach the pharyngeal pouches, they must continue proliferation and differentiate. The importance of this phase is underscored in the case of *endothelin-1*-deficient mice, which have neural crest cells that migrate properly into the third and fourth arch, but fail to proliferate, leading to aortic defects and craniofacial abnormalities (Thomas et al., 1998).

Differentiation, also a key event, takes place as a result of both NCM-autonomous signals, as previous work in our lab has shown (Merrill et al., 2008; Eames and Schneider, 2008; Tokita and Schneider, 2009; Solem et al, 2011), and as a result of reciprocal interactions with overlying epithelium. One of these example of reciprocal interaction relies on Sonic hedgehog signaling from the surface ectoderm, which can affect cell proliferation in the palate, and generate the majority of morphological variation in the upper jaw in a dosage-dependent fashion (Young et al, 2010). Other transcription factors expressed in the mesenchyme, including Bmp4, Msx1, Fgf8, and Fgf10 can also affect cell proliferation and size of mesenchymal primordia (Hu et al., 2003; Lan and Jiang, 2009). In general, as the loosely associated stellate neural crest mesenchyme begins to differentiate under these signals, the cells take on morphologies specific to their function, (e.g. osteoblasts and chondrocytes become cuboidal, and increase ribosomal and Golgi activity for secretion of cartilage and bone matrix), and decrease proliferation. In addition, many cell types, including muscle, cartilage, and bone, form condensations, whereby a concentrated population of cells is able to reach a critical mass of signaling to further promote differentiation within the local area (Hall and Miyake, 2002). It is during this period, as osteogenic cells switch from proliferation to differentiation, and condensations begin to form, that we also detect the expression of, and regulation by, the transcription factor Runx2, which will be a major focus throughout this dissertation.

In the complex developmental landscape built of multiple hierarchical

levels of regulation, it turns out that proper cell numbers, rate of proliferation, and timing of histogenic movements are absolutely essential to build a functional face and jaw. This is partly because what in the adult looks like a solid upper and lower jaw is actually derived from multiple mesenchymal primordia. These mesenchymal primordia are at first separated by space and overlying epithelium, but they eventually move toward each other and fuse to form continuous elements (Figure 1D). Any misstep in related processes can cause the common birth defects we know as cleft palate and cleft lip, both of which are direct results of defective fusion. For this reason, isolated divergences from the established forms of any of the mesenchymal primordia comes at high risk to fitness for the organism. We will touch upon this point in again in **Chapter 3**.

In terms providing identity to the premandibular mesenchyme, it has been postulated that much in the way that rostrocaudal identity is determined by a metamerically expressed Hox code of expression, there is also a metamerically expressed Dlx code that determines pattern and polarity across the proximodistal axis of the first arch, comprised of overlapping expression patterns of the transcription factors Dlx1, Dlx2, Dlx3, Dlx5, and Dlx6 (Qiu et al., 1995, 1997; Depew et al., 2002, 2005). Moreover, recent *in vitro* studies increasingly suggest that cell fate and identity strongly are affected by the material properties of the surrounding extracellular matrix (reviewed by Guilak, et al., 2009).

The consideration that multiple major processes that occur mid-development could go on to produce craniofacial variation, including polarity patterning, mesenchymal proliferation and differentiation, and size regulation

highlights the importance of spatial distribution of NCM, as well as the timing of such distribution.

During these steps, variation in eventual morphologies could arise as a result of differences in:

1. Chemotactic signals
2. Survival and maintenance signals (versus neglect and cell death)
3. Cellular distribution along the proximo-distal axis of the arches
4. Spatiotemporal expression of Dlx factors determining tissue identity
5. Spatiotemporal expression of transcription factors influencing proliferation and differentiation
6. Cell density and formation of condensations
7. Deposition of extracellular matrix and matrix material properties
8. Timing of the above processes, as well as of fusion of mesenchymal primordia

From the mid-phase to the end of development, and even after hatching (or birth), we observe continuous growth and expansion of many of NCM-derived tissues, as well as interactions with non-NCM derived tissues. Signaling between the brain and facial ectoderm is particularly well-studied in the context of frontonasal process patterning (Foppiano et al, 2007; Hu and Marcucio, 2009, 2012), but other neighboring tissues, e.g. optic and muscle, are also likely to impact shape and function. Physical constraints and geometries also play a role in affecting continuous changes to shape and size. One example of a process that affects physical constraints that is often presented in the context of

craniofacial birth defects (specifically, craniosynostoses), is that of craniofacial ossification. As the skull grows during development and early life, fibrous sutures connect bony elements to allow lateral growth. However, if the ossification of any of these sutures occurs prematurely, the newly rigid line of fusion, composed of differentiated (non-proliferative) cells and mineralized bone matrix, prevents further expansion, and growth occurs differentially on the remaining free edges of the bony elements, contributing to skull, and often facial, malformations (reviewed by Robin, et al., 1993) especially in the presence of, or perhaps primarily due to, other growth factor signaling defects (Martínez-Abadías et al., 2010). Constraints of the developing craniofacial skeleton can also include weight, balance, density, flexibility, fracture resistance, and more, depending on the multitudes of ways in which an animal optimally interacts with its ever-changing environment.

So, let us see how the amount and quality of bone laid down to form the face and jaw may vary: As neural crest-derived mesenchyme forms condensations and begins to differentiate into osteogenic cell types, they will prefigure the skeletal elements both by the shape and size of their condensations but also by the secretion of bone matrix, which is referred to as osteoid. During this early differentiation, the cells express enzymes such as alkaline phosphatase to build and expand this matrix. As they continue to differentiate into osteoblasts, they also lay down the organic components of the matrix, composed mostly of Type I Collagen (Col1), but also including proteins that are essential for the nucleation and incorporation of bone mineral, to form the hardened bone

structure. The proteins include bone sialoprotein (Bsp), osteopontin (Opn), and osteocalcin (OC). The combinatorial expression pattern of these proteins plays a role in dictating the structure of bone minerals, including mineral length and density, which in turn affect the material properties of the bone. (Erlebacher et al., 1995)

However, the building of the organic and inorganic components of the bone matrix does not end during development, nor even when the organism has finished growing. In reality, the skeleton is incredibly dynamic, and is continually remodeled throughout the life of the organism, or until the tissues lose their generative capacity, in a process called bone remodeling (Frost, 1963). As osteoblasts continue to differentiate, they reach a terminal state, where they are referred to as osteocytes. Osteocytes are completely embedded and immobile in mineralized bone matrix, but have long cellular extensions that likely foster cell-cell communication and sense forces and strain around them. As bone succumbs to age, microfractures, and other changes in integrity, it is broken down and resorbed by a non-NCM derived cell type, osteoclasts. As soon as osteoclasts remove old bone by enzymatic and acidic means, osteoblasts quickly follow in their wake to replace the affected areas with new bone. Thus, it is the interplay between these two cell types after the initial formation of bone that help to maintain its structure over time. Altered activity or communication by either cell type can easily offset the balance of bone deposition and resorption, leading to such common diseases as osteoporosis, which is defined by loss in bone density.

Although this review of possible sources of craniofacial variation is by no means exhaustive, what I hope to have conveyed is a breadth of possibility, in addition to a sense that generation of variation can occur continuously throughout the developmental process, at times aggregating traits to shift morphologies further from the norm, and at times limiting, minimizing, or almost negating the effects of these earlier divergences. That is, in producing shapes and patterns, it is likely that no developmental steps are truly independent or discrete, but rather that all later steps build on those that come before. Of course, whether our limits of detection allow us to identify the connectivity of events or not, is another question.

1E. The Transcription Factor Runx2 – a Model for Sources of Variation

In **Chapter 2**, I outline the experimental portion of my dissertation work, done in conjunction with other lab members (see Acknowledgements). These data provide the first evidence that Runx2 expression levels in the jaw are NCM-dependent and species-specific. Moreover, we are the first to report that its over-expression is able to alter patterning of the face, and that its levels can be affected by NCM-driven changes to cell cycle regulation.

Taken together, these new findings, along with previous data from other groups, point to Runx2 being an interesting case study as a possible driver of facial evolution. Runx2 is well known to affect many processes in osteogenesis, which is a key component of facial and jaw development. Furthermore, *in vitro* models show that Runx2 can affect both cell proliferation and differentiation, as

well as respond to changes in cell cycle, while human genetic surveys tie variation in Runx2 expression levels to congenital birth defects, and thus phenotypic outcomes. Lastly, the gene may be highly “evolvable,” while many layers of molecular and genetic regulation allow fine-tuning of expression levels and morphological effects. A subset of the data that has been published on Runx2 function and regulation prior to our own work is presented below, and shall complete **Chapter 1**.

1E i. Roles of Runx2 in Osteogenesis

Runx2, i.e., Runt-related transcription factor 2, is a member of the Runx transcription factor family, which is characterized by its Runt DNA-binding domain. Although other members of the Runx family are expressed in tissues including the hematopoietic lineage and epithelium, Runx2 is uniquely expressed in mesenchymal condensations of the developing skeleton, and becomes gradually restricted only to cells of the osteoblastic lineage during the course of skeletogenesis, and is maintained postnatally in fully differentiated osteoblasts. As a transcription factor, it regulates and directly binds to the promoters of several key osteoblast-specific genes including osteocalcin (OC); collagen type 1, $\alpha 1$ subunit (Col1a1); Bone sialoprotein (Bsp); and osteopontin (Opn), which have various roles as the organic components of bone matrix and in the nucleation and formation of bone mineral crystal structures, which comprise inorganic components of the bone matrix. (Ducy et al., 1997)

In vitro it has been shown to drive osteogenesis in a variety of primary cells and cell lines (including those from, muscle, fibroblastic, mesenchymal, and osteoblastic lineages), to varying degrees. In MC3T3-E1 calvarial cells (a pre-osteoblastic cell line that is committed to the osteoblast lineage, but does not normally express osteoblast-specific genes, over-expression of Runx2 induces the expression of OC, Col1a1, Bsp, and Opn. In C3H10T1/2 cells, a pluripotent fibroblastic cell line, and in skin fibroblasts, over-expression of Runx2 induces the expression of OC and Bsp (Ducy, et al., 1997). Forced Runx2 expression can also accelerate the onset of osteogenic activity, such as alkaline phosphatase deposition, when applied in conjunction with exogenous Bmp, and media formulated to support osteogenic differentiation (e.g. Kang and Alliston et al., 2005).

In vivo, Runx2 has been shown to be absolutely essential for bone formation. In 1997, two groups independently created Runx2-deficient mice, and found that the resulting pups completely lacked bone matrix, osteoblasts, and the anatomical elements that form direct ossification without a cartilage intermediate (e.g. calvaria and clavicles). However, the cartilage anlagen prefiguring the bones that form via endochondral ossification, e.g. tibia, ribcage, humerus, were patterned normally when compared to wild type mice. (Komori et al., 1997; Otto et al., 1997)

To specifically examine the role of Runx2 postnatally, a transgenic mouse model was created to express a truncated, dominant-negative form of Runx2, under control of the osteocalcin promoter (and thus expressed only in

differentiated osteoblasts). It was found that these transgenic mice had a normal number of osteoblasts and a normally patterned skeleton, but that osteoblastic function was reduced, resulting in decreased bone matrix deposition, such that the mice began to lose bone by two weeks of age. Confirming the loss of osteoblastic function were decreased levels of Opn, OC, and Bsp proteins in the bone matrix. In contrast with these markers expressed late in osteoblast differentiation (after endogenous OC comes on – and thus, after the transgene promoter is activated), early markers of osteogenesis were intact, including Col1 expression and alkaline phosphatase activity. (Ducy, et al., 1999)

At the time, the combined data from these mouse models were interpreted by some researchers to mean that although Runx2 controls osteoblast differentiation and function, it “is not implicated in patterning the skeletal elements” (Ducy, 2000), a view which may not be altogether true. For one thing, a complete lack of Runx2 participation may leave cartilaginous skeletal anlagen normally patterned, but this would not necessarily be the case if decreased or increased Runx2 levels could play a role. It must be pointed out, for example, that a Runx2-deficient mouse with no calvaria at all gives us no information the role of Runx2 in calvarial patterning.

In fact, a few years later, when the role of Runx2 was analyzed in avian limbs, as well as in a transgenic mouse model where Runx2 expression was driven by the Collagen Type II promoter (and thus only expressed in chondrocytes) it was found that over-expression could result in overt phenotypic changes, such as such joint fusions and shortening of limbs (Stricker, et al.,

2002). This was traced back to functions of Runx2 in regulation of chondrocyte differentiation. However, since Runx2 was over-active only in chondrocytes in the mouse model, this study does not rule out the possibility that Runx2 over-expression in other cell types could be capable of affecting shape as well. Moreover, the role of Runx2 over-expression in skeletal elements that do not form through a cartilage intermediate, including many of those in the jaw and face, was not examined in either the avian over-expression studies, or the mouse Col II promoter-driven Runx2 expression model. Thus, the data gathered during my dissertation research brings us new insight on the involvement of Runx2 in craniofacial patterning, but does not directly contradict data from previous studies.

In addition to being necessary for osteogenesis, Runx2 expression is also sufficient to drive premature ossification in a Prx1 (mesenchyme-specific) promoter-driven mouse model. In these transgenic mice, ectopic mineralization begins as early as E11.5 in the calvaria, as compared to E15.5 in wild-type littermates (Maeno et al., 2011). However, a full picture of the cellular and molecular processes that help to promote cell differentiation and accelerate osteogenesis *in vivo* has not yet emerged. Further, any effects of the transgene on facial and jaw patterning were left either un-examined or un-described.

1E ii. Interactions Between Runx2 and Cell Cycle

Based on extensive published *in vitro*, biochemical, and DNA-/protein-interaction data, we know that Runx2 can also affect cells in ways that do not

strictly have to do with the function of differentiated osteoblasts. Notably, Runx2 has been shown to interact closely with cell cycle regulators. As I hope to show through a short review of these data, the interplay between Runx2 and cell cycle provides many clues as to how Runx2 can accelerate osteogenesis *in vivo* (potentially also affecting patterning along the way). To follow up on these possibilities, I performed several experiments *in ovo* (**Chapter 2**).

As briefly mentioned in **Chapter 1D**, at early stages of craniofacial development, the mandibular primordium is largely composed of highly proliferative mesenchyme. However, at the onset of osteogenesis, a subset of these mesenchymal cells take on osteoblast cell fates, simultaneously increasing expression of genes that regulate and encode proteins for bone matrix synthesis, and decreasing proliferative capacity (Stein et al., 1996, Aubin et al., 1998). At the level of the cell cycle, the transition between proliferation to differentiation is regulated at a checkpoint between the G1 and S phases, where G1 is the phase that follows immediately after mitosis, and S phase is when the cell begins to synthesize DNA in preparation for the next round of cell division. At this checkpoint, G1 arrest allows further differentiation, while progression past G1 into S phase allows continued cell cycling and proliferation (Figure 2A). Below, we examine some mechanisms by which this checkpoint is regulated in osteoblasts, and how crosstalk between proliferation programs and differentiation programs may be established via Runx2.

In vitro, Runx2 mRNA and protein levels correlate to stages of the cell cycle, rising to maximal levels at the G0/G1 transition, and dropping to minimal

levels at early S and M phase, suggesting that regulation of cell cycle progression and Runx2 expression are intertwined. This phenomenon has been observed exclusively in cells of an osteoblastic lineage, and does not occur in cells of chondrocytic or fibroblastic lineages (Galindo et al., 2005).

One explanation for why Runx2 expression and cell cycle progression seem to correlate could be that the same upstream signals control both processes. This idea is bolstered by data showing that contact inhibition and serum starvation in cell culture conditions can also up-regulate levels of Runx2 mRNA and protein. These same conditions cause up-regulation of p27, which is a cyclin-dependent kinase inhibitor and negative regulator of S-phase entry, and causes down-regulation of cyclin-dependent kinases (enzymes that promote cell cycle) and cyclins (the activating binding partners of these kinases), including cyclin D1, cdk2, cyclin E, cyclin A (each important for S phase entry), and cyclin B1 (important for M phase entry). In this model, osteoblastic cells are likely monitoring growth factor concentrations or the signaling milieu, since heparin treatment blocking osteogenic cell surface receptors can also mimic the effects of serum starvation (Pratap et al., 2003). Interestingly, chondrocytic cell lines have a different response entirely, and exhibit a decrease in runx2 levels with serum deprivation. This has led others to point out that this unique regulation of runx2 may also provide a tissue-specific mechanism for driving differentiation (Pratap et al., 2003).

On the other hand, Runx2 gain- and loss-of-function experiments seem to place Runx2 upstream of cell cycle regulation, with Runx2 demonstrating an anti-

proliferative function. Runx2 over-expression in synchronized MC3T3s delayed entry into G1, while cultured calvarial osteoblasts from runx2-deficient mice exhibited increased proliferation and cell density as compared to those of wild-type mice. Moreover, administration of exogenous Runx2 by adenovirus restored growth regulatory control (Pratap et al., 2003). Similarly, forced Runx2 expression in MC3T3-E1 cells has also been shown to induce p27, which is normally expressed in differentiating, but not proliferating calvarial osteoblasts (Drissi et al., 1999; Thomas et al., 2004). Runx2-dependent induction of p27 *in vitro* also leads to de-phosphorylation of Retinoblastoma (Rb) and G1 cell cycle arrest. This effect on cell cycle arrest seems specific to Runx2-dependent regulation of p27, since administration of p27 siRNA is able to rescue the proliferation defect.

Additional data tracking Runx2 at the sub-cellular level also supports an anti-proliferative function for Runx2. Runx2 can directly bind the ribosomal RNA (rRNA) gene promoter to affect chromatin histone modifications at ribosomal DNA (rDNA) regulatory regions, resulting in repression of RNA Pol1-mediated ribosomal synthesis, and thus, inhibition of the cell cycle. Further confirming that repression of ribosomal synthesis is a direct result of rDNA binding interactions are data showing that Runx2 over-expression decreases rDNA promoter activity, and Runx2 ablation and RNAi treatment in SAOS cells that show increased rRNA transcript and protein synthesis (Young, et al., 2007)

1E iii. Runx2 in disease

Perhaps as a consequence of Runx2 playing critical roles in both osteoblast cell cycle regulation and differentiation, loss or over-expression of Runx2 has also been observed in numerous instances of human disease. So far, at least 50 unique mutations in Runx2 have been reported to cause cleidocranial dysplasia (CCD), presumably due to decreased Runx2 function (Mundlos, et al., 1997). The severity of the disease varies widely, as does the location of the mutation within the Runx2 sequence. However, most mutations affect the Runt DNA-binding domain. In cleidocranial dysplasia, patients display missing clavicles, delayed closure of cranial sutures (Figure 2B), ectopic bones in sutures (known as Wormian bones), problems in tooth development, and in severe cases, limb defects. These same features have also been corroborated in transgenic mice with one copy of the Runx2 allele lacking a functional transactivation domain (Otto et al., 1997).

Of particular relevance to our studies is a report of jaw proportions for 14 CCD versus non-CCD patients, which reported subtle effects on jaw length: Prior to puberty, jaw proportions in CCD patients were no different from unaffected individuals. However, by adulthood, CCD patients showed longer horizontal mandible growth (but shorter vertical maxillary growth) than their unaffected counterparts (Ishii et al., 1998). These data suggest that differences in Runx2 expression levels can affect patterning of the jaw, during juvenile growth – an idea that we will come back to.

On the other end of the spectrum are the disease phenotypes caused by over-expression of Runx2 (Figure 2B). Mice that carry a fibroblast growth factor

receptor 1 (FGFR1) mutation that is an ortholog of a mutation in humans causing Pfeiffer syndrome (Pfeiffer, 1964), display increased Runx2 expression. Possibly as a result, the mutant mice also exhibit craniosynostosis (premature fusion of cranial sutures – directly opposite to the phenotype observed in cleidocranial dysplasia) and accelerated osteoblast proliferation and differentiation in the sutures (Zhou, et al., 2000). Interestingly, this FGFR1 mutation mirrors a craniosynostosis phenotype that is also observed in transgenic mice over-expressing Runx2 under the Prx1 promoter (Maeno, et al., 2011), suggesting that Runx2 expression may be partly regulated by FGF signaling. However, this is not nearly the only pathway that can modulate Runx2 levels, as we shall see in the next section.

1E iv. Molecular Regulation of Runx2

A dizzying array of possibilities is presented in the literature for the molecular regulation of Runx2 at both the transcriptional and post-translational levels. However, there may be several reasons for this complexity: multi-faceted control over Runx2 expression may help with tissue-specific expression, stage-specific expression, differential expression in distinct anatomical locations (e.g. maxilla versus mandible); it may be an artifact of the myriad ways in which random mutations could affect Runx2 levels to produce helpful facial morphologies; or it could be a system of balances, in place to decrease the

possibility that spontaneous mutations could alter expression levels too dramatically and result in disease phenotypes.

To begin, the Runx2 exonic sequence contains several motifs that are essential for its regulation. The first N-terminal 19 amino acids, along with a poly-glutamine/poly-alanine domain act as activation domains, while the C-terminal region contains a proline/serine/threonine-rich domain that can be repressed by HES1, a basic helix loop helix protein, and a VWRPY motif, which can be repressed by TLE2, a mammalian homolog of the Groucho gene found in *Drosophila* (Thirunavukkarasu et al., 1998). In addition, the Runx2 promoter contains functional Runx2 binding sites, allowing it to auto-regulate its expression (Ducy et al., 1999).

Runx2 has also shown to be regulated by a number of homeobox genes, transcription factors, and growth factors. Though there are many examples, here I present only one or two in each category.

1. Homeobox genes: Mice that are deficient in Msx-2 display decreased Runx2 expression, delayed osteoblast differentiation, and delayed ossification in skull and long bones (Winograd et al., 1997). However, loss of Msx-2 may be partially compensated for by expression of Msx-1; Mice that lack both Msx-1 and Msx-2 present a much more dramatic phenotype, including complete lack of frontal bones of the skull, and no detectable Runx2 expression (Han et al., 2007). Interestingly, in a NC-specific conditional Msx-1/Msx-2 inactivation model, loss of up to three functional Msx alleles caused progressively more bone loss, but loss

of four alleles caused ectopic Bmp expression in normally non-osteogenic NC derivatives, and resulted in ectopic bone islands in the skull, phenocopying the appearance of Wormian bones observed in cleidocranial dysplasia (Roybal et al., 2010).

2. Transcription Factors: Normally, Twist-1 and Twist-2 are expressed in Runx2-expressing cells during early skeletogenesis, and it is only after their expression decreases that osteoblast-specific gene expression is observed. Furthermore, mice with Twist-1 or Twist-2 haploinsufficiency display premature osteoblast differentiation, whereas Twist-1 over-expression inhibits osteoblast differentiation despite the presence of normal Runx2 expression levels. This is due to the fact that Twist-1 and Twist-2 can bind directly to the DNA-binding domain of Runx2 to inhibit its function, thus acting in an anti-osteogenic capacity. In addition, it seems that Twist-1 and Twist-2 temporal expression is important for modulating timing of onset of osteogenesis (Bialek et al., 2004).

3. Growth factors: One of the clues to the osteogenic function of Runx2 upon its characterization was the fact that it was the first osteoblast-specific transcription expressed after Bmp-7 treatment *in vitro* for differentiation assays (Ducy et al., 1997). Runx2 also interacts with seemingly endless components of the TGF β pathway, and the MAPK pathway. For example, Smad3, one of the main downstream effectors of TGF β , can bind to the Runx2 target promoter sequences (e.g. of OC, Opn, Runx2 itself) to inhibit osteoblast differentiation. Smad3 can also co-localize to these sequence regions with HDAC4 and/or HDAC5 to promote histone de-acetylation and block transcription at Runx2 target

sequences. CBP and p300, which are acetyltransferases can also act as co-activators by associating with Smads (Alliston et al., 2001; Kang et al., 2005). Runx2 levels are also responsive to levels of circulating glucocorticoids and estrogen (Ducy, 1997), and can itself induce expression of the Type I TGF β receptor to complete a regulatory feedback loop (Ji et al, 1998). This loop provides a way by which TGF β signaling could quickly and efficiently shut off Runx2 expression and activity. The functional relevance of TGF β regulation is apparent *in vivo*, since mice that conditionally over-express TGF β in osteoblasts also display an osteoporotic and CCD-related phenotype seen in Runx2-deficient mice (Erlebacher and Derynck, 1996). On the other hand, over-expression of Runx2 in osteoblasts or Smad3 deficiency can also lead to bone loss, since both can cause premature osteocyte apoptosis (Borton, et al., 2001).

To complicate matters further, Runx2 can be regulated post-translationally through phosphorylation, acetylation and ubiquitination, downstream of multiple, possibly redundant, inputs. For example, both Bmp2 and TGF β can promote p300-dependent acetylation of Runx2, preventing ubiquitination by Smurf ligases, and subsequent degradation. Phosphorylation of Runx2 through the MAPK pathway, which again is affected by both TGF β and Bmp signaling, can also enhance Runx2 transactivation, as can TGF β -dependent activation of the c-Fos/c-Jun transcription complex which can act as a co-activator to help Runx2 up-regulate transcription at target promoters (e.g. Col1) (Selvamurugan et al. 2002).

Among the experiments that help to shed light on Runx2 regulation and function, there are a multitude of others that cloud and confuse our understanding, through sheer contradiction. Some of the reason for this is the enormous variety of aberrant, immortal cell lines or culture conditions used for *in vitro* studies; the inclusion of data from fish, bird, and mouse models, or even different anatomical elements; the stage-specific effects of Runx2, TGFb, Bmp, and MAPK signaling, which often induce distinct responses in context of cell maturity, density, and surrounding growth factors; dosage-specific effects,; or even simply differences in endochondral versus direct ossification, which may be a large factor considering that Runx2 certainly plays chondrocyte- and osteoblast-specific roles. However, as suggested earlier, perhaps this complex regulation arose as a consequence of big, risky changes in Runx2 levels too often affecting skeletal structure, shape, and fitness adversely. To follow, in the next chapter I present the experimental data of my dissertation, linking mesenchymal proliferation and differentiation to effects of Runx2 on facial size, shape, and developmental timing, and in Chapter 3, how changes to facial size and shape may be readily modulated, but also form integrated structures during evolutionary adaptation.

Chapter 2. Neural Crest Controls Osteogenesis and Species-Specific Patterning of the Facial Skeleton By Regulating Cell Cycle

Modified from manuscript of the same title, with contributions by Andrew H. Jheon, Erin Ealba, B. Frank Eames, Kristin Butcher, Suzanne Mak, Raj Ladher, Tamara Alliston, and Richard A. Schneider

Chapter 2A. The Avian Chimeric System

In our lab, we use a unique avian chimeric model, which allows us to investigate changes to timing of molecular, cellular, and histological processes in osteogenesis *in vivo*. To do so, we perform transplants of pre-migratory neural crest mesenchyme (NCM) and track its behavior and properties as it goes on to give rise to all the bones in the face (Figure 3C-F). We take advantage of two avian species with divergent growth rates and species-specific facial and jaw morphologies: quail, a faster-developing species with a small, pointed beak, hatches in 17 days; and duck, a slower-developing species with a large, broad bill, hatches in 28 days (Figure 3A,B). When faster-developing quail NCM is transplanted into a slower-developing duck host, osteogenic events occur on the accelerated donor timetable, which maintains about a 3-stage lead over control duck. While this work shows that NCM is instructive in controlling the timing of osteogenic events, the mechanisms by which it is able to coordinate each step of this complex process, including cell proliferation, differentiation, matrix deposition, and mineralization are mostly unknown. We originally hypothesized

that one mechanism by which NCM-dependent *Runx2* expression could drive accelerated osteogenesis in chimeras is by *Runx2* playing a dual role regulating both cell proliferation and osteogenic differentiation, which has previously only been demonstrated *in vitro*. Although this may still be the case, we ended up uncovering a larger pattern of NCM instruction. Here, we present our findings that NCM is able to regulate cell cycle to drive species-specific timing of osteogenic events, including *Runx2* expression, and thus modulate species-specific facial patterning.

2B. Results: NCM Controls Timing of Osteogenesis

2B i. Neural crest mesenchyme establishes the timing of mineralization

To determine the extent to which neural crest mesenchyme governs the timing of mineralization, we transplanted neural crest cells from quail to duck, producing chimeric quack. The onset and progression of mineralization during development was analyzed in quail, duck, and quack by whole-mount Alizarin red staining (Wasserug, 1976). The first evidence of any mineralization was observed in the distal hindlimb (i.e., tibia) of quail and duck at HH33 (data not shown), but there was no Alizarin red staining anywhere in the head skeleton (Fig. 4A). In the jaw skeleton of quail (Fig. 4C) and duck (Fig. 4D), the bones mineralized at HH34. In quack, initiation of craniofacial mineralization on the quail donor side occurred three stages earlier at HH31 (Fig. 4B), long before the onset of tibial mineralization. Moreover, quack mineralization at HH34 (Fig. 4E) was like that of quail at HH37 (Fig. 4F), and quack at HH36 (Fig. 4H) were equivalent to

HH39 quail (Fig. 4I). The host side of quack was always similar to that observed in the stage-matched duck control (Fig. 4D,G). In duail at HH34, the presence of duck donor-derived (i.e., Q ϕ PN-negative) mesenchyme (Fig. 4J) resulted in a delay of craniofacial mineralization by three stages (Fig. 4K). Duail mesenchyme eventually mineralized but maintained its slower progression (Fig. 4L).

2B ii. Neural crest mesenchyme regulates spatiotemporal expression of genes involved in mineralization

To ascertain the ability of quail donor NCM to regulate genes known to play a role during mineralization, we performed *in situ* hybridization on tissues from duck, quack, and quail (Fig. 5). We focused on the angular bone adjacent to Meckel's cartilage (Fig. 5D). In HH32 duck and the host side of stage-matched quack, we observed little or no expression of *Tissue non-specific alkaline phosphatase (TNAP)* (Fig. 5E, F), *Bone sialoprotein (Bsp)* (Fig. 5I, J), and *Osteopontin (Opn)* (Fig. 5M, N). This gene expression profile was identical to quail at HH32 (not shown). However, on the quail donor side, these genes were all highly expressed (Fig. 5G, K, O), coincident with the presence of donor NCM (Fig. 5C) and equivalent to that observed in HH35 quail (Fig. 5H, L, P).

2B iii. Host vasculature and blood mineral levels provide a permissive environment for donor-directed osteogenesis

To determine whether donor NCM regulates systemic levels of blood minerals required for mineralization, calcium and phosphorus levels were first measured in duck at time points ranging from HH28 (just before the first evidence

of mineralization in the embryo) to HH38 (less than one week before hatching. (Fig. 5Q). Calcium levels were relatively constant between HH28 to HH38, whereas phosphorus levels nearly tripled by HH31 ($p=0.0040$) and steadily decreased until HH38. No differences were detected between quack and duck. Quail blood sera from several stages were also measured, and calcium and phosphorus levels were similar to that observed in duck and quack (data not shown).

In order for blood minerals and systemic osteogenic factors to reach the tissues to be ossified, vascularization must also take place. Thus, we decided to assess influence of donor NCM on host blood vessel formation, by measuring vasculature in sectioned and whole-mount chimeric mandibles at HH24, when the osteogenic program is beginning induction. To measure vasculature from sections, we triple-stained tissues with *Lens Culinaris* Agglutinin, Q ϕ PN, and Hoescht dye to visualize vasculature, quail donor NCM, and total cells, respectively (Fig. 7H) and quantified total vasculature over a fixed volume. Surprisingly, we found no difference between quail donor and host sides in quack HH24 (Fig. 7J). To measure vasculature in whole mandibles, we filled the bloodstream with fluorescent microspheres (Fig. 7I). Fluorescence as a measure of blood volume was quantified, and again, no differences in the amount of vasculature between quail donor and host sides in HH24 quack were detected (Fig. 7K). Lastly, *in situ* hybridization for two markers of developing vasculature, *Vegf* and its receptor, *Flk1*, was performed on sections from HH24 quack. No

apparent difference was detected between quail donor and host sides (data not shown).

2B iv. Neural crest mesenchyme controls timing of osteoid deposition

We measured the effect of NCM on deposition of extracellular matrix (osteoid) histologically in quail, duck, and quack by trichrome staining of the jaw joint. Osteoid was present in the jaw at HH34 in quail (Fig. 6D,H), and duck (not shown), but not at HH31 (Fig. 6A,E). In quack, osteoid was visible three-stages earlier on the quail-donor side at HH31 (Fig. 6C,G) coincident with Q ϕ PN-positive staining (Fig. 6L).

To test the limits of the ability of NCM to accelerate osteogenic processes, we created chimeras using two avian species with even more disparate developmental timing than quail and duck: quail and emu. Emu take 58 days to hatch, versus duck (28 days), and quail (17 days). In resulting “qumu” we found that donor quail NCM was able to dramatically accelerate osteogenesis in the slow-developing emu host. At HH27, when the control, un-operated side of the emu mandible was composed mainly of mesenchyme just beginning to differentiate, the quail donor side showed robust Meckel’s cartilage and the first signs of osteoid deposition – an acceleration of about seven stages (Fig. 6N, O).

2B v. Neural crest mesenchyme controls timing of osteoblast differentiation

To investigate NCM influence on osteoblast differentiation, we assayed for the enzymatic activity of alkaline phosphatase in the mandibular arch. Low levels of alkaline phosphatase were detected in HH26 duck (Fig. 7A) and quail (not

shown), and much higher levels at HH29 (Fig. 7C). The donor side of HH26 quack chimeras stained considerably darker like that observed in older HH29 quail (Fig. 7B).

We then tested NCM ability to modulate gene expression required for differentiation. For gene expression analyses, we used qPCR to measure mRNA levels of *Runx2*, a transcription factor which drives osteogenesis, and *Col1*, the most abundant protein in bone matrix, via qPCR (Fig. 7E, G). In both control quail and duck, a significant up-regulation of both *Runx2* ($p < 0.01$, $p < 0.05$) and *Col1* ($p < 0.01$, $p < 0.01$) mRNA took place between HH24 and HH27. However, in chimeric quack, this up-regulation took place three stages earlier, between HH21 and HH24 ($p < 0.01$; $p < 0.01$). A similar trend was confirmed visually, when we performed section *in situ* hybridization to detect *Runx2* and *Col1* mRNA expression. At HH24, *Runx2* and *Col1* mRNA are not yet expressed in either control quail or duck, however expression is very apparent by HH27 (data not shown). In quack, *Runx2* and *Col1* expression is apparent three stages earlier on the side containing quail NCM (visualized by Q ϕ PN staining), while not yet detected on the control side (Fig. 7D, F).

2C. Neural crest mesenchyme regulates cell cycle progression

2C i. Neural crest mesenchyme regulates proliferation at the G1/S checkpoint

At early stages of craniofacial development, the mandibular primordium is largely composed of highly proliferative mesenchyme. However, at the onset of osteogenesis, a subset of these mesenchymal cells take on osteoblast cell fates,

simultaneously increasing expression of genes that regulate and encode proteins for bone matrix synthesis, and decreasing proliferative capacity (Stein et al., 1996, Aubin et al., 1998). At the level of the cell cycle, the transition between proliferation to differentiation is regulated at a checkpoint between the G1 and S phases: At this checkpoint, G1 arrest allows further differentiation, while progression past G1 into S phase allows continued cell cycling and proliferation.

To examine the extent to which NCM regulates this developmental transition, we used several methods. First, rates of cell division were measured by BrdU incorporation in HH24 quack mandibles. Anti-BrdU staining showed less BrdU incorporation on quail donor side relative to duck host side, suggesting a premature decrease in proliferative capacity (Fig. 8B). Quantitative measurements demonstrated an approximately 40% decrease in the number of proliferating cells on quail donor side relative to duck host side in the same volume of mandible in quack ($p=0.0132$) (Fig. 8C).

We also monitored progression through the cell cycle from HH21 to HH27 quail, duck, and quack via propidium iodide incorporation (to label proliferating cells), and subsequent FACS sorting. To ascertain the ability of NCM to control progression past the G1/S checkpoint and thus control a developmental transition from proliferation to differentiation, we quantified the percentage of cells G1 phase, versus the percentage of those actively cycling in S, G2/M phases. (Fig. 8D) In quail and duck, there was a significant increase in G1-phase cells, along with the expected reciprocal decrease in S+G2/M-phase cells

between HH24 and HH27 ($p=0.003$, $p=0.049$). In quack, the increase in G1-phase cells occurred three stages earlier, between HH21 and HH24 ($p=0.029$).

2C ii. Neural crest mesenchyme modulates expression of cell cycle regulators

To identify mechanisms by which NCM regulates cell cycle, we monitored cyclin and CKI protein expression in quail, duck, and quack from HH24 to HH30, when mandibular mesenchyme first undergoes differentiation. Proteins analyzed included cyclin E, which is required for G1/S phase transition; cyclin B1, which is required for G2/M phase transition; and p27, a cyclin-dependent kinase inhibitor that decreases proliferation in a range of cell types including differentiating rat calvarial osteoblasts (Zavitz et al., 1997; Coats et al., 1996; Drissi et al., 1999).

Surveying control quail and duck, we found stage-, species-, and tissue-specific patterns of protein expression. In both species, protein levels of cyclin B1 decreased from HH24-HH30, though levels showed down-regulation earlier in quail ($p=0.0165$ HH24 to HH27; $p=0.0381$ HH27 to HH30) than duck (no statistically significant decrease HH24 to HH27; $p=0.030$ HH27 to HH30; Fig. 8G). Cyclin E expression also decreased in control duck ($p=0.0045$ HH24 to HH27; $p=0.0066$ HH27 to HH30; Fig. 8F). However, at all stages studied in quail, we detected almost no intact cyclin E, observing instead a large smear at a higher molecular weight like that resulting from post-translational modification, or cyclin E protein degradation (Doronkin, 2003).

Expression of *p27* mRNA rose steadily from HH21 to HH30 in both species, yet p27 protein expression remained relatively constant in duck, and

rose only marginally in quail during the same time frame (Fig. 8E). We also noted that a single isoform of p27 pre-dominated in the mandible at the time points studied, in contrast to the two isoforms detected in HH17 to HH31 chicken and duck frontonasal processes in a recent report (Powder et al., 2012).

In chimeric mandibles, the cyclin E, cyclin B1, and p27 expression patterns on the quail donor side were similar to control quail three stages older, and in the case of cyclin E ($p < 0.0001$) and cyclin B1 ($p < 0.041$), were significantly different than those of duck the duck host side (Fig. 8J-M).

2D. Transient, early over-expression of D-type cyclins accelerates osteogenic differentiation

To evaluate whether timing of osteogenic differentiation in NCM depends on cell cycle progression, we decided to modify timing of mesenchymal proliferation via transient, early over-expression of D-type cyclins in NCM.

D-type cyclins promote proliferation, and over-expression has been sufficient to alter timing of differentiation or cell fates in other systems (Lobjois et al., 2004). To map out when D-type cyclins are endogenously expressed in our model, we performed qPCR (data not shown) and Western blot (Fig. 9A) on quail mandibular mesenchyme, and found that cyclin D1 expression is relatively constant during the onset of osteoblast differentiation.

By electroporating a combination of bicistronic Cyclin D1/GFP and Cyclin D2/GFP constructs into HH8 quail, we were able to drive NCM expression of these genes throughout early development (Fig. 9B). GFP expression was

confirmed to be bright at HH18, much less so at HH21, and no longer visible by HH24, the time of collection (Fig. 9C). Using qPCR analysis, we found that during the period of active cyclin D1 over-expression at HH18, Runx2 levels were slightly lower on the treated than untreated side, and Col1 was not yet expressed at consistently detectable levels (Fig. 9D). Cyclin D1 had diluted to endogenous levels by HH24 (Fig. 9C), at which point Runx2 and Col1 showed 5-fold ($p=0.01$) and 1.4-fold (not statistically significant) increases in expression levels in treated versus controlled tissue, respectively (Fig. 9D). Thus, by over-expressing D-type cyclins well before osteogenesis would normally occur, we were able to drive early up-regulation of *Runx2*, closely mimicking the effect of quail donor NCM in a duck host (as shown previously in Fig. 7F, G).

2E. Runx2 levels affect mandible size

2E i. Continuous runx2 over-expression decreases overall mandible size

To understand the effects of premature *Runx2* up-regulation, as observed in our chimeric and cyclin D1/D2 over-expression experiments, we turned to RCAS, an avian retrovirus, as a tool to continuously over-express Runx2 (or GFP in control chick) starting from HH8.

RCAS-driven Runx2 over-expression was confirmed by *in situ* hybridization for a viral envelope gene (*env*) and *runx2* (Fig. 9E, F), and RCAS-GFP infection was confirmed visually by epifluorescence (data not shown). Evaluating gross morphology and skeletal preparations, we were able to see a decrease in the size of treated versus control mandibles at HH38, a phenotype

consistent with results previously observed in *Runx2* over-expression experiments from our lab (Eames et al., 2004; Fig. 9C). By examining earlier stages in development, we found this effect on size was already apparent by HH26, with severely decreased size of mandibular, frontonasal process, and maxillary primordia (data not shown).

2E ii. Endogenous *Runx2* levels during development correlate with species-specific mandible size

In considering the relationship between *Runx2* expression and mandible size, we decided to investigate endogenous *Runx2* expression in the small-beaked quail, versus the large-billed duck. We found that prior to the first instance of bone deposition in the mandible, differences in *Runx2* expression levels were not statistically different. However, as the skeletogenic program continued throughout development, the gap between quail and duck *Runx2* levels grew, resulting in quail *Runx2* levels more than double that of duck ($p=0.0143$; Fig. 9H).

2F. Discussion: Proposed Mechanisms by Which NCM controls size of facial elements

Our results demonstrate that NCM establishes the timing of bone formation and does so by autonomously executing molecular and cellular programs for osteogenesis. Following transplantation, quail donor mesenchyme maintains its faster timetable for molecular and cellular programs of osteogenesis within the slower environment of the duck host, which is consistent with that

observed in previous experiments (Noden, 1983; Merrill et al., 2007). Further, NCM closely regulates cell cycle progression in a stage- and species-specific manner.

One of the striking species-specific differences in cell cycle regulation between species was expression of cyclin E in the mandible. Quail mandibles consistently showed heavy cyclin E post-translational modification at all stages studied, in stark contrast to a single dominant cyclin E band in duck samples at all stages examined. Given the strong conservation of the cyclins between species (e.g. cytosol from arrested mammalian cells drives *Xenopus* oocyte maturation; Adlakha et al., 1983), we did not predict such a distinctive difference in regulation within the same Class. However, these cell regulatory differences may have great impact on species-specific adaptive evolution, whereby lower levels of functional cyclin E may be a mechanism by which quail dampens mesenchymal proliferation, to form a faster-developing, and ultimately, smaller beak. From our studies, species-specific cell cycle regulation also appears to be linked to size through p27 up-regulation in quail during osteogenic differentiation (versus no apparent change in duck at the same stages), and an earlier decline in cyclin B1.

Already in the literature are studies correlating p27 and size. Perhaps the most telling is a study of p27-deficient mice, which finds them significantly larger than their wild-type littermates, yet with no overt defects in skeletal development (Drissi et al., 1999). Perhaps in duck versus quail, mandibular tissues are able to grow larger as well, with skeletal elements scaling up, supporting isometric

growth. In avians, it was also recently found that developing duck frontonasal processes (FNPs) have lower p27 levels than chick, although a possible connection to size was not discussed (Powder et al, 2012). Interestingly, in comparing the single isoform-dominated p27 expression pattern in our mandibular samples to the doublet pattern from FNP reported in the Powder paper, we also find what appears to be a tissue-specific p27 post-translational regulation, which has been previously described in other systems (Hirano et al., 2001; Zhang et al., 2005), and may be a mechanism for tissue-specific growth and allometric growth in general.

In addition to species-specific cell cycle regulation, we also find species-specific regulation of the osteogenic transcription factor, *Runx2*. As osteogenesis proceeds, the mandibular *Runx2* levels of the small-beaked quail rise to more than double those of the large-billed duck. Moreover, by over-expressing *Runx2* expression in chick, we are able to decrease jaw size. Although correlations have been drawn between predicted *Runx2* expression levels and jaw length in adult dogs and Carnivora (Fondon and Garner 2004; Sears et al., 2007), to our knowledge this is the first study that presents a functional connection in an *in vivo* model, and traces size differences back to developmental origins.

Although we can say that NCM controls timing of osteogenesis *and* cell cycle progression, in reality, these two processes are tightly interwoven. This is highlighted by our experiments in which we over-expressed D-type cyclins to manipulate cell cycle progression, which resulted in dramatic early up-regulation of *runx2*. It has previously been shown *in vitro* that *Runx2* can both respond to

and modulate cell cycle progression. For example, levels of Runx2 mRNA and protein levels increase with entry into G1 arrest due to cell density dynamics or serum starvation, but it can also promote cell cycle exit through direct and indirect mechanisms, including repressing rRNA synthesis, and up-regulating p27 expression (Young et al., 2007; Galindo et al. 2005; Thomas et al., 2004; Pratap et al., 2003). Further, calvarial osteoblasts from Runx2-deficient mice have diminished stringency of cell growth control, but this defect is rescued by re-introduction of exogenous Runx2 (Galindo et al., 2003).

Connections between proliferative capacity, differentiation, and ultimately, size of skeletal elements can be examined in the context of a critical phase of osteogenesis: condensation. Osteogenic condensations are composed of pre-osteoblastic mesenchymal cells, densely packed among glycoprotein-rich ECM facilitating local osteogenic signaling necessary for differentiation. Thus, in order to proceed to bone formation, numbers of pre-osteoblasts must reach critical condensation size (Dunlop and Hall, 1995, Hall and Miyake, 2000), much the way *in vitro* bone formation assays are not performed until plated cells have reached confluency (Orriss et al., 2012), which may be related to the fact that in cell culture conditions, simple contact inhibition and serum starvation may be responsible for up-regulation of Runx2 mRNA and protein, up-regulation of p27, and decreased levels of cyclins and cdks needed for cell cycle progression. It seems more likely that osteoblastic populations can monitor a scarcity of certain growth factors or signals to drive differentiation since blocking osteogenic cell surfaces with heparin treatment can mimic the effects of serum starvation (Pratap

et al., 2003). Variations in condensation shape, size, and location, are all sources of morphological variation in development and evolution (Atchley and Hall, 1991; Dunlop and Hall, 1995; Ettinger and Doljanski, 1992; Smith and Hall, 1999; Hall and Miyake, 2000). Therefore, our data can be understood to incorporate several possible ways by which NCM controls species-specific timing of osteogenesis and jaw size.

1. Migration effect / Starting population size. Quail and duck may have different starting numbers of NCM, and/or migration may concentrate cell numbers in different species-specific locations. This is supported by the fact that quail NCM maintains species-specific size and shape of jaw elements.
2. Early condensation (quail model). In our D-type cyclin gain-of-function model, by providing signals to drive cell cycle progression, areas that normally have sparse pre-osteoblast populations reach threshold of condensation earlier, thus driving earlier differentiation. Earlier osteoblast commitment reduces numbers of proliferative cells, leading to smaller overall mandible size.
3. Continued slow proliferation plus expansion (duck model). When comparing quail and duck cell cycle regulation, we find that quail suppresses proliferative signals, and shows more dramatic signs of cell cycle exit. In contrast, the duck supports continued growth along with continued differentiation, resulting in larger overall mandible size.

4. Intrinsic differences in response to growth and differentiation signals. Even in the same organism, it has been shown that condensations from different anatomical structures (e.g. wing versus leg) can maintain distinct cellular morphologies and have differential responses to TGF-beta signaling, resulting in different condensation sizes. (Downie and Newman, 1995)
5. Interaction of osteogenic genes with species-specific expression patterns of homeobox transcription factors. For example, *Hoxa2* is known to downregulate *runx2* signaling to cause overproliferation of mesenchymal cells, create additional sites of condensation and result in ectopic cartilage formation (Rijlie et al 1994; Kanzler, 1998; Smith and Schneider, 1998).

In all likelihood, all of these factors play a role in providing NCM with the ability to autonomously regulate cell cycle progression and timing of osteogenic differentiation. We now show that, in line with previously published *in vitro* data, cell cycle and osteogenesis are inexorably linked *in vivo*. The ability of NCM to control and coordinate shifts in timing to both processes, combined with a generally permissive environment provided by surrounding non-NCM derived tissues, such as vasculature, may lend a particular plasticity to the evolution of craniofacial shape and size.

Chapter 3. Evolvability in the Craniofacial Complex

3a. Debates on Evolvability

3a i. What is Evolvability?

It is impossible to deny that evolvability exists, since it is simply defined as: “the capacity to generate heritable, selectable phenotypic variation” (Gerhart and Kirschner, 1998) or in slightly different wording, “the ability of random variations to sometimes produce improvement” (Wagner and Altenberg, 1996). That is, it is a word meant to encompass the roots of evolutionary capacity. Inevitably, however, when we reflect upon the application of this term, we begin to ask, “What constitutes evolvability? What generates or provides variation? What allows, versus what hinders, evolution?” We start to use it to represent more complex genetic and organismal properties – and this is when we run into some very difficult conceptual problems.

To prevent this dissertation from getting trapped in a similar quagmire, after we have dedicated considerable time to discussing the generation of variation, the context of evolvability demands an important re-framing, surrounding two key questions that we are greeted with frequently in biology: “How?” and “So what?” That is, how is variation constantly available for selection to draw on? Up to this point, I have only mentioned places where biological processes *have the potential* to vary. And what do so many variations contribute to actual evolution and speciation, where I have so far only suggested that the accumulation of variation vaguely *leads to more profound changes?*

3a ii. Laws of Variation

Questions surrounding the elemental basis of evolvability have been a source of consideration since Darwin first conceived of evolutionary theory. Even though Darwin himself based Origin of Species on inheritance of variation and natural selection, he admitted, “our ignorance of the laws of variation is profound” (1859). However, even in this phrase, he names an important possibility: that there may be indeed laws, or at least logic, behind mechanisms underlying organic change and the generation of living forms. This idea in itself echoes the tradition of thinking of Rational Morphologists such as Wolfgang von Goethe, Georges Cuvier, and Geoffroy Saint-Hilaire, who sought to understand how fixed elements are recurrently deployed in different organisms (Kaufmann, 1993).

Although Darwinian schools of thought at times clashed sharply with those of contemporaries such as Sir Richard Owen, by examining specific examples of contention we are able to come upon some resolution and synthesis of their meaning in terms of modern biology. Let us start with the examinations of vertebrate limb homology, which was investigated first by Saint-Hilaire, who espoused the presence of homologous forms as the basis of his *principe des connexions* (Takechi and Kuratani, 2010). Saint-Hilaire, and later Owen, believed that vertebrate limbs could be considered equivalent, ordered members of a group or series, which could be transformed between each other by changes in a few characters (Kaufmann, 1993).

We now know that dramatic transformations through single-step mutations in the genome are actually plausible – extending to even more anatomical elements than only the limb. In the most famous example, the *Drosophila Antennapedia* mutant grows legs in the place of its antenna (reviewed in Carroll, 1995; Fig. 10A, B). Similarly, limb branches characteristic of posterior body segments can be shifted anteriorly to form feeding apparatuses when the Hox code is altered in the crustacean *Parhyale* (Pavlopoulos et al, 2009).

In studying other systems, such as the evolution of the mammalian middle ear, we find a textbook example of how homologous structures with fixed relations can indeed be co-opted for different functions (Fig. 10C). Reptiles and avians have only one bone, the columella auris, to connect the eardrum to the inner ear, which corresponds to the mammalian stapes. However, the mammalian ear also includes a malleus (“hammer”), which is homologous to a posterior portion of the articular bone of the lower jaw, and the incus (“anvil”), which is homologous to a portion of the quadrate of the jaw joint. These evolutionary changes were complemented by an extension of the mammalian jaw’s dentary bone to complete the functions of a jaw joint (Allin, 1975; Takechi and Kuratani, 2010). Although we cannot be sure of how these evolutionary changes actually took place, several gene knockout models in mice have suggested ways in which ectopic cartilages could form, mimicking primitive forms and components of reptilian and avian jaws (Chisaka et al., 1992; Gendron-Maguire, 1993; Yamada et al., 1995; Qiu et al., 1995).

Indeed, the laws of form, which at first glance can seem insufficient for explaining biological complexity, are taken as a matter of fact in so many other fields, such as crystallography (an example that is given in Kaufmann, 1993), electrical circuitry, or wave physics. In these fields, the combinations of a few known forms are capable of generating an immense array of complex morphologies. Thus, as we gain knowledge in seeing the relevance between the previously shunned theories (as Lamarckian epigenetics once was), we can no longer afford to be so black and white, going along with old beliefs that these other ideas are *anti-Darwinian*. As Michael Conrad stated in a very peppery (but, extremely incisive) essay in 1990, "...so far as evolvability is concerned, the contrary structuralist view is **just** as Darwinian, if not **twice** as Darwinian" [emphasis mine].

What then, are the modern structuralist principles of evolutionary adaptability? Conrad provides visuals for the beautiful conceptual landscape that was first brought to our collective consciousness by Wright (1932) and Fisher (1934). In a summary and slight re-interpretation, Conrad proposes the "Geometry of Evolution" based on two simple assumptions. (1) That structures are mostly stable under the current conditions – these structures can be imagined in a 3-D model as sitting in low energy basins where rising out of the basins is more difficult depending on the depth of the basin (Fig. 10D). (2) Each structure confers a certain level of fitness in the current conditions – this can be imagined in a separate model, a linear graph whereby each structure is a peak, the height of the peak correlating to the amount of fitness the structure confers,

and distance between peaks denotes how different structures are from each other (Fig. 10E). However, in the set up of this model is an inherent difficulty: i.e., the character basins are stable, meaning they resist change, but the fitness peaks are separated, and genetic variability is required for any kind of travel between them. Conrad resolves this by positing that in order for evolution to occur, “biological structures must be characterized by a high degree of component redundancy and multiple weak interactions (1990).” He clarifies that this is possible if the genetics of each structure are unstable, but physiological structures themselves are quite stable under a variety of conditions. Then, in order for a structure to change, and “move from one fit position on the landscape to another there must be a 'smooth' connecting path. This means a path that can be traversed in single steps... peaks have to be densely packed or connected in at least one dimension,” presumably through incremental, non-detrimental change. In **Chapter 3b**, I shall propose genetic mechanisms that may provide these “smooth connecting paths.” First, however, let us turn to the stable structures at each fitness peak, since the existence of stable structures (in stable organisms) also implies stable populations, which may seem at odds with providing variation required for evolution.

3a iii. Variation in Stable Populations

How is variability maintained in a population? Kauffman (1993) describes two viewpoints: that of Neutralists, who believe that spontaneously generated mutations are passively retained in a population through random drift as well as continuous fixation and loss (Kimura, 1968); and that of Selectionists, who

believe that heterozygote genotypes may confer phenotypic advantages, and as a result, are actively selected for. Of course, we do know of some examples where the latter holds true, e.g. the locus at which homozygosity can cause sickle cell anemia or malaria susceptibility, whereas heterozygosity leads to resistance to malaria (reviewed by Ashley-Koch et al., 2000). However, it is quite a bit more difficult to know when mutations are truly neutral. Even some of the early model examples proposed in 1968 of non-harmful mutations, e.g. intronic amino acid changes, are now recognized to have potential effects on gene and protein regulation. In any case, I do not discount the contribution of either *some* neutral changes, and *some* advantageous heterozygosities to the generation of variation, but I shall bring our attention to what I consider a critical property of populations that is not addressed by the two theories: simply, the fact that populations are not isolated.

3a iv. Population Mixing

What defines a population, and why do we consider them stable or unstable? Our model organisms certainly seem close to stable, in that we keep them in controlled environments for many generations, but then, these systems are terribly inbred by our own hand, and as such, it is difficult to entertain any suppositions about what maintains their variation.

Let us imagine instead one wild population that is separate from another, as with two different species. Surely then, we can consider each species to be an isolated population, because they cannot interbreed? Unfortunately not – the

myth of the impossibility of breeding between species or of producing fertile offspring a common misinterpretation of Ernst Mayr's biological species concept, published in 1942, which states: "Species are groups of actually or potentially interbreeding populations that are reproductively isolated from other such groups." It is not a fixed, intrinsic property of any species group, but rather an informed snapshot of the often dynamic amount of inter-breeding that is currently active between two groups, where inter-breeding can be prevented by offspring viability, physical constraints, or sexual selection, certainly, but also spatial distribution, mating season, offspring diet, and more. Not only can the relationships between two species populations change over time in response to alterations in seasonal weather, invasion of habitats, expansion of habitats, etc., but the human observers who classify species as separate, reproductively isolated populations may not be fully informed about the extent of interbreeding. It is easy to imagine that the extent of interbreeding may be especially hard to keep track of in some organisms, such as avians, which are capable of flight and widespread migration. In The Birder's Handbook, we have this example:

"... the western populations of the Yellow-rumped Warbler (which have yellow throats) were previously considered a species, Audubon's Warbler, distinct from the eastern Myrtle Warblers (which have white throats), largely because of differences in appearance. Then it was discovered that the breeding ranges of Audubon's and Myrtle Warblers overlap broadly in a band from southeastern Alaska through central British Columbia to

southern Alberta, and that the two 'species' hybridize freely within this area' (Erlich et al., 1988).

Furthermore, Erlich et al., continue on to say that some populations (i.e. Red-breasted Sapsuckers and Yellow-bellied Sapsuckers) hybridize where they meet in certain geographical locations, but not others. Although the nomenclature and classification become very cloudy, another point becomes clear: intermixing brings new traits and diversity to more populations than we often take into consideration.

3a v. Re-interpreting the Framework

When we acknowledge that almost no natural populations in which we study variation and evolution are truly isolated, we can see stabilization (Schmalhausen, 1949), introduction of variation, and selective selection as cyclical processes of organic movement and change. Thus, neutral evolution or heterozygote selection may have less of an impact on maintenance of variation than sporadic inter-mixing. For example, if we follow two populations composed of mixed species, sub-species, or even regional breeds, we might see a cycle proceed as:

- One population is temporarily isolated from another, under relatively constant environmental conditions, and each population undergoes adaptive, then stabilizing selection. Phenotypic variation is lost to some degree, but some mix of distinct genotypes is still maintained.
- As populations intersect, less common genetic variants are increased in

number, or more rarely, new variants are introduced, thus changing proportions of different genetic combinations (haplotypes). Naturally, this decreases fitness in some offspring compared to the better-adapted parental generation, although it may increase fitness in a small minority.

- As environmental conditions change, new haplotypes may be selected for, and may flood the gene pool of one population or the other.
- The populations may part ways again, now with more diverse haplotypes.

Of course, these processes could occur in a number of ways. The population intersection itself could be a result of change in environmental condition, which adds selective pressure. This has been the case with Barred Owls and Northern Spotted Owls, which are mixing in unfamiliar lands due to deforestation, giving rise to “spurred owls” (Dugger et al., 2011). Another possibility is that more than one population could potentially intermix, as with the coyote, red wolf, gray wolf, and Great Lakes wolf (Von Holdt et al., 2011). Migration routes can change, directing populations to new breeding grounds where food may be more abundant, as with the Serin, a relative of the canary, whose migration routes and expansion from the Mediterranean region to central Europe was studied by Mayr for his doctorate (Berthold, 1999), etc.

Importantly, it has been recently shown that genetic mixing, followed by enrichment of genotypes contributing fitness advantage, is sufficient to create new, hardy, adaptive genotypes. In a study examining sunflower hybridization, Rieseberg et al. traced the lineages of both wild and synthetic heritage varieties, and found offspring adapted to soil, weather, and nutrient conditions very

different than those adapted to by parental generations, but that new offspring genotype combinations could be directly accounted for from parental genetic variation (2003). This principle was also confirmed and corroborated by Cypionka et al., in studies of two species of sculpin, a type of freshwater fish, as well as a natural hybrid, termed the “invasive sculpin” for obvious reasons (2012). Moreover, studies in stickleback populations have led researchers to believe that the majority of mutations useful for adaptation pre-exist in sticklebacks globally (although concentrated in some groups locally) and that these mutations are transferred through hybridization of divergent freshwater and saltwater forms at coastal rivers, far more often than they arise *de novo* (Jones et al., 2012).

Though we might, for a moment, be satisfied with population mixing as a source of variation, we would invariably run into the next logical question: where does the variation *between* populations come from? Thus, in the next section, I describe a major source of genetic mutability often tied to phenotypes that can readily undergo selection (fulfilling both of Conrad’s conditions in his Geometry model): tandem repeats in the DNA sequence.

3b. Biological Relevance of Tandem Repeats

Tandem repeat regions have the fascinating potential to act as a strong mediator of evolutionary modifications. Mutation rates via slipped-strand mispriming in tandem repeat regions occur up to 10,000x more frequently than single base pair point mutations. In addition, mutations are reversible and can create a range of quantitative changes from small (e.g., the addition of a few

repeats) to large (e.g., the duplication of an entire repeat region), resulting in subtle or drastic morphological changes (Kashi and King, 2006). Small changes, in particular, may contribute to creating a “smooth connecting path” that allows evolution between fitness peaks in the Conrad model, while large-effect changes may be risky, but still useful when a structure necessary for fitness is far from optimized (Orr, 1998). Furthermore, based on the size and integrity of the repeats, the likelihood that mutations will occur in the next replicative iteration (i.e., the mutability) can determine level of stability (Kashi and King, 2006).

Tandem repeats are found in an enormous number of DNA transcription factors, and can have activating, repressing, or neutral effects on gene transcription. In one of the first studies on tandem repeat function, it was found that proline or glutamine repeat domains could increase *in vitro* transcription when fused to the binding domain of GAL4, and that the increase in transcription correlated to the number of repeats (Gerber et al., 1994). Since then, tandem repeats have also been shown to play a role in affecting basal transcription machinery (i.e., the transcription factors, RNA Polymerase II subunits and polypeptides that directly bind promoter DNA at the TATA box). For example, Dr1, a negative regulator of basal transcription has a glutamine- and alanine-rich domain, which can repress transcription at promoter sites by directly binding the TATA binding protein (Yeung et al., 1997).

The biological significance of tandem repeats has also been reported in several classic developmental processes, including polarity patterning in *Drosophila*. Normally, at the anterior pole of the embryo, the transcriptional

activity of the morphogen Bicoid is down-regulated by Torso. However, it turns out that Bicoid actually possesses three autonomous activation domains, where two of them are serine/threonine-rich and down-regulated by Torso, while the third domain is glutamine-rich and is insensitive to Torso. A separate alanine-rich domain can also repress activity through a non-Torso dependent pathway (Janody et al., 2001), offering multiple, highly mutable sites allowing modulation of Torso regulation.

3C. Correlations Between Tandem Repeats in Runx2 and Craniofacial Proportions

Runx2 transcript levels, protein levels, and activity, are controlled by a variety of mechanisms, including HDACs, phosphorylation, acetylation, co-factors, and other transcription factors, as reviewed in **Chapter 1D**. Although evolution has occurred at many of these DNA and protein interaction sites, one DNA sequence site in particular has been shown to undergo enormous change is a tandem repeat region composed of multiple glutamines (Q) followed by multiple alanines (A) at the 5' end of the exonic transcript, where it overlaps with the HDAC4 binding domain. The Q/A domain, along with the first 19 N-terminal amino acids specific to Runx2 among the Runt family, was initially described as an activation domain (Thirunavukkarasu et al., 1998). Recently, it has been found that higher Q:A ratios are correlated with higher Runx2 basal transcription levels, and lower Q:A ratios are correlated with lower Runx2 basal transcription levels *in vitro* (Sears et al., 2007).

Sequence differences in a Glu-Ala tandem repeat region of the *Runx2* gene have been found to correlate to variation in rostrum length of adult dogs and other Carnivora (Fondon and Garner, 2004; Sears et al., 2007). The current interpretation of these findings rely on the *in vitro* data: it is believed that the higher the Q:A ratio in the repeat region, the higher *Runx2* expression, and the shorter the rostrum (Sears et al., 2007). It has also been noted by Fondon and Garner that dogs with low Q:A ratios seem to phenocopy humans with *Runx2* haploinsufficiency, supporting the idea that low Q:A ratios are linked to low *Runx2* expression (2004). Furthermore, a mild form of CCD, usually linked to a loss-of-function mutation in a *Runx2*, has been discovered in a family with a ten alanine expansion in the tandem repeat region, also implying that the length, or at least proportion, of alanines in the sequence has a repressive effect on *Runx2* transcription (Mundlos et al., 1997).

Interestingly, Fondon and Garner reported that *Runx2* Q:A ratio was not correlated to jaw length alone, but also dorso-lateral flare, and dorso-ventral nose bend, which are both variables associated with dorsal mid-facial growth. In our retroviral *Runx2* over-expression studies, we saw similar phenotypes of bending, length, and shape changes (Fig. 11B-E). In the context of our findings that *Runx2* levels are intimately tied to cell cycle regulation *in vivo* (**Chapter 2**), it seems possible that the shorter, narrower, and downward-bent rostrum of both models could be tied to a smaller or less proliferative mesenchymal cell population, and a lesser amount of tissue under the same physical (musculoskeletal) forces and connective relationships in the jaw, could cause the deformation of the normally

straighter jaw line.

Also of note is that early this year, Pointer et al. surveyed placental mammals and found no correlation between tandem repeats and rostrum length or between tandem repeats and any of several other craniofacial measurements (2012). However, it must be clarified that correlation between Q:A and facial length had not been found equivalent across mammals, even in previous studies. That is, although Fondon and Garner found Q:A ratio and facial length to be strongly correlated across 92 breeds of dogs, when Sears et al. examined 30 species of Carnivorans, they found the correlation was stronger among Caniforms (e.g. dogs, bears, raccoons), than Feliforms (e.g., cats, civets, and mongooses). The authors attributed this difference to the fact that Caniforms show more positive allometry during growth than in Feliforms, with preferential dorso-ventral expansion of the rostrum, compared to the braincase, for example (Fig. 11F). Thus, the argument seems to be that Runx2 Q:A and transcript levels are tied more strongly to facial morphologies that change dramatically during early life. If this is the case, perhaps we can expand this mode of thinking to avians.

In all mammals, neonatal rostral length is constrained by the requirement to latch for feeding, and nearly all dorso-ventral expansion of the rostrum occurs postnatally. In contrast, many bird species must be able to feed as soon as they are hatched. These species are easily identified, since ornithologists have traditionally sorted birds into two broad categories based on developmental maturity at hatching: altricial and precocial. Altricial birds usually lack the ability to

thermo-regulate or feed on their own when first hatched. A classic example is the nearly naked little sparrow fledgling, which chirps loudly in the nest, expectant for the return of its mother. However, precocial birds such as quail and duck begin to peck for seed or sieve pond silt for insects on their first day out of the shell. For this reason, their rostrum must be developed for either the adult diet, or a precursor juvenile diet, which usually demands roughly the same mechanical requirements. Thus, much of the allometric growth of the face and jaw must take place before hatching.

In addition to the requirement for allometric establishment of functional feeding apparatus *in ovo*, there may be another mechanism that tightens the correlation of Q:A ratio and adaptive craniofacial morphologies: constraints of flight. It has been recently argued that feeding mechanisms in bats are under strong pressure to minimize mass and maximize functional performance. Thus, a selection signature would be “more apparent...where the penalty is larger for being overbuilt” (Dumont, 2007). Along the same line of reasoning, there may be less noise caused by non-functional variation in jaw length among birds of flight that might otherwise frustrate our ability to draw correlations to Q:A ratios. In other words, if Q:A ratios are truly strong regulators of jaw length, then avians cannot afford to have Q:A ratios that would conflict with optimal morphology, and correlations should be very tight. In the following section, I review my findings resulting from my re-examinations of the relationships between Q:A ratios and jaw length using a cross-avian model.

3D. Survey and Implications of Runx2 Tandem Repeats in Avians

The bulk of the *Runx2* DNA sequence is remarkably conserved. With the exception of the Q/A tandem repeat region, and the variable presence of a 20 AA mid-sequence insertion, chick *Runx2* differs from mouse *Runx2* by only seven amino acids. In fact, in a survey of mouse, rat, human, chick, and xenopus *Runx2*, there are only eleven total AA discrepancies in the entire 450 AA sequence, outside of the repeat and insertion domains. On the other hand, the number of repeats at the Q/A region varies widely between organisms, as we have seen, and this is also the case among avian species. Here, I present the first survey of Runx2 Q:A ratios in avians, from my own sequence analyses as well as published NCBI sequences (Fig. 11A and Table 1).

Table 1. *Runx2* Q:A ratios in avian species

Species	Q Repeats	A Repeats	Q:A Ratio
Quail	12	1	12
Chick (NCBI)	12	2	6
Duck	17	4	4.2
Zebrafinch (NCBI)	11	4	2.7
White-Throated Sparrow (NCBI)	10	4	2.5

The first *Runx2* tandem repeat regions I sequenced were those of quail and duck. In these birds, I found a Q:A ratio of 12.0, 6.0, and 4.2, respectively. According to previous data from dogs, *in vitro* transcription, and other Carnivora, a higher Q:A ratio would imply a higher level of *Runx2* expression. By performing

qRT-PCR on quail and duck tissue, we found that this was indeed the case. After osteogenesis had begun, until hatching, average *Runx2* levels in quail were more than three times that of duck. Further, by late development, when expansion of the jaw was proceeding rapidly, *Runx2* levels in quail reached nearly four times that of duck. Also in line with Canid and Carnivoran models, the level of *Runx2* correlated to the length of the jaw, and possibly also the shape of the face. Our retroviral *Runx2* and electroporated *Cyclin D1/D2* over-expression experiments in **Chapter 2C** suggest that these correlations are glimpses of a functional connection between cell cycle and bone patterning.

As I continued to survey avian species, however, I began to see a very different pattern emerge. *Runx2* Q:A ratios seemed more likely to be correlated to the proportions of jaw length to cranial size at hatching (Fig. 12). A lower Q:A ratio presumably led to lower *Runx2* expression, and thus a relatively larger beak compared to total cranial size. This could make sense in the context that decreased *Runx2* expression could allow increased cell proliferation. It is also possible from our findings regarding species- and tissue- specific cell cycle regulation that the non-NCM derived tissues are able to respond to levels of *Runx2* differently than the NCM-derived jaw elements.

Interestingly, Q:A repeats and the relative size of the jaw, was also tied to where the birds fell on the precocial-altricial spectrum. It has been noted that in altricial birds, which depend completely and directly on maternal feeding upon hatching, compete with their siblings in the nest by opening their beaks widely to beg for food. Fierce direct competition (e.g. scarce food conditions) can lead to

increased growth of the beak to allow wider jaw openings, larger jaws, and brightening of oral coloration, in a characteristic known collectively as “gape” in a bid for maternal attention, compared to the slower growth rates observed when food, nutrition, and maternal attention are abundant (Gil et al., 2008; Soler et al., 2010).

It is a tantalizing possibility that changes in nutrition and metabolic signaling pathways could alter cell cycle signaling to promote slow sustained growth (as we have called the “duck model” in **Chapter 2F**) or fast differentiation (“quail model”), in turn affecting jaw morphologies and modulating adaptive function. Undoubtedly one of the strongest selective forces in evolution is that of feeding and energy requirements, which are necessary for promoting fitness, strength, and presentation for sexual selection, including a multitude of displays such as bright colors, glossy fur, dances, songs, fighting, hunting and gifting, etc. Furthermore, starvation or near-starvation quickly shifts an organism’s energy balance to self-maintenance, usually at the cost of short- or long-term growth and reproductive capacity. In some animals, entering reproductive diapause is a normal part of the life cycle as food availability varies across the seasons and years (e.g. in caribou, mice, *C. elegans*, etc.; Cameron, 1994; Lopes et al., 2004; Padilla et al., 2012), and many other animals simply enter dormancy or hibernation (reviewed in Wang et al., 2006). By removing individuals or populations from activity and breeding, we can again see a factor that may contribute to selection in evolution. Still, there is yet another evolutionarily relevant component of the response to low food supplies that occurs at the level

of gene regulation – a combination of consequences of, and defense mechanisms against, the oxidative and ER stress that inevitably results from starvation conditions (e.g, Morales et al., 2004).

In one striking study, authors find that oxidative stress alone may globally affect transcription factor expression through SIRT family proteins and homologs, which have been implicated in age-related disease and DNA changes (Oberdoerffer et al., 2008). Loss of SIRT family proteins and homologs has been shown to lead to decreased DNA repair and increased mutation rates, while gain-of-function mutations lead to increased cellular replicative lifespan, implying perhaps, that when nutritional conditions are good and fitness is high, cell growth and strength are favored, while when nutritional conditions are extremely poor, mutations are favored. Of course, in the latter case, this may be a negative consequence of starvation, not necessarily an adaptive germ line response that we might like to suppose would contribute to genetic variation and adaptation in the next generation.

SIRT-1 in particular can directly bind and silence expression at tandem repeats, which exist at coding and non-coding regulatory regions of many transcription factors. However, oxidative damage can decrease the direct interaction between SIRT-1 and repeat regions, causing transcriptional deregulation (Oberdoerffer et al., 2008). Again, this may be an individual's survival mechanism, an unintended negative consequence, or a glimpse at yet another way in which repeat regions may be useful in generating adaptive responses, especially when considering that these regulatory events often occur during

ontogenesis to generate adult morphological variants. Certainly, it would not be a stretch to consider that nutrition affects morphology epigenetically: consider the canonical example of camouflaged, reticent grasshoppers whose offspring morph into aggressive, brightly colored locust swarms when food resources are patchy (reviewed in Burrow et al., 2011).

Is it possible that under environmental stress, some creatures arrest their whole metabolism, development, and growth; some arrest only cell cycle in key tissues to drive rapid tissue differentiation and maturation to adulthood, and in all creatures, if the stress is severe enough, the DNA becomes mutation-prone or undergoes epigenetic changes? And that on the other side of the coin, during periods of nutritional abundance or decreased competition, organisms have the luxury of growing slowly, to a larger size, with their DNA remaining largely intact? The last point especially, I realize, hints at the existence of *selection of evolvability*, a hotly debated topic that I shall not enter into for the purposes of this dissertation (instead, see Kirschner and Gerhart, 1998). Let me say instead that the above may be an oversimplification, but given our ability to synthesize data in the literature surrounding metabolism, cell cycle, tissue differentiation, mutation rate, it would be blind to ignore the possible connections.

As a case in point, let us survey organisms back in Aves, our model Class. Since at least the early 1940s, the growth rates of more than 100 birds have been described mathematically, along with their feeding habits, developmental characters at hatching, brood sizes, and more. Based on these data, ornithologist and evolutionary biologist Robert Ricklefs noted a strong correlation between

body size and growth rate, suggesting an interaction between the two outcomes (1968). He further postulated that these outcomes were modulated by three factors:

1. Interactions between physiology and growth. Links between basal metabolism, caloric use, and allometric growth have already been described as far back as 1961 by King and Farner.
2. Adaptions to direct selective pressures, such as predation. Ricklefs provides the comparison of heavily predated-upon hole-nesting species, such as passerines, which develop quickly and hatch small, versus the generally more carefree open-nesting species, which grow more slowly, resulting in larger young (Lack, 1948).
3. The chance to increase numbers of viable offspring via brood size. If there is enough food availability to meet the energy requirements of more young, brood size should be maximized, evolutionarily, for more chances at contributing to the gene pool of the next generation. However, if food availability is too scarce even to support one offspring very easily, energy budgeting may require that offspring develop quite slowly (Lack, 1948).

One particularly interesting set of examples of avians in energetically-limiting environmental conditions are seabirds, extensively studied by Ricklefs throughout his career. Many seabirds scour their habitats for scarce food

resources and lay only a single small brood of a maximum of three eggs each year. In an extreme example, the frigate-bird may lay only a single egg every two years, underlining importance of energy budgeting for offspring. This scarcity of resources, along with a relative lack of predators at sea, likely contributes to a developmental timeline that is uncommon in mammals and nearly unheard of in avians: after hatching, immature frigate-bird fledglings take over a year to develop under unflagging parental care (1968).

Observations like those made in the frigate-bird led Ricklefs to predict that it should be possible to correlate rate of growth with external danger and energy availability. Indeed, when we plot the growth rates and adult weights of 118 bird species originally surveyed by Ricklefs (1968) onto a graph, we can see that the vast majority of points fall along a curve whereby incremental increases in growth rate are correlated to exponential increases in adult weight ($y = -0.078 \ln(x) + 0.6783$; $R^2 = 0.56$; Fig. 13A). Notably, the frigate-bird falls far from the curve, making the lowest growth-rate point on the graph, but it is only one of several fascinating divergences. Some of the others are wrens, which are a family of very small passerines; the glittering-throated hummingbird, with an extremely high metabolism, a diet heavily reliant on nutrient-poor nectar supplemented with insects, and the ability to enter a state of hypothermic torpor (similar to hibernation; Carpenter, 1974); and a fast-growing nest parasite, the brown-headed cowbird, and its many host nestling competitors (Remes, 2006).

These interesting cases seem to further support Ricklefs' idea that it should be possible to correlate rate of growth with external danger and energy

availability. However, an addendum that I would like to put forth is that we should also be able to correlate metabolic inputs to global changes to cell cycle regulation as well as tissue-specific growth responses caused by transcription factor variation. Moreover, mutations in labile DNA regions over evolutionary time have likely contributed to the hugely variable gene pool that allows selection in the face to take place at a rapid pace. In combination, these metabolism/cell cycle/mutability relationships may have been necessary in order to regulate feeding apparatuses in response to metabolic signaling inputs that have their basis in organismal fitness and ability to acquire nutritional resources.

3E. Mutation-prone sequences in other transcription factors involved in craniofacial patterning

Mutation-prone regions are ubiquitous in living forms. The type that we have been referring to as tandem repeats, are also known as simple-sequence repeats, or microsatellites. These can be composed of di-nucleotide or tri-nucleotide sequences, and although some sequences are more common in certain organisms than others, they have been detected in all species examined so far. Triplet repeats are very common in transcription factors, where the majority lie in non-coding regulatory regions, and a small portion lie in the coding region itself (reviewed in Kashi and King, 2006).

To probe the extent to which genes involved in craniofacial patterning are mutable, and thus capable of driving rapid morphological changes, I surveyed a small, but essential subset. I found that transcription factor DNA was more often

labile than not, as I came across many microsatellite regions that had evidence of “slipped” mis-priming causing insertions, expansions, and contractions during replication, instability leading to chromosomal breaks, translocations, deletions, and inversions, and low binding affinity AT-rich regions.

Table 2. Mutability of genes involved in craniofacial patterning

Gene	Reference	Mutation-prone sequence	Found in	Role of gene in development and disease
<i>alx4</i>	Fondon and Garner, 2004	51 bp deletion in (PQ) _n microsatellite region	Dogs	Inhibits runx2, but necessary for skull osteogenesis. May be downstream of msx2 (Antonopoulou et al., 2004)
<i>bmp4</i>	Zhong et al 2010	(CA) _n dinucleotide microsatellite in 3' exon flanking region	Cows, humans, mice, sheep, goats	Cartilage development, facial patterning. Linked to holoprosencephaly, and in extreme cases, cyclopia. (Foppiano et al., 2007)
<i>dlx2</i>	Fondon and Garner, 2004	Tightly linked to HoxD cluster repeats, Combines with Hoxd8, Hoxd11, and Hoxd13 to form a minimum of 36 haplotypes	Dogs	First and second branchial arch identity (Qiu et al., 1995)
<i>foxc1/foxc2</i>	Lehmann et al., 2000	Deletion in (CCG) _n microsatellite region	Human	Skull formation, eye development (Zarbalis et al., 2007)
HoxA Cluster	Fondon and	Seven different repeat loci in	Dogs	Identity and homeotic transformations of the

	Garner, 2004	the Hox-a2, Hox-a7, and Hox-a11 genes combine for at least 28 distinct haplotypes		skull (Trainor et al., 2003)
<i>hoxa7</i>	Fondon and Garner, 2004	33 bp deletion in microsatellite region	Dogs	"
<i>hoxa13</i>	Reviewed in Brown and Brown, 2004	Expansion of 18 alanines to 24-26 alanines	Human	"
HoxD Cluster	Fondon and Garner, 2004	Eight repeats in the Hox-d8, Hox-d11, and Hox-d13 genes combine for a minimum of 30 haplotypes	Dogs	Identity in neck, vertebrae, base of skull (Condie and Capecchi, 1993)
<i>hoxd13</i>	Albrecht et al., 2004	Expansion of 15 alanines to 22-29 alanines	Human	"
<i>msx2</i>	Ott et al., 2012	Microduplications in upstream noncoding region	Human	Inhibits runx2, but necessary for skull osteogenesis. Hypomorphic alleles are linked to Cleidocranial Dysplasia (CCD).
<i>Phox2b</i>	Reviewed in Brown and Brown, 2004; Meguro et al., 2007	Expansion of 20 alanines to 25-29 alanines	Human	Associated with Congenital Hypoventilation Syndrome, marked by depressed autonomic response. Approximately 20% of all cases are comorbid with Hirschsprung's Disease, a rare defect of gut innervation,

				suggesting involvement with neural crest migration. Some cases of facial defects also reported (Croaker et al., 1998)
<i>pitx3</i>	Semina et al., 2000	652 bp deletion in microsatellite region	Zebrafish	Pituitary, lens, olfactory, and trigeminal placode development (Zilinski et al., 2005)
<i>runx2</i>	Albrecht et al., 2004	Glutamine repeats followed by alanine repeats in the <i>Runx2</i> coding region	Human	Necessary for osteogenic differentiation, Linked to CCD (Mundlos et al., 1997; Komori et al., 1997; Otto et al., 1997).
	Fondon and Garner, 2004; Sears et al., 2007; Pointer et al 2012	Insert of up to 45 bp in Q/A repeat region resulting in 18-20Q and 12-17A	Dogs	"
	Mundlos et al., 1997	Expansion of additional 10 alanines	Human	"
<i>satb2</i>	Fish et al., 2011 and NCBI gene	AT-Rich domain in <i>satb2</i> coding region	Human, Mice, Chick	Necessary for structural integration and size of jaw elements. Microdeletions can result in cleft lip and palate (Fish et al., 2011)
<i>six3</i>	Fondon and Garner, 2004	54 bp deletion in microsatellite region	Dogs	Represses <i>wnt1</i> and activates <i>shh</i> in the forebrain, associated with schizencephaly (Jeong et al., 2008;

<i>sox9</i>	Hill-Harfe et al., 2005	17 chromosomal breakpoints upstream of coding region, leading to translocation/inversion	Human	Hehr et al., 2010) Cartilage patterning (Eames and Schneider, 2008). Linked to Campomelic Dysplasia, as well as milder skeletal dysplasias (Hill-Harfe et al., 2005)
<i>tfap2a</i>	Lehmann et al., 2000	Functional proximity to foxc1/foxc2 (CCG) _n microsatellite region	Human	Neural crest survival and induction (Wang et al., 2011)
<i>twist1</i>	Kress et al., 2005	Trinucleotide insertion in polyglycine repeat region (GGC) ₅ GCG (GGC) ₅ ; in-frame deletions in the 5' DNA binding domain	Human	Represses Runx2 at DNA binding domain (Bialek et al., 2044). Linked to Saethre-Chotzen syndrome (Kress et al., 2005)
<i>zic2</i>	Brown et al., 2001	Expansion of alanine repeats	Human	Linked to holoprosencephaly (Brown et al., 2001)

At the conclusion of my search, I was surprised by how many transcription factors and their associated mutations were linked to human disease. This connection could be the result of several things. First, I admit that there must be bias in reporting disease phenotypes – few of us are able to publish human genetic variations related to normal patterning and function. However, this bias does not detract from the fact that these necessary genes and transcription factors are indeed labile, that their lability continues to result in detrimental

phenotypes and morphologies (craniofacial defects in humans are the third most common birth defects, after Down syndrome and heart malformation, occurring in one out of every 476 live births; Parker et al., 2010), and the property of lability itself remains the gene pool – and yet *it does remain*. Thus, let us presume that our genetic selves are harboring some essential hope to counter such omnipresent latent risk.

3F. Craniofacial Defects as a Consequence of a Genetic “Shotgun Approach”

As I have mentioned, since I began my dissertation work, I have most desired to understand the confusing existence of rapid adaptation. Evo-devo biologist Alexander Badyaev recently observed radiation of house finches (*Carpodacus mexicanus*) first-hand, by tracking their migration to new environments. Using careful morphometrics, he described dramatic changes to beak length, width, and depth, forming well-integrated facial structures over the course of only three to five generations, on average (2009). Inspired by the work of ornithologist and evolutionary biologist Peter Raymond Grant, Badyaev describes the paradox nicely, writing that finches illustrate “rapid, and essentially unconstrained evolution of precise local adaptation...that close correspondence between genetic and developmental integration should prevent.” In other words, how does nature generate such wonderfully optimized structures if it is working so quickly, and with all likelihood, so *haphazardly*?

Going backward in time, we find fellows even more upset by these issues

– Robert Beverly MacKenzie, a nineteenth-century critic of Darwin wrote:

“In the theory with which we have to deal, Absolute Ignorance is the artificer; so that we may enunciate as the fundamental principle of the whole system, that, **in order to make a perfect and beautiful machine, it is not requisite to know how to make it.** This proposition will be found, on careful examination, to express, in condensed form, the essential purport of the Theory, and to express in a few words all Mr. Darwin's meaning; who, by a strange inversion of reasoning, seems to think Absolute Ignorance fully qualified to take the place of Absolute Wisdom in all the achievements of creative skill” (1868; emphasis mine).

However, there are indeed signs that nature does not know how to make “it,” i.e., the perfect machine. In the same 2009 study by Badyaev, he finds that upon entering a new environment, house finch populations show a significant number of facial defects in early generations, including side-curved beaks (upper or lower beaks curved toward one side of the face), cross-bill (upper and lower beak skewed in opposite directions), under-bite or over-bite (longer upper or longer lower beaks), shape abnormalities (flattened, wide beaks), and ectopic outgrowths on beaks (grooves, ridges, condensations).

An equally interesting finding came from Badyaev's quantification of phenotypic adjustments. Apparently, beak depth, which, as previously mentioned, is crucial for species-specific gape and garnering parental attention, was under stabilizing selection. Surprisingly though, this was the only trait whose additive genetic variance was very substantial. On the other hand, the traits of beak length and width, which were under directional selection in new environments, showed very low additive genetic variance. He interpreted these

results in this paper to suggest that diverse phenotypic adjustments could “replenish genetic and developmental variation” even during selection, or perhaps protect the variation from getting too out of hand. Both of these explanations may hold some truth. However, in the context of the lability of the DNA sequences, it may be that under environmental stress, these genes have developed many variants over evolutionary time, maintaining diversity in the population. As long as variants exist, they sometimes helpfully, and sometimes harmfully recombine, mixing every which way, in what I term a “genetic shotgun approach” to adaptation. Although birth defects result at a high rate, a subset of the population quickly finds a more suitable beak phenotype, and an extra bit of luck allows functional integration. In this model, I do not intend to discount modularity, which certainly has a role, but rather to point out that even when a portion of the compensatory mechanisms of DNA modification are quite fast and loose, integration can be achieved, due to the sheer number of quickly moving parts (i.e. labile genes).

Since the time of Fisher’s geometric model, it has been debated whether the changes driving the majority of adaptation are many, small- (or even micro-) effect, weakly linked genes, connecting multiple fitness peaks, or whether it could be plausible that large-effect genes could be mutated for adaptation without causing lethality or detriment to individual organisms. This has led people to support the idea that intermediate-effect genes are more often at play (Kimura, 1968). Interestingly, with modern sequencing and computing capabilities allowing QTL analyses to be completed almost daily, we now know that many phenotypic

traits do, in fact, arise from combinations of innumerable genetic predispositions combined with epigenetic changes due to diet and other environmental factors.

A refinement of the ideas surrounding travel between peaks has come about recently, from evolutionary biologist Andreas Wagner. In his model, selection is not, in fact, step-wise, as the classical model would seem to represent, with organisms hopping from fitness peak to peak. Instead, he says that a population goes through a “neutralist regime” where “innovation occurs via cycles of exploration of nearly neutral spaces” (2008). In theory, after exploration and accumulation of a number of mutations, genetic diversity has increased and its genotype overtakes the population to fixation in a “selectionist regime” as diversity then decreases. Although I quite agree with a model of adaptation in novel environments as generally a period exploration, followed by a period of fixation, I would argue that the exploration that promotes diversity is not *de novo* mutations, but rather the seemingly random increase in proportion of individuals harboring less common genetic variations within the population. The numbers of these individuals may have been suppressed in previous environments where much of the rest of the population was better adapted, but now that conditions have changed, these ex-pariahs may become able to compete in terms of having also a moderate level of fitness. The increase of these genetic variants also increases the combinations of new haplotypes, some of which may be adaptive, and eventually, become more dominant in the population.

The last point that I would like to include in our understanding of adaptation addresses small- versus large-effect genetic changes. Although

clearly, adaptive biology does not result exclusively from one type or another, there is a likely pattern by which genetic changes can accumulate to generate new, useful morphologies. H. Allen Orr proposed an “adaptive walk” toward an adaptive morphology, where a population begins quite far from an optimized state. During this phase, large-effect genetic changes can be quite useful. However, as the population nears optimization, the genetic changes would have to be smaller to balance risk and reward (1998). He likens this to a quote from Fisher who stated, "conformity of these statistical requirements with common experience will be perceived by comparison with the mechanical adaptation of an instrument, such as a microscope, when adjusted for distinct vision." That is, when focusing a microscope, once we have the settings quite close to where we want them using the coarse adjustment knob, we would really prefer to optimize using the fine adjustment knob, rather than risk knocking it back to a worse condition by continuing to fumble around with the coarse.

Biologically, the use of coarse and fine adjustment in tuning functional morphologies over the course of an adaptive walk is absolutely plausible. As I have presented, natural populations are full of variants of both large- and small-effect that have come about over evolutionary time, or recurred recently, due to many highly labile sequences in transcription factors, genes involved in patterning genes, or their regulatory regions. I have also pointed out that some types of environmental stress can reduce regulation specifically at these sites and alter expression epigenetically as well. Although by no means does mixing of labile sequences always avoid detrimental phenotypes, populations gain an

advantage in that new adaptive morphologies can form and integrate quickly.

3G. Conclusion

In this dissertation, we have explored Runx2 regulation and evolution as a model for drivers of adaptation (Figure 21). Through a combination of observational and functional studies, we have found that Runx2 expression can generate shifts in timing of development and size of craniofacial elements. We also find that Runx2 expression levels are responsive to changes in cell cycle, raising the fascinating possibility that signaling events surrounding metabolic outcomes relevant to fitness and survival, such as nutrient availability, may affect rate of growth and facial morphologies during ontogenesis, while the fact that Runx2 is expressed at species-specific levels regulated autonomously by neural crest highlights its heritability, and thus its ability to be selected for. Further, due to the presence of a tandem repeat region in the *Runx2* DNA sequence, there exists enormous capacity for mutation over evolutionary time, at many times the rate at which point mutations occur. Ultimately, the accumulation of variants of Runx2, and in other, highly labile sequences of genes involved in craniofacial patterning, may be a major contributor to the genetic diversity needed for rapid generation of adaptive haplotypes within a population and eventual fixation of evolved structures.

Chapter 4: Methods and Technique Development

4A. Bone Formation Rate

Fluorochrome Labeling of Newly Formed Bone Surfaces

To understand the role of NCM in determining the rate of bone formation, we tested a sequential fluorochrome injection assay. A range of fluorochromes such as calcein and xylenol orange, while in circulation in the bloodstream, can be deposited in newly forming bone surfaces along with bone minerals. In healing chicken humeral fractures, it has been shown that by measuring the distance between bone surfaces that have formed over a fixed amount of time, one can estimate bone formation rate (Stuart and Smith, 1992). For example, a large distance between fluorochrome incorporation suggests a large amount of bone has formed in a fixed amount of time, and thus points to a high rate of bone formation, whereas a small distance points to a low rate of bone formation.

- *Reagents:*
 - Calcein and xylenol orange concentrations were determined from adult and juvenile mouse subcutaneous and IV injections from the literature. The published range for calcein was 8-20mg/kg, and xylenol orange 90mg/kg. Estimated HH36 quail embryonic weight was 0.62g, and estimated HH36 duck weight was 1.713g, based on our measurements. Calcein powder was dissolved in PBS, and xylenol orange was dissolved in

1.4%NaHCO₃ in PBS, and filter sterilized with a 0.22µm filter syringe. Solutions were stored in the dark at room temperature.

- *Sequential Injection:*
 - Calcein and xylenol orange were sequentially injected into intravitelline veins of HH37 duck embryos. I found complete overlap of calcein and xylenol orange incorporation in mandibular bone. Attempts to reduce the range of overlap included reducing the concentration of calcein (from 15mg/kg starting concentration to ¼, 1/10th, and 1/50th doses), and extending the interval between sequential injection (from every 4 hours, to every 8 hours, to 4 days).
- *Visualization of Fluorochrome Incorporation:*
 - Embryos younger than HH38 were cryosectioned, and embryos older than HH38 were embedded in PMMA (Poly Methyl methacrylate) and sectioned by tungsten-carbide blade. Fluorochrome incorporated sections were visualized under epifluorescence.
- *Interpretation:*
 - Studies of fish opercle published after my initial tests seem to suggest that embryonic woven bone is continuously laid down across a large area during maturation (Kimmel et al., 2012). This may contribute to the overlapping ranges bone formation within a short time frame, in contrast to the layering effect that

can be observed more easily in adult bone with sequential labeling by fluorochrome.

4B. Bone Material Properties

Tissue Diagnostic Instrument (TDI)

We used TDI to measure peak dynamic elastic modulus (EM) of embryonic quail and duck bone, to determine how NCM impacts bone material properties. The elastic modulus refers the slope on a stress-strain curve of the bone as force is applied to it. Thus, elastic modulus correlates to the stiffness of a material.

- *Settings:*
 - 800mV maximum force, 1 Hz indentation frequency, Flat punch soft tissue probe, Type V, 0.024-inch radius.
 - Note: A mineralized tissue probe punches through lightly mineralized embryonic avian tissue, even at HH44, and should not be used.
- *Tissue preparation:*
 - QHH44 (dry) and DHH44 (wet) mandibles were used.
 - Ideally, tissues should be collected fresh, kept in sterile PBS with antibiotics and antifungal reagents and kept in cold room until ready to use.

- We may have incorporated errors in measurement due to tissue bending and displacement. In the future, it may be better to embed jaws in a soft flexible media to generally immobilize them.
- *Results (Fig. 1E):*
 - HH44 quail. Distal tip: 110MPa, Mandibular shaft: 130-156Mpa, Jaw joint: 60-70 MPa.
 - HH44 duck. Distal tip: 16-23MPa, Mandibular shaft: 48-85Mpa, Jaw joint 55-58: MPa.
- *Interpretation:*
 - The protocol needs further optimization. A smaller probe would be useful, as the current probe diameter is larger than the embryonic jaw sample width. Immobilization and consistency of sample treatment should be considered.
 - Currently the data suggests that the distal tip of avian jaws has a lower EM than the rest of the jaw. The EM of the mandibular shaft is higher than that of the jaw joint in quail, but these EMs are nearly equivalent in duck.
 - Low EM at the distal tip may be related to distal jaw kinesis, or adaptive movement for avian feeding, as in the fast opening and closing of the beak in duck for sifting silt.
 - Low EM at the jaw joint may relate to flexibility in withstanding tension upon impact as in the pecking of quail. However, in duck, the heavy lifting of silt likely requires stiffness at the jaw joint

equivalent to that of the mandibular shaft so that applied force is not wasted in bending.

- *Alternative techniques:*
 - Nanoindentation may be more sensitive to differences between species' bone material properties at early embryonic stages

Mineral Content by X-Ray

We used X-ray as a fast, low-cost method for detecting total mineral content, in a non-quantitative fashion. Mineral content would be estimated visually from film, based on attenuation in the X-ray path.

- *Equipment:*
 - Portable X-Ray was used to scan QHH41, QHH44, DHH41, and DHH44 mandibles.
- *Result:*
 - Signal was very faint. Even using a high-resolution scanner, sensitivity does not seem adequate for detecting stage- or species-specific differences in embryonic bone.
- *Alternative techniques:*
 - A micro-radiography facility has been set up at UC Berkeley, as of 2008.

Bone Mineral Density by DEXA

DEXA, or dual-energy X-ray absorptiometry, measures mineral in the area of focus by X-ray attenuation. This technique presents a semi-quantitative 2-D map of mineral distribution.

- *Equipment:*
 - Lunar PIXimus, calibrated with a hydroxyapatite standard.
- *Samples:*
 - Quail and duck at HH35, HH37, and HH44; quck at HH35.
- *Results:*
 - Very little bone was detected at all stages.
- *Alternative techniques:*
 - Radiography in sections.

Tissue Mineral Density by Micro-Computed Tomography (μ CT)

μ CT is a high-resolution form of X-ray tomography that can be used for *in vivo* scanning of small animals. It can measure tissue mineral density (TMD), which is the density at voxel, and is not dependent on the volume of tissue analyzed. This is in contrast to techniques such as DEXA, which measure in 2-D, and depth of sample contributes to total bone mineral density measurements. In this way, μ CT is useful for understanding local osteoblast and bone formation activity separate from bone geometry. We used μ CT to measure TMD in quail, duck, and quck, and to determine whether NCM could control TMD.

- *Methods:*

- Tissues were collected in a neutral pH fixative such as 4% PFA or 10% NBF. If previously dehydrated to 100% EtOH for storage, tissues were rehydrated for uCT. Measurements and analyses were performed by the UCSF Radiology uCT core by Bryan Hermannsson and Andrew Burghardt with a SCANCO μ CT scanner.
- *Results:*
 - HH38 quail had an average TMD across the mandible of about 180 mg hydroxyapatite/cm³, while HH38 duck mandibles had a TMD distribution averaging about 300 mg hydroxyapatite/cm³. TMD distribution in HH35 quail mandibles was similar to that of HH38 quail, with an average around 190 mg hydroxyapatite/cm³ (Fig. 14A). In 3-D Reconstructions, we found that mineralized bone in HH38 duck had a smoother appearance (characteristic of more mature bone) than HH38 quail (Fig. 14B, 14D). In quail, the maturation on the donor side appeared similar to that of HH38 quail (Fig. 14C).
- *Interpretation:*
 - Quail and duck have species-specific TMDs: across the mandible, TMD is higher in duck on average. TMD seems to be a NCM-dependent characteristic, since TMD in chimeras seems to follow that of donor quail at the same stage.

Biochemical inhibition of TGF β Type I receptor

It has been shown that TGF β signaling can regulate the mechanical properties of bone and the composition of bone matrix in long bones (Balooch et al., 2005). Thus, in order to: (1) describe the expression pattern of TGF β pathway members during development of the mandibular skeleton, and (2) Determine whether TGF β pathway inhibition is necessary and/or sufficient to species- or stage-specific material properties through the regulation of Runx2 expression or timing of mineralization, we sampled expression of TGF β pathway members over a developmental timecourse, and used SB431542, a biochemical inhibitor of TGF β Type I receptor (TBRI) to evaluate effects of loss of signaling on osteogenesis. SB431542 may also inhibit TGF β family receptors ALK4 and ALK7.

- *Samples:*

- HH32, HH35, HH38 quail mandibles treated with SB431542 or DMSO vehicle control.

- *Protocol:*

- SB431542 reagent or DMSO vehicle solutions were injected in varying doses into the intravitelline veins of HH32 chick. Chick were incubated until time of collection. At collection, mandibles were dissected and processed for RNA purification and cDNA synthesis. qRT-PCR was performed to measure levels of TGF β Type II receptor (necessary for TGF β activation along with TBRI), Runx2 (downstream transcription factor required for osteogenesis), PAI1 (downstream pathway component often used as a readout of TGF β activity), and Smad 3 (downstream effector).

- *Protocol Notes:*

- An injection volume of 2ul of DMSO vehicle control in HH32 quail caused no overt problems to embryonic development. (In contrast, an injection of 10ul DMSO vehicle control caused lethality in 100% of embryos; n=42).
- A 10mM SB431542 solution injected even at 2ul volumes was lethal to embryos, likely due to lack of solubility in the bloodstream.
- 2ul of a 5mM SB431542 solution or 2mM SB431542 solution allowed embryo survival. These treatment groups were collected for mRNA expression analyses (n=3 per group)
- Dissection of mandibles at this time was unskilled and inconsistent due to my unfamiliarity with avian jaw anatomy at the time that I performed these experiments. Much of the epithelium and mesenchyme surrounding the Meckel's cartilage was lost during this time, including the bulk of the mineralized tissue.

- *Results:*

- At first glance, it seemed as though mRNA expression of *TGBRI* increased 2-fold, *Runx2* increased 3-fold, *PAI1* decreased 0.7-fold, and *Smad3* increased 3.4-fold, when comparing SB431542-treated to DMSO-treated mandibles. However, examination of the unlikely mRNA expression patterns in DMSO-treated embryos (e.g. a 2.5-fold increase in *Runx2* from HH32 to HH35, and then a 0.5-fold decrease in *Runx2* from HH35 to HH38) along with high standard

deviations between replicates, reveal that the data collected are probably unreliable (Fig. 14F).

- Alternative techniques: SB525334 is a newer reagent that is marketed as a selective inhibitor of TGBRI. The increased selectivity may overcome the solubility or lethality issues we experienced in attempting to administer a high dose *in ovo*.
- A skilled dissection to promote consistency between replicates should include fixed surgical landmarks and prevent removal or loss of any tissue distal to the jaw joint.

4C. Gain- and Loss-of-Function Techniques

Mesenchymal electroporation at HH21

For plasmid over-expression in the mandibular mesenchyme, we attempted several settings for electroporation *in ovo* at HH21. This timepoint was chosen as a window in which we could affect osteogenic processes just before the beginning of differentiation between HH24 and HH27. I first used pMES plasmid, which drives eGFP expression by a chick B-actin promoter and IRES site to look for preliminary presence and localization of signal. I then switched to Hsp-LacZ plasmid, which drives B-galactosidase expression by a chick heat shock protein promoter, for permanent staining and increased resolution of localization.

- *Equipment:*

- INTRACEL TSS20 Ovodyne electroporator, Picospritzer injection apparatus, 0.5mm diameter platinum electrodes.
- *Protocol:*
 - Removed embryonic membranes at region to be electroporated using fine forceps. Injected 2-4ug DNA solution with Fast Green tracer dye under epidermis of mandible (Fig. 15A). Placed one electrode dorsal to hindbrain, and one proximal to the mandible (Fig. 15D). Embryos were given 8-10V, 5 pulses, with 30ms space and 20ms width.
- *Results:*
 - In QHH21 and DHH21 pMES electroporations, eGFP signal was detected in epithelium of FNP, maxilla, and mandible, as well as heart and brain tissue, in about one fifth of the cases, at the HH25 collection time point (+24h; Quail n=36, Duck n=24; Fig. 15E, 15F).
 - In DHH21 Hsp-LacZ electroporations, LacZ was expressed in the mandibular and FNP epithelium (n=34).
- *Interpretation:*
 - Mesenchyme is poorly conductive as loosely connected cells, compared to epithelium, which is composed of tightly connected cell sheets. An electric charge flows along the most highly conductive channel, in this case, targeting the epithelium, bypassing and insulating the mandibular mesenchyme completely.
- *Alternate techniques:*

- I electroporated DHH21 with homemade tungsten electrodes used by Diane Hu in the lab of Ralph Marcucio. These were used at 10-15V, with 25-100ms pulse length. No signal was detected (n=15).
- Because of a combination of high resistance of duck albumin versus Dr. Hu's usual chick samples, and the reduced radius of tungsten electrodes versus our lab's wide-radius platinum electrodes, I raised the voltage to 13-18V. I also increased the space of electric pulse, since some papers suggest this may help electroporation efficiency in refractory tissue. Lastly, I added 1/3 glycerol to the DNA solution to add viscosity and keep the DNA solution localized to the interior of the mandible. Most of these embryos died, likely due to the high voltage. LacZ expression was detected in the epithelium of the FNP, mandible, hyoid, and oral cavity.
- CuSO₄ added into the DNA solution may increase conductivity. This method is commonly used in the plant community (e.g. Siegemund and Eimert, 1995).

Ex ovo mesenchymal electroporation at HH21

In order to optimize electroporation conditions without the resistance of albumin and physical constraints of electrode placement within the confines of the egg, I dissected mandibles at HH21 for electroporation in Hank's Balanced Salt Solution, and subsequent organ culture. Equipment was kept constant from *in ovo* electroporation at HH21.

- *Reagents:* Embryos were cultured on Corning Transwell plates (0.4 μ m size, 6-well) in BGJb media.
- *Result:*
 - o No eGFP signal in mesenchyme was detected (n=22).

Confined mesenchymal electroporation at HH21

In order to bypass the issue of epithelial conductivity, I made new tungsten electrodes with propane torch-sharpened tips, insulated by nail polish with only the distal 1mm exposed. During electroporation, these electrode tips were inserted directly into the mandibular mesenchyme, past the point of insulation such that electric current would not be conducted to the epithelium, instead retaining the charge entirely in the mesenchyme (Fig. 15G).

- *Protocol:*
 - o Electroporation settings were 15- 50V, 5-20 pulses, 15-25ms space, 50 ms width, using 2 μ g Hsp-LacZ plasmid and Fast Green loading dye.
- *Results:*
 - o The optimal voltage for confined electroporation under these conditions was 30V, at 25 ms space, 50 ms width. Epithelial expression was still detected in the mandible and maxilla; additionally, a small volume punctate bolus was detected in the mesenchyme, with equivalent frequency under 5, 15, or 20 pulse conditions (n=75).

Mesenchymal lipofection

Since electroporation was not successful in driving plasmid over-expression at the critical HH21 timepoint, I tried *in ovo* lipofection using a number of reagents. In the book chapter “Gene Transfer Techniques in Whole Embryos” by Daisuke Sakai and Paul Trainor, the authors wrote that they were successful in obtaining plasmid over-expression in mouse embryo cultures using Lipofectamine 2000 as a carrier. In addition, a paper from Joy Richman’s lab showed good eGFP over-expression in chick maxillary mesenchyme using a custom lipid blend of N,N-dioleoyl-N,N-dimethylammonium chloride (DODAC)/1,2 dioleoyl glycerol-3-phosphorylethanolamine (DOPE) used at 18mM concentration (Geetha-Loganathan et al., 2011).

- *Protocol:*

- I tried four different commercial lipofection reagents: Superfect (0.5ug DNA, 1ul Superfect), Effectene (5ul Effectene, 4ul enhancer, 0.5ug DNA), Fugene (3ul Fugene, 1ug DNA), GeneIn (1ug DNA, 4ul GeneIn RED, 4ul GeneIn BLUE). Each lipofection mix was made fresh before injection into mandibles at HH21. The DNA used was pMES. Embryos were evaluated for over-expression at HH24.
- For DODAC/DOPE, I followed instructions from correspondence with the authors. The lipid mix was vortexed before use, and 1.1ul lipid mix was added to 1ug of plasmid. This solution rested at 15-20min at RT during formation of lipoplexes. The solution was mixed gently with Fast Green loading dye and injected directly into CHH18

facial structures. The DNA used was pMES, pRK5- β gal, RCAS-GFP. Embryos were evaluated for over-expression at HH24 and HH27.

- To bypass the potential problem of dilution of DODAC/DOPE due to embryonic circulation, mandibles were also cultured *ex ovo* for 24 hours until HH24 and HH27. DODAC/DOPE was injected at the time of dissection using the same protocol as *in ovo* lipofection.

- *Results:*

- Commercial lipofection resulted in no detectable signal (n=21).
- pMES and DODAC/DOPE resulted in no detectable signal (n=8). Correspondence with authors confirms that DODAC/DOPE has not worked with IRES-containing constructs.
- pMES and pRK5- β gal and RCAS-GFP result in small boluses of localized expression in the mandible in both *in ovo* and *ex ovo* tests (Fig. 15H, 15I). However, the majority of mandibular mesenchyme is unaffected (n=8).

Neural Crest Electroporation at HH8

Despite attempts at developing new techniques, the only continuous, reliable method for plasmid over-expression in the mesenchyme remained the well-described one of neural crest electroporation at HH8 (Krull, 2004). At HH8, the neural tube lumen forms an excellent reservoir for DNA solution, while the neural crest are currently in an epithelial, and thus what I assume to be a current-carrying, state.

- *Protocol:*
 - Embryo was hydrated with a few drops of HBSS to prevent tissue damage by charged electrodes. Embryonic membrane was cut and pulled away from the area of interest using sharpened tungsten wire. pMES DNA solution was injected directly into the lumen of the neural tube from the mid-forebrain region rostrally, to the first somite, caudally. 0.2mm diameter homemade platinum electrodes were placed parallel to the neural tube for 10V, 5 pulses, 50ms space, and 50 ms width.
- *Result:*
 - Strong eGFP signal was detected in neural tube, and migrating neural crest, 16h post-electroporation ~HH15. eGFP signal was still readily apparent in brain tissue and pharyngeal arches 1-2 days later at HH21 (Fig. 15J). By HH24, eGFP was very faint, and usually only detectable in brain tissue. eGFP was not detected at HH27 in any cases (N=20+).

Electroporation of Stable, Neural Crest-Specific, Tetracycline-Inducible Constructs

Stable, neural crest-specific, tetracycline-inducible constructs were a gift from Yoshiko Takahashi, as described in Takahashi et al., 2008 and Yokota et al., 2011. Stable expression is conferred by Cre-LoxP mediated excision and a Transposase-expression construct. The constructs use an enhancer that shares expression patterns with Sox10 and Hnk1 mRNA in the trunk to drive Cre

recombinase expression, thus it is considered neural-crest specific, though specificity has not been validated in the head. An alternative Cre recombinase construct that is constitutively expressed under the CAGGS promoter was also provided. A construct with a reverse-tetracycline controlled transcriptional activator flanked by Tol2 site, which requires Cre excision of dsRed in a Stop cassette for genomic integration confers inducibility. Lastly, the gene of interest can be subcloned into a Tol2-flanked IRES-eGFP containing construct for genomic integration and subsequent lineage tracing.

- *Protocol:*

- The combination of four constructs conferring constitutive stable expression of eGFP, along with Fast Green tracer dye, was administered by electroporation of the neural tube at HH8 according to conditions optimized in our lab. The concentration of each construct was 1ug/ul, such that the solution was 4ug/ul. At HH18-21, doxycycline was administered to induce construct expression. These embryos were collected at HH21-24 and checked for eGFP expression, denoting successful integration and recombination/excision, or DsRed expression, denoting successful electroporation.

- *Results:*

- Efficiency was very low, and few embryos expressed eGFP. Of the eGFP expressing embryos, signal was spotty and weak (Fig. 15K, 15L).

- *Interpretation:*
 - o Low efficiency may have been due to the necessity of all four constructs working in tandem. We did not sequence the constructs after receiving them – at the time of correspondence not all sequences were yet available.

4D. Transient Gain and Loss of Function

p27 knockdown in quail and quack by shRNA

In order to slow cell differentiation and test whether we could delay osteogenesis to recapitulate a duail-like phenotype in quail and rescue quack, we decided to knockdown p27, which is tied to be exit from the cell cycle and osteoblastic differentiation *in vitro*.

- *Methods:*
 - o The basic shRNA template designs were created using the MIT Whitehead Institute's Online siRNA Selection Program (Yuan et al., 2004) and expression cloning into pSilencer 2.1-U6 Neo was based on Chestnutt and Niswander, 2004.
 - o Based on methods described in McIntyre and Fanning, 2006, we designed and synthesized three shRNA sequences targeted against quail p27 only. To create species-specific p27 shRNA, we cloned quail, duck, and chick p27 and only chose quail target sequences with mismatches to duck and chick.

- Briefly, synthesis included designing overlapping PCR primers to form the bulk of the sequence, and end extension by Phi29 polymerase, a polymerase that works well in DNA with secondary structures.

- Primers for synthesizing shRNA, features sous-labeled:

- Generic 3' Primer:

5' - CGC GAAGCTT CC AAA AAA - 3'

seat HindIII termination

- p27 (KB2; 43% GC; N22)

5' - GCGC GGATCC G TTT CGA TTT CCA GAA CCA

seat BamHI Sense Stem

CTT A CTCGAG A **G TGG TTC TGG AAA TCG AAA**

Loop/XhoI Anti-Sense Stem

TTC TTT TTT GGAAGCTT - 3'

term HindIII

- p27 (T2; 47% GC; N22)

5' - GCGC GGATCC **GT AAA CGG GAA TTG CCA GT**

seat BamHI Sense Stem

TT A CTCGAG A **AC TGG CAA TTC CCG TTT AC**

Loop/XhoI

Anti-Sense Stem

TTA TTT TTT GGAAGCTT - 3'

term

HindIII

- p27 (T3; 47%GC; N22)

5' - GCGC GGATCC **GAA TCT CAG AGG ACA CTC A**

seat BamHI

Sense Stem

TT A CTCGAG A T GAG TGT CCT CTG AGA TTC

Loop/XhoI

Anti-Sense Stem

TTA TTT TTT GGAAGCTT - 3'

term

HindIII

- shRNA templates (flanked by cut sites for ligation into pSilencer):

- KB2:

GGATCCGTTTCGATTTCCAGAACCACTTACTCGAGAGTG

GTTCTGGAAATCGAAATTCTTTTTTGGAAAGCTT

- T36:

GGATCCGAATCTCAGAGGACACTCATTACTCGAGATGA

GTGTCCTCTGAGATTCTTATTTTTTGGAAAGCTT

- T2:

GGATCCGTAACGGGAATTGCCAGTTTACTCGAGAACT

GGCAATTCCCGTTTACTTATTTTTTGGAAAGCTT

- As a control, we used Ambion GFP shRNA, which is part of the pSilencer RNAi expression vector kit.
- p27 shRNA was electroporated at HH8 and targeted to regions of known high endogenous p27 expression including the brain, FNP, and post-orbital region (Fig. 16E). Control embryos were electroporated with pCAX (B-actin eGFP), knockdown control embryos were electroporated with pCAX and eGFP shRNA, and experimental embryos were collected at HH27 for eGFP visualization and protein.
- *Results:*
 - pCAX-electroporated embryos showed eGFP over-expression, similar to that observed in previous tests of HH8 electroporation efficiency. However, Ambion eGFP shRNA did not show consistent decrease in eGFP signal.
 - Although the low levels of endogenous p27 protein made quantification difficult, of the three p27 shRNA sequences KB2 appeared to increase cyclin E levels (Fig. 16A). Increase in cyclin E would be an expected outcome of successful p27 knockdown due to decreased inhibition of proliferation.
 - Following up on p27 shRNA KB2 with more treatments showed only small differences in expression levels of p27 and cyclin E in transfected versus control embryos, well within the margins of error (Fig. 16B, 16C, 16D).

- *Interpretation:*
 - Difficulties visualizing eGFP knockdown may have been due to variation in over-expression between transfected embryos. Or, there could have been a problem with the eGFP sub-cloned sequence – without the proprietary sequence, we could not check to rule out this possibility.
 - None of the three shRNAs we designed caused significant knockdown in p27 under the current lipofection conditions. This could be due to a biological reason (lack of response or recognition of these sequences upon binding) or a technical one (the lipofection simply has such low efficiency that knockdown cannot be detected).
- *Alternate Techniques:*
 - Since the time of our p27 shRNA synthesis, avian miR-222 has been identified (Powder et al., 2012).
 - Seven molecules (inhibitors of miR-189, -153, -133a, -186, -27a, -148b, and -489) have been observed to significantly affect alkaline phosphatase activity during *in vitro* mineralization assays of mesenchymal stem cells (Thermofisher miRNA Application Note). The molecules showing the most specificity and promise from additional testing are miR-27a, -148b, and -489a. Although some of these miRNAs have roles in proliferation, tumor suppression, and tumorigenesis, their effects on osteogenesis have not yet been described outside of this *in vitro* study.

- The shRNAs could be electroporated at HH8 for maximum efficiency of expression. However, endogenous p27 expression would have to be identified in the HH13-18 (i.e., +24h) range in a tissue that could be collected in adequate volume (by size or number of embryos) in order to check for knockdown by Western.

Electroporation of D-Type Cyclins *in ovo*

In order to understand the effects of forced cell cycle progression on osteogenesis, *in ovo* electroporation was performed using a 1:1 solution of 2 ug/ul pCIG-CyclinD1-IRES-eGFP and pCIG-CyclinD2-IRES-eGFP constructs (a gift from F. Pituello, described in Lobjois, et al. 2004, 2008). The optimized protocol for neural crest electroporation at HH8 was used (see previous section). I designed qRT-PCR primers to detect, and distinguish between, endogenous quail *cyclin D1* and exogenous mouse *cyclin D1* from the over-expression construct. Exogenous *cyclin D1* mRNA was clearly expressed during early development up to HH18, but was undetectable by HH24 (Chapter 2). Cyclin D1 protein over-expression in electroporated mandibles was only 1.5 to 2-fold over control embryos mandibles by HH24, as detected by Western blot (Fig. 16F, 16G).

Runx2 over-expression for *in vitro* osteogenesis

To test the ability of Runx2 to accelerate osteogenesis, we evaluated the effects of several plasmid Runx2 over-expression constructs in cells cultured in osteogenic conditions.

- *Reagents:*
 - Cell line used was CAR1B 2T3 (from Tamara Alliston). The transfection reagent used was Effectene. Plasmids were pMES (from Cathy Krull), pMES-Runx2, pRK5- β gal (from Tamara Alliston), and pXF1F-Runx2 (from Tamara Alliston).
- *Protocol:*
 - Cells were grown in DMEM with 10% FBS in 6-well dishes until confluence, when they were switched to osteogenic media (alpha-MEM, 2% FBS, 100ug/ml ascorbic acid, and 5mM β -glycerophosphate; as in Alliston et al., 2001).
 - 3-wells was collected at 24h for transfection efficiency by staining for β -gal. Cells were collected from the other plates in triplicate at t=day 0, day 1.5, 3.5, 5.5, and 7.5 for qRT-PCR) and alkaline phosphatase.
 - For alkaline phosphatase assay, see Alliston et al., 2001.
- *Results:*
 - eGFP expression was detected in pMES and pMES-Runx2 transfected cells. Expression peaked at the first timepoint, and decreased steadily for the next three days. No expression was detected by day 3.5 by qRT-PCR (Fig. 17C).
 - Runx2 over-expression was no longer detected by day 1.5 (Fig. 17A).

- There was no difference in Col1 expression over the time course of active plasmid expression in Runx2 over-expressing versus control pMES transfected cells. All samples equivalently up-regulated levels of Col1 up to day 3.5 of culture in osteogenic media (Fig. 17B).

- *Interpretation*

- Plasmid over-expression of Runx2 did not last long enough, or was not strong enough, to impact the bulk of changes to osteogenic gene expression or alkaline phosphatase activity which would occur around day 5.5 of culture.
- Due to the limiting nature of transient over-expression, stable Runx2 over-expression should instead be used for *in vitro* osteogenesis assays.

Runx2 knockdown in quail and quack by siRNA

In order to transiently decrease Runx2 expression and possibly delay mineralization, we hoped to recapitulate a duck-like phenotype in quail, and rescue the chimeric phenotype in quack. This experiment was meant to be a proof-of-principle to show that timing of Runx2 expression can control timing of osteogenesis. It was already known at the time of these studies that minimal levels of Runx2 are required for osteogenesis to proceed.

- *Reagents:*

- Two 20 nmol custom synthesized siRNA was ordered from Ambion. siRNA was designed by Ambion based on sense and

antisense sequences for chick Runx2 that I submitted in their online application. Ambion NeoFX liposomal transfection reagent, Ambion amine transfection reagent, and a negative control siRNA for mouse were also used.

- *Protocol:*

- Control and pMES-Runx2 transfected DF-1 cells were cultured for siRNA treatment. pMES-Runx2 was transfected using Superfect, a reagent our lab often uses to transfect DF-1 cells with plasmid DNA. 50 μ M of control or Runx2 siRNA was administered via either amine-based transfection or liposomal transfection. Cells were collected for RNA, and *Runx2* gene expression was analyzed via qPCR versus the *GAPDH*.

- *Results:*

- *Runx2* expression was low in control DF-1 cells, but fairly equivalent also in pMES-Runx2 treated DF-1 cells. The control and *Runx2* siRNAs did not affect *Runx2* expression levels over a 1.25-fold change within the margins of error. It seemed that neither the plasmid nor siRNA transfections were successful. Indeed, visualization of eGFP fluorescence of pMES-Runx2 treated DF-1 cells 24 hours post-transfection showed only 3-5% efficiency. A representative DF-1 transfection with pMES-Runx2 in my hands had generally yielded 15-25% efficiency prior to these experiments.

- *Interpretation:*

- I ran into technical issues with low transfection efficiency of the initial pMES-Runx2 transfection, since the DF-1 cells do not have endogenous Runx2 expression for knockdown. Even with stronger pMES-Runx2 expression, I had no way to guarantee that over-expression was equivalent in all treatment groups before beginning the knockdown experiment.
- Since the siRNA is specific to avian Runx2, an avian osteosarcoma line with endogenous Runx2 would be optimal for these studies.
- An important factor to note is that even if Runx2 siRNA causes mRNA degradation, if certain mRNA fragments are intact, the qPCR primers can detect them as if mRNA levels are still high. A better test of knockdown is to check for decrease in protein levels by Western.
- Lastly, GAPDH has been shown to have TGF β -mediated changes to expression. Feedback from Runx2 may alter these conditions and make baseline comparisons difficult. In the future, the more stable expression pattern of RPL19 (Ribosomal Protein L19) may be more useful for normalization.

4E. Stable Gain of Function

Retroviral Over-expression of Runx2

For stable over-expression, we used RCAS, a replication-competent retrovirus, which is derived from avian sarcomavirus.

- *Reagents:*

- The RCAS-Runx2 construct was a gift from S. Mundlos (Stricker et al., 2002), and RCAS-GFP was developed in the lab of Connie Cepko (Chen et al., 1999). RCAS virus was produced as described (Morgan and Fekete, 1996). DF-1 cells were American Type Culture Collection (Manassus, VA).

- *Protocol:*

- With the addition of Fast Green tracer dye, DNA solution was injected profusely into HH8 neural tubes of virus-free SPAFAS chick (Charles River Labs) and/or adjacent paraxial mesoderm was using pulled glass micropipettes and a Picospritzer fluid injector. For unilateral treatments, only a single, tiny bolus was administered to paraxial mesoderm at the midbrain-hindbrain boundary immediately adjacent to neural tube.

- *Results:*

- Validating RCAS-Runx2 construct for functional protein expression
 - RCAS-Runx2 was sequenced and insertion was confirmed to be mouse Runx2.
 - Over-expression of mouse Runx2 transcript – I amplified the full mouse Runx2 gene by step-wise PCR, detecting no gaps

the expressed gene, and found high levels of expression by qRT-PCR in RCAS-Runx2 infected DF-1 cells.

- Over-expression of Runx2 protein – Although I had difficulty with Western Blotting for Runx2 during the time of my thesis work due to a lack of constant access to a reliable sonicator, I did eventually detect good over-expression of Runx2 in a double-sonicated pellet of DF-1 cells transfected with pMES-Runx2 (which contains the subcloned *Runx2* from RCAS-Runx2) and 80ug of sonicated DF-1 cells infected with RCAS-Runx2. Since the RCAS-Runx2 construct can drive good protein over-expression *in vitro*, it is likely that it can do the same *in vivo* (Fig. 20B).
- Recapitulating the ectopic mineralization phenotype in Eames et al., 2004 – The presence of ectopic mineralization seemed to be dose-dependent. Unilateral infection resulted in barely visible spots of ectopic mineralization. A bulky, deformed jaw was found only in two samples. In the jaw mineralization did not look “ectopic” as previously described, but rather expanded along the same general growth axes. In the calvaria, scattered mineralization began about four stages earlier than it would usually for that region (Fig. 18D).
- Recapitulating the limb phenotype in Stricker et al., 2002 – RCAS-Runx2 was injected into presumptive limb region at

HH13-15. Unlike the published data, we saw no evidence of joint fusion at the digits or limb shortening. Instead, we saw hip, elbow, and knee joint fusion (Fig. 18B), as well as wavy long bones characteristic of weak cartilages.

- Changes to facial morphology and osteogenesis
 - Lethality – RCAS-GFP treated embryos have a peak in lethality at HH13-15 (at the time of vascularization) due to damage during injection or windowing causing exsanguination. Other deaths are dispersed throughout the rest of the developmental period. However, RCAS-Runx2 treated embryos have a peak in lethality at HH25-34, suggesting a RCAS-Runx2 specific mechanism causing death.
 - Facial Hypoplasia: At HH24-34, all embryos that died during development (n=7), and about half of those that survive (n=13) show extremely hypoplastic FNP, maxillary, and mandibular primordia which fail to fuse (Fig. 18E-18H). In addition, at least one case showed a skull closure defect, and in RCAS-Runx2 limb region (distal somite) injections, I observed a ventral body wall closure defect in the majority of embryos.
 - Facial Asymmetry: Asymmetry was observed in the mandible in about 1/3 of the RCAS-Runx2 treated embryos

in both unilateral and bilateral infection scenarios (a bilateral infection does not guarantee equal dosing on both sides of the embryo). In unilateral infections, the untreated side was larger (Fig. 18I, 18J). This trait was observed both in whole mount and in Trichrome-stained sections. In embryos that survived to HH36, this resulted in significant cross-beaking (where the upper and lower beaks point in opposite directions; Fig. 18K, 18L).

- Eye defects: I observed eye defects including a hypoplastic eye (n=3) and blood in the pupils (n=2).
- Proliferation: No effect was seen on proliferation when assayed with BrdU (Fig. 17I, 17J), despite detection of viral infection at the time of collection by *in situ* hybridization (Fig. 17H). However, only mandibles with unilateral RCAS-Runx2 spread were used for the BrdU assay so that one side of the mandible could be used as a unilateral control. It is likely that the extremely low doses of Runx2 used to achieve this limited spread were below the threshold needed to induce a detectable change to cell cycle.
- p27 expression: A p27 *in situ* hybridization probe was generated from a p27 fragment product amplified from an HH27 chick library using the qRT-PCR primers. Upon visualization of quail, duck, and chick section *in situ* analyses

from HH25-32, we found that p27 mRNA expression was ubiquitous, but more highly expressed in the developing forebrain, myogenic condensations, and osteogenic condensations (Fig. 17 D-F). In RCAS-Runx2 unilaterally treated embryos, it appeared that p27 was up-regulated on the treated side (Fig. 17G).

- Early differentiation: No striking effects were seen on alkaline phosphatase activity in control v.s. treated embryos, collected at HH25-27. Low viral doses were also used in these embryos in an attempt to keep spread unilateral.

- *Interpretation*:

- In general, the over-expression of Runx2 causes hypoplasia when compared to control untreated or RCAS-GFP tissues. This points to either a defect in proliferation or an increase in cell death. A TUNEL assay across developmental timepoints in treated and control embryos would let us know whether apoptosis is a major factor in generating the hypoplastic phenotype. Similarly, a BrdU assay in high-dose RCAS-Runx2 injected embryos compared to RCAS-GFP embryos could be much more informative than the very low-dose RCAS-Runx2 unilateral comparisons against the contralateral side. In this context, we also cannot rule out the possibility that high viral doses could also affect early

differentiation, especially since morphology is affected in treated embryos.

- The possibility that Runx2 over-expression can up-regulate p27 *in vivo* is an intriguing one, and would be in line with data from *in vitro* studies. However, we would need a larger sample size to confirm this phenotype.

Retroviral Over-expression of RANKL and OPG

Unpublished data in the lab shows that donor NCM can control the pattern of osteoclast activity in chimeras, although osteoclasts are a host-derived cell type. In addition, the administration of recombinant mouse and human RANKL and OPG proteins through the bloodstream seems to be able to preferentially increase or decrease the length of the lower jaw compared to the upper jaw. We presume the mechanism by which this occurs is that RANKL (an activating ligand) binds RANK (a cell surface receptor on osteoclasts) to drive osteoclast proliferation, differentiation and function. In this way, exogenous RANKL increases the degradation of bone and prevents elongation of the jaw. In contrast, the administration of OPG (a decoy RANK-like receptor) binds and sequesters RANKL, preventing activation of osteoclasts. This allows bone formation to continue unimpeded, resulting in increased growth and length of the jaw. How these proteins differentially affect the lower jaw is unknown. To our knowledge, this is the first time that modulation of osteoclast activity has been linked to developmental shape of skeletal elements.

The development of a RCAS retroviral-mediated RANKL and OPG administration over an intravenous protein injection affords a few advantages. First, RCAS is replication competent, and could be active throughout development, while proteins naturally degrade in the bloodstream in a couple days. Second, RCAS can be targeted by injection to only the head, whereas systemic RANKL and OPG protein injection may affect other organs and lead to off-target effects. Lastly, RCAS production affords us an enormous, cheap supply of reagent, allowing larger sample sizes of treated embryos – in contrast, RANKL and OPG proteins are quite expensive and have an upper limit in dosing based on solubility.

- *Protocol:*

- I cloned full-length chick OPG (ch.OPG) from HH44 chick cDNA, whereas mouse soluble RANKL (m.RANKL) and mouse OPG (m.OPG) were a gift from the Tanaka lab. Each gene was subcloned into RCAS. Virus was produced in DF-1 cells, as described, and virus-free SPAFAS chick were used for injection at HH8 along the paraxial mesoderm and neural tube, or HH24 directly into mandibular mesenchyme. Embryos were collected at HH37/38 for analysis osteoclast activity (via TRAP staining) and morphometrics (via measurements of Alizarin Red-stained jaw proportions).

- *Results:*

- Over-expression was confirmed in treated embryos or DF-1 cells

two days after infection via qRT-PCR for chick *OPG*, mouse *OPG*, and soluble *RANKL*, respectively. All infected samples were also confirmed to be expressing viral *gag* by qRT-PCR.

- To test whether RCAS-ch.OPG was generating functional protein, I attempted an apoptosis rescue experiment, by which Sigma tests the functionality of its recombinant OPG protein. In this experiment, L929 cells are treated with recombinant TRAIL (Peprotech) protein, which triggers cell death. Functional OPG protein should neutralize this phenotype (Shipman and Croucher, 2003). I plated 5,000 L929 cells/well in an 8-well slide culture and tried 5 conditions: (1) BSA, DMEM (2) TRAIL, DMEM (3) TRAIL, RCAS-ch.OPG conditioned media (4) TRAIL, RCAS-GFP conditioned media, and (5) TRAIL, Sigma recombinant human OPG. TRAIL was used at a concentration of 500ng/ml, which was described as the LD50 for L929 cells. However, in a live/dead count using trypan blue, I found roughly equivalent numbers of cell death in all wells. The dosing may need to be optimized in the future.
- RCAS-ch.OPG-treated embryos collected for alizarin red (n=7) and TRAP (n=8) had no overt phenotype compared to controls. Nothing stood out about the RCAS-mo.OPG and RCAS-mo.RANKL treatments either, when examined for gross morphological and TRAP activity pattern changes.
- In morphometric analyses, we had higher sensitivity in detecting

differences between treatment and control groups. Although the higher range of upper:lower beak ratios in treated embryos overlapped with those of control embryos, both RANKL and OPG treated embryos had lower upper:lower ratios on average. Looking at the distribution of cases, the median 50% of treated samples fell well below the median 50% of control samples. Furthermore, no single control sample fell below the upper:lower ratio of 0.34, whereas nine treated embryos had an upper:lower ratio of 0.33 or lower (Fig. 19A).

- The average upper:lower ratio of OPG-treated embryos was significantly lower than that of control embryos (Fig. 19B).
- A survey of beak morphologies sorted by treatment group and upper:lower beak ratios reveals a few possibilities (Fig. 19C-19E). The shorter upper and lower beaks seem to be correlated to beak curvature, as seen in RCAS-Runx2 treated embryos (Chapter 2) and canine dorsal nose bend (Chapter 3). Lower jaw extension (past the upper jaw) was overt only in RCAS-OPG treated embryos.
- Of the control batch of embryos, one had a severe neural tube defect at the time of windowing, and a dome-shaped skull, edema, and encephalocele upon collection. This sample was not counted in control analyses, but had an upper:lower ratio of below 0.33. No treated samples showed this common developmental defect in control samples either at the time of windowing or collection.

However, even if this severe developmental defect went unnoticed throughout the processing of treated embryos, we still saw 9/33 embryos with treated embryos with upper:lower ratios of 0.33 or lower, which would be at least 3x what we would expect from the frequency of occurrence of a spontaneous natural defect.

- *Interpretation:*

- My data of RCAS-OPG treatment corroborates previous unpublished findings in our lab that OPG may be able to affect beak morphology, specifically increasing the lower:upper beak ratio, likely by blocking osteoclast activity.
- RCAS-RANKL treatments may point to a dysregulation of coordination of lower:upper beak ratios, though not necessarily causing a preferential decrease in lower beak length as we might have expected from our lab's previous systemic recombinant RANKL injection treatments.
- Upper and lower jaw coordination otherwise seems strong enough to prevent lower jaw extension past the upper jaw even in the very low upper:lower beak ratios in the RCAS-RANKL and control embryos. Instead, the lower jaw, when especially long compared to the upper, seems to extend further dorsally so that the tip of the beak is not out of line. There may be a constraint built into this system to help with adaptive fitness, as there are very few birds that have stable protruding lower beak morphologies (e.g. the black

skimmer, *Rynchops niger*).

4F. Cell Cycle Analyses

Wst-1 Cell Viability and Proliferation Assay

Wst-1 reagent undergoes an enzymatic color reaction in the presence of viable cells. Thus, absorbance of Wst-1 can be used to estimate cell number and cell proliferation over a time course. We used Wst-1 to determine the effects of Runx2 over-expression on primary chick mesenchymal cells *in vitro*.

- *Protocol:*

- Chick mandibles were infected with RCAS-GFP, RCAS-Runx2, or no virus, the morning of the assay. In the evening (+8hrs), mandibles were dissected, were treated in 0.05% trypsin at room temperature, and epithelium was removed. Mandibles were transferred to MEMalpha growth media. Mandibular mesenchyme was dissociated by pipetting, pooled by treatment group, and spun down at 1500 rpm for 5 minutes at 4C, resuspended 1 ml of growth media for counting with a hemacytometer. Cells were plated in a 96-well plate with 10,000 cells per well. Each treatment received 4x replicates and 4 timepoints for measurement, 0h, 4h, 11h, 16h. At each timepoint, Wst1 was added, incubated for one hour, and read by spectrophotometric plate reader. Readings of uninfected cells

were subtracted from the readings of RCAS-GFP and RCAS-Runx2 treated cells as a baseline.

- *Protocol notes:*

- We previously attempted to apply Wst-1 to all samples at 0h, and perform readings at each timepoint following. However, the manufacturer's protocol recommends only a 2-hour incubation for adherent cells (in addition, we only used a 1-hour incubation). These previous attempts at continuous readings were thrown out, since Wst-1 saturation may have lent inaccuracy to readings past the 2-hour timepoint.

- *Results:*

- No difference was detected in proliferation potential between RCAS-GFP and RCAS-Runx2 cells. However, no proliferation was detected during the 16-hour time course. Instead, we observed a decrease in cell viability after first plating (0-4 hours), and a constant number of viable cells for the remainder of the study (4-16 hours).

BrdU Injection

BrdU was used to visualize and quantify cell proliferation at specific developmental stages *in ovo* (Chapter 2, Fig. 8B, 17I, and 27J)

- *Protocol:*

- 1 μL of BrdU (Invitrogen, Carlsbad, CA) was injected into an intravitelline vein and the embryo was incubated for 20 min at 37°C. Embryos were fixed in Serra's solution, sectioned, and stained using the BrdU staining kit (Invitrogen). BrdU-positive cells were quantified as follows: using ImageJ software, the rectangular selection tool was used to define equal areas (ranging from approximately 0.0625 mm² to 0.16 mm²) on donor and host sides of quack through a depth of 0.5 – 0.9 mm (average volume of 0.06 – 0.1 mm³). Levels were relative to BrdU-positive cells on host side in quack.

- *Results:*

- In Chapter 2.

Flow cytometry

Fluorescence-activated cell sorting (FACS) was used to quantify the percentages of cells in each phase of the cell cycle across stages of development. Dissociated NCM from mandibular primordia of quail, duck, and bilaterally transplanted quack were fixed in 70% ethanol and treated with 1 mg/mL propidium iodide (PI; Invitrogen), 2 μg RNase (Roche), and 0.1% Triton X-100 for 15 min at 37°C. Flow cytometry was performed using a Cytomation MoFlo High Speed Sorter to detect PI and cell cycle phases were estimated using the Watson model analyses in the FlowJo software (Ver. 7.2.2). Results in Chapter 2 and Fig. 8D.

Analysis of genes regulating cell death and cell cycle

To get a sense of the regulation of cell death and cell cycle in the developing mandible, I surveyed the mRNA expression pattern of p53 (which drives apoptosis), p21 (which is expressed in proliferating pre-osteoblasts and terminally differentiated osteoblasts *in vitro*), and p27 (which is expressed in differentiating osteoblasts *in vitro*) by qRT-PCR. I found that p53 was not expressed at detectable levels at HH21, HH24, or HH27. p21 was expressed at these stages, but did not clearly trend with or against differentiation (Fig. 20C). p27 increased as osteogenesis continued, as discussed in Chapter 2, and Fig. 8E.

4G. Section Histology, Immunohistochemistry, and Tissue Staining

Skeletal Preparations

Skeletal preparations were used to visualize mineralized bone and cartilage morphology in whole mount. Embryos were fixed in 10% neutral buffered formalin overnight, stained with Alcian blue and/or Alizarin red, and cleared in glycerol as described (Wasserug, 1976). Results in Chapter 2, Figure 4, Fig. 18D, 18L, 19D, and Fig. 19E.

Alkaline Phosphatase Assay

Detection of alkaline phosphatase was used to visualize the activation of enzymes characteristic of early osteogenesis. Embryos were fixed in 4% paraformaldehyde for 20 min at 4°C, and stained using 4-nitro blue tetrazolium

chloride (NBT; Roche) and 5-bromo-4-chloro-3-indolyl-phosphate (BCIP; Roche) as described (Liu, 1999). Results in Chapter 2 and Figure 6.

Milligan's Trichrome

Trichrome staining was used to visualize osteoid deposition and gross morphology in tissue sections. Refer to Presnell and Schreiber, 1997. Results in Chapter 2 and Figure 6.

Antibody staining

For standard protocol, refer to Schneider, 1999.

- *Q α PN*:
 - o Primary antibody from Developmental Studies Hybridoma Bank (DSHB), University of Iowa. Tissues fixed in Serra's fixative, 4C, overnight, embedded in paraffin, and sectioned at 7 μ m (Fig. 3D, 4J, 5B-C, 8I-M, 8B).
- *GFP*:
 - o I tried three antibodies, anti-GFP from Abcam (ab290), from Molecular Probes, and from Santa Cruz. Antigen binding was detected only with ab290 (at a dilution of 1:500-1:1000). Specificity of binding was confirmed by checking localization of over-expression with notes taken of eGFP visualization at the time of embryo collection.
 - o I tried three fixatives. Carnoy's allowed the best antigen binding with the least background, Serra's allowed antigen binding of equal

strength with some background, and 4% PFA did not allow antigen binding.

- I tried two embedding conditions: fixed frozen, and fixed paraffin-embedded. Both allowed equivalent antigen binding.
- Antigen retrieval with a 5 min treatment of Ficin at 37C did not drastically affect signal strength.

- *Cyclin and cdk antibodies*

- Antibodies against cyclin E, B1, and A, as well as cdk2, cdk4 and KI-67 from Santa Cruz, were tested on 4% PFA fixed, paraffin embedded sections; with HRP and fluorescent secondary antibody; in frozen sections fixed in Carnoy's, Serra's, and 4% PFA; without antigen retrieval and with antigen retrieval in pH 9.0 TE Buffer and citrate buffer. However, I could not recognize patterns of expression specific to any tissues or cellular localization under any condition, and all antibody stains looked equivalent to background. The procedure was always run with one Q ϕ PN positive control section and antibody, which was fine.

- *Viral coat:*

- AMV-3C2 from DSHB recognizes viral gag protein.
- Work from the lab of Cliff Tabin (Smith et al., 2000) describes AMV-3C2 antibody staining on 4% PFA sections, but cites another lab that used Zamboni's fixative on frozen sections.

- I used AMV-3C2 at a dilution of 1:50. In 4% PFA fixed frozen sections, antibody binding localized to areas of confirmed viral expression (by RCAS-GFP visualization at time of collection). However, in 4% PFA fixed paraffin sections, antibody binding was ubiquitous in the tissue, whereas in an adjacent section, viral envelope mRNA was detected only unilaterally by *in situ* hybridization. Thus, the antibody seems only to work with 4% PFA frozen sections and not paraffin sections under these conditions.
- *Fluorescent secondary antibodies:*
 - Seem to cross-react with BrdU, causing nuclear fluorescence in all channels for BrdU injected embryos.

4H. Protein Expression Analyses

Western Blot

Western Blot was used to detect protein expression and quantify levels relative to β -actin. This was especially useful for understanding cell cycle expression, since cyclins are controlled by degradation at the protein level; for Q ϕ PN, which has only been described as a protein, and for detecting functional protein in over-expression/gain-of-function experiments.

- *Reagents:*

Table 3. Primary Antibodies for Western Blot

Antigen Specificity	Manufacturer; Product Name
Q ϕ PN	Dev. Studies Hybridoma Bank
B-actin	Abcam; ab8229
Cyclin E	Santa Cruz; M-20
Cyclin B1	Santa Cruz; H-433
p27	BD Biosciences; BD610241
Cyclin D1/D2	Santa Cruz; C-17
Runx2	Santa Cruz; S-19
Cdk2	Santa Cruz; D-12

Table 4. Secondary Antibodies for Western Blot

Product Name	Manufacturer
Alexa Fluor 488 goat anti-mouse	Invitrogen
goat anti-mouse IRDye 800CW	LICOR
goat anti-rabbit IRDye 680LT	LICOR

- *Protocol:*
 - o Mandibles from HH24-HH30 control embryos and HH27 chimeric embryos were syringe-lysed with a 22½G needle in 1X RIPA Buffer with cOmplete, Mini Protease Inhibitor Cocktail (Roche) and 0.5 mM PMSF. The samples tested for cyclins and p27 expression were sonicated using a Misonix cup-horn sonicator at 3x5 sec at 100%. However, prior to purchasing the Misonix sonicator, I relied

on an intermittently working, unlabeled, stick sonicator to process samples tested for Q ϕ PN and Runx2.

- Proteins were separated on 10% SDS-polyacrylamide gels, transferred onto nitrocellulose membranes at 300mA for 1.5 hours, blocked in 5% milk, and detected with the appropriate primary antibody. Appropriate secondary was applied prior to imaging. Antibody-bound proteins were visualized using a LICOR Odyssey Infrared Imager, and quantifications were performed using LICOR Odyssey software.

- *Results:*

- No difference in protein visualization was observed between 3-5X, 5, 10, 15 second pulses of Misonix cup-horn sonication at 50%, 75% or 100%. For this reason I continued my studies with the briefest sonication to prevent degradation (3 X 5sec at 100%). However, I did not optimize the cup-horn sonicator to detect Runx2 expression. Since Runx2 is a DNA-binding transcription factor, it may more sonication to best release it. This is readily apparent in the Western blot of a pellet from lysed DF-1 cells transfected with pMES-Runx2, sonicated by an old machine – upon resonation, a clear, strong band is visible on the blot (Fig. 20B).
- Western Blot with Q ϕ PN bound a larger than 250 kDa protein complex present only in quail tissues in a dose-dependent manner. This band was not observed in duck tissues (Fig. 20A).

- Cdk2 was detected at low levels in HH24, HH27, and HH30 quail. No overt stage-specific protein expression pattern was seen. Duck tissue was not tested for cdk2 expression.

4I. Vascularization Analyses

Calcium and phosphorus levels in blood

Calcium and phosphorous levels were measured to evaluate the ability of a chimeric host environment to provide systemic minerals necessary for mineralization. Blood (20-100 μ L) was collected from embryos via a heat-pulled Pasteur pipette inserted into the vitelline vein. Blood serum was isolated by incubating for 1h at 37°C, followed by centrifugation (700g, 10 min). Calcium and phosphorus levels in collected or commercially available control serum (DC-Trol, Diagnostic Chemicals Ltd., Charlottetown, PEI) were measured in a Spectra Max M5 multi-well plate reader (Molecular Devices, Sunnyvale, CA) using the Calcium and Phosphorus Assay kit following manufacturer's protocol (Diagnostic Chemicals Ltd.). Results in Chapter 2 and Fig. 5Q.

Quantification of Blood Vessel Volume

Blood vessel was quantified to evaluate the ability of the host environment to provide supportive tissues and vasculature to distribute growth factors and minerals necessary for mineralization. Using needles from hollow glass rods (diameter 0.5 mm, Sutter Instruments Co.) pulled on a mechanical needle puller

(Sutter Instruments Co., Model P-87), 5 μ L of FluoSphere carboxylate-modified microspheres (0.2 μ m, 580/605; Invitrogen) or rhodamine-conjugated *Lens Culinaris Agglutinin* (Vector Laboratories, Inc.) was injected into a vitelline vein using a PV830 Pneumatic Picopump (World Precision Instruments, Sarasota, FL). Fifteen min after injection, embryos were fixed in 4% formaldehyde overnight. For FluoSphere-injected embryos, embryos were cleared in glycerin and visualized under a MZFLIII stereoscope (Leica). For quantification, relative fluorescent units (RFU) measured on donor versus host sides using a Spectra Max M5 multi-well plate reader. For lectin-injected embryos, embryos were incubated in 5-30% sucrose/PBS overnight, embedded in tissue freezing media (Triangle Biomedical Sciences, Durham, N.C.), and cryosectioned (20 μ m intervals). Embryos were stained with Q ϕ PN and Alexa Fluor 488 goat anti-mouse IgG (Invitrogen) secondary antibody, and Hoescht reagent. Quantification of blood vessels was performed as described above for quantifying BrdU-positive cells. Results in Chapter 2 and Fig. 7H-K.

4J. Cell and Tissue Culture

Transfection of DF-1 Cells

Transfection was performed for transient plasmid over-expression or RCAS production.

- *Reagents:* Superfect for transfection, alpha-MEM w/o nucleosides with 10% FBS is used for DF-1 growth media.

- *Ratios*: 10ug DNA in 300ul media (without FBS), 60ul superfect.
- *Protocol*: Follow Superfect manufacturer's instructions

Production of RCAS Virus

RCAS Virus was produced in the lab, for *in ovo* stable over-expression experiments.

- *Protocol*:
 - o Originally described by Morgan and Fekete, 1996.
 - o Transfect DF-1 chick fibroblast cells (American Type Culture Collection; Manassus, VA) with RCAS plasmid using Superfect. Viral titer can be increased with addition of Polybrene at 0.8ug/ml. Always grow RCAS-GFP in tandem with virus-of-interest for a positive control of transfection success.
 - o Expand cells up to 3 x T-125s at 90% confluence in growth media (alphaMEM without nucleosides +10% FBS),
 - o At 90% confluence, switch over to media with only 1% FBS and begin supernatant collections the following day, always replacing media with Media + 1% FBS. Collect for three days, snap freezing and storing supernatants in -80C.
 - o Thaw and spin supernatants using ultra-centrifuge: SW-28 rotor, 25,000 RPM, for 2 hours at 4C. Use compatible ultra-centrifuge tubes.

- Gently pour off supernatant, dab lip of tube with kimwipe to further decrease amount of supernatant
- Pipet up and down to resuspend virus, pool samples if necessary
- Aliquot to 5ul in microfuge tubes, snap freeze on dry ice → store in -80C.

4K. Molecular Biology

In situ hybridization

In situ hybridization was used to detect localization of mRNA expression.

- *Protocol:*

- *In situ* hybridization analyses were performed as described in Albrecht et al., 1997. Briefly, sections were hybridized with ³⁵S-labeled chick riboprobes generated from plasmids containing chicken collagen type I α (COL1), Runx2, tissue non-specific alkaline phosphatase (TNAP), bone sialoprotein (BSP), and osteopontin (OPN). Results in Chapter 2, Fig. 5E-P, Fig. 7D, 7F, Fig. 9E-F, Fig. 17D-H.

qRT-PCR

Quantitative real-time PCR (qRT-PCR) was performed to quantify changes to gene expression over time as development and osteogenesis proceeded, or to quantify changes induced by gain-of-function experiments.

- *Protocol:*

- Analyses were performed on total RNA (RNeasy kit, Qiagen) isolated from embryonic mandibles of quail, duck, and bilaterally transplanted quack. cDNA was generated using the iScript cDNA synthesis kit (BioRad) and qPCR was performed in triplicates using the iScript SYBR Green RT-PCR kit (Biorad) on an iQ5 cycler (Biorad). Primers were generated using NCBI Primer-BLAST software. Primers were tested on avian samples and DEPC-treated water before experimental runs. Melt curves were checked for binding specificity and amplification of only a single target product. DEPC-treated water was always used as a negative control during negative runs. In early runs, GAPDH was used for normalization in quantifications. In later runs, RPL19 was used as a TGF β -insensitive gene for normalization (Results in Chapter, 2, Fig. 7E, 7G, 8E, 9D, 9H, 14F, 17A-C, and Fig. 20C)

4L. Generation of chimeras

Neural crest transplants allow us determine the instructive effects of neural crest when surrounded by a foreign environment. Eggs from Japanese quail (*Coturnix coturnix japonica*) and white Pekin duck (*Anas platyrhynchos*) (AA Labs, Westminster, CA) were incubated at 37°C until reaching HH9.5. Embryos were handled following University and NIH guidelines. Tungsten needles and Spemann pipettes were used for operations (Noden, 2006; Schneider and Helms, 2003). Unilateral grafts of rostral hindbrain and midbrain neural crest

were excised from quail donors and transplanted into stage-matched duck hosts, producing chimeric 'quck' (Schneider and Helms, 2003; Figure 3). Equivalent transplants were also made from duck to quail ('duail'). Donor tissue was inserted into a host that had comparable regions of tissue removed. Control orthotopic grafts and sham operations were made within each species. Controls were incubated alongside chimeras to ensure that stages of grafted cells were accurately assessed. In addition, unilateral transplants provided an internal control on the un-operated host side.

4M. Tools

Pulling Needles for Injection

- Borosilicate glass: 10 cm length, O.D. 1.0mm, I.D. 0.75 mm
- Sutter P-97 Micro-capillary Puller Settings: Heat 450, Pull 150, Vel. 40, Time 150

Tungsten needles for surgery

- Pull Pasteur pipets, separate halves to use as handles
- Cut tungsten wire to manageable length (usually half)
- Insert one end of wire into thin end of pulled pipet, set with hot glue
- Use forceps to bend wire to 120 degree angle. For a sharp bend, pull and bend at the same time.
- Hold outer end of wire into a propane torch flame until sharpened.

4N. Statistical methods

Unpaired Student's t-tests were used for comparisons of continuous variables between exactly two groups. Two-tailed $P < 0.05$ was considered statistically significant (*), and $P < 0.01$ was considered very statistically significant (**).

4O. Oligonucleotide Sequences

All primers are designed against chick sequences unless otherwise noted (prefix of "mo." denotes mouse, and "av." denotes universal avian primer working in quail, chick, and duck. All oligos are listed 5' to 3', a suffix of "F" denotes forward, "R" denotes reverse, and a number before F or R indicates the base pair number at which oligo binding begins when aligned with the NCBI gene sequence. All primers were designed by me, unless a reference or initials are noted for other members of the lab (AJ = Andrew Jheon, ELE = Erin Ealba, KB = Kristin Butcher).

Table 5. Primers for detecting mRNA expression by qRT-PCR

Primer Name	Primer Sequence	Designed by
	TGG ACC TTT CCA GAC CAG CAG	
av.Runx2 F	CA	ELE

	GGC AAG TTT GGG TTT AGC AGC	
av.Runx2 R	GT	
av.RPL19 F	ACG CCA CT CGC GTC AG	ELE
av.RPL19 R	ATA TGC CTG CCC TTC CGG CG	
Bsp F	CGC TGC ATC GCT ACA AGG GCA	
Bsp R	CCC CAC ATC CCC GAG GGT CA	
Col1a1 F	CCC GAC CCT AAG ACA AAG AG	AJ
Col1a1 R	GCT ACT TAC TGT CCT CTT CTC C	
cyclin D1 422F	CTT GGA TGC TGG AGG TCT GC	
cyclin D1 601R	CTG CGG TCA GAG GAA TCG TT	
cyclin D2 44F	TGC CGG ACC CGA ACT TGC TC	
cyclin D2 286R	ACT TTC GAG TGG GCA CCA CAG C	
eGFP F	GCA GAA GAA CGG CAT CAA GGT	Li et al, 2006
eGFP R	ACG AAC TCC AGC AGG ACC ATG	
mo.cyclinD1 204F	TGA GGA GCA GAA GTG CGA AG	
mo.cyclinD1 379R	AGA TGC ACA ACT TCT CGG CA	
mo.OPG 904F	CTG CCT GGG AAG AAG ATC AG	

mo.OPG 1129 R	TG TGA AGC TGT GCA GGA AC
mo.RANKL 256F	ACC AGC ATC AAA ATC CCA Ag
mo.RANKL 461R	TTT GAA AGC CCC AAA GTA CG
mo.Runx2 357F	CTG GTC CGC ACC GAC AGT CC
mo.Runx2 1510R	CAG CGT CAA CAC CAT CAT TC
OPG F	ACG CTT GTG CTC TTG GAC AT
OPG R	TAC TGG TCT GGG TAC GGA GC
p21 1201F	TGT GCC GAG AGT GTC TTC AGG C
p21 1425R	TGG GCC CGT ATG CTT TCC GTG
p27 692F	CAT GCC AGA GGA AGT GGA AT
p27 928 R	TTC GGC CTA CAC AGT GAG TG
p53 360F	GGA GGC GGG CAC AGC CAA AT
p53 609R	CCG GAT GAG GTG CTG TGC GG
PAI1 F	AAG AGC GTG GAC TTT GAG GA
PAI1 R	GAT TTC CAC AAG CCC TTG AA
RANKL F	TGT TGG CTC TGC TTG TC
RANKL R	CCT GCT TCT GGC TCT CAA TC

RCAS gag F	GGT TGC TTA TGT CTC CCT CAG
RCAS gag R	GTT GTT TT CCC ACC TCC TC
RPL19 F	ACG AAA TTC CAG CCG CCC CC
	ACT GCC AAC GTA GAA CTC GGG
RPL19 R	GA
Runx2 F	TGG CAG AGG GAA GAG CTT TA
Runx2 R	ATA CTG GGA TGA GGA ATG CG
Smad 3 F	CAT CCC AGA GAC ACC TCC TC
Smad 3 R	GTG TGC CGG AGA CAT AGG AT
βgal 725F	CTG CGA TCA CGA CTA CCT CA
βgal 910R	AGC ATT GCC CAG ATT TGG TC
TBR1 F	TGT AGG CAC ACA AGG CAA AC
TBR1 R	TTC CTA CTC TGT GGT TGG GG

Table 6. Primers for Cloning

Primer Name	Primer Sequence	Designed by
OPG CLAI F	CTG ACC ATC GAT GGC ACC ATG	

	AAC AAG TTC CT
	CTG ACC ATC GAT GGT TAG ACA
OPG CLAI R	CAT CTT AC
RUNX2 36F	CTC TTC AGC GTG ACA CC
RUNX2 46F	CGT GAC ACC ATG TCA GCA A
RUNX2 379R	TCT CCT AAG GCC ACC ACC TT
RUNX2 562R	GGG GGA TTT GTC AGG ACA GT

Table 7. Primers for Sequencing

Primer Name	Primer Sequence	Designed by
OPG 41F	ACG CTT GTG CTC TTG GAC A	
OPG 1205R	TCA GTT GAC TCC CTA CCA TTT C	
	TAG TAA TCA ATT ACG GGG TCA	
pcDNA3.1 CMV F	TTA G	
	CTC ATT TTA TTA GGA AAG GAC	
pcDNA3.1 polyA R	AGT G	
	TGC TGG TTG TTG TGC TGT CTC	Laboratory of
pMES F	ATC	Cathy Krull

pMES R	TAA CAT ATA GAC AAA CGC ACA CC	
RCAS insert	CTT AAT AAT GCG GCC TGA CC	Diane Hu
		Xin Li, Lab of Ralph
RCAS Gateway	CTG AGC TGA CTC TGC TGG TGG	marcucio
RUNX2 36F	CTC TTC AGC GTG ACA CC	
	GTT GCA ACA AAT TGA TGA GCA	
TOPO Gateway F	ATG C	Invitrogen
	GTT GCA ACA AAT TGA TGA GCA	
TOPO Gateway R	ATT A	

Table 8. Primers for shRNA Synthesis

Primer Name	Primer Sequence	Designed by
Generic shRNA 3'	CGC GAA GCT TCC AAA AAA GCG CGG ATC CGT TTC GAT TTC CAG AAC CAC TTA CTC GAG AGT GGT TCT GGA AAT CGA AAT TCT	
p27 KB2 shRNA 5'	TTT TTG GAA GCT T	KB
p27 T2 shRNA 5'	GCG CGG ATC CGT AAA CGG GAA	KB

TGG CCA GTT TAC TCG AGA ACT

GGC AAT TCC CGT TTA CTT ATT TTT

TGG AAG CTT

GCG CGG ATC CGA ATC TCA GAG

GAC ACT CAT TAC TCG AGA TGA

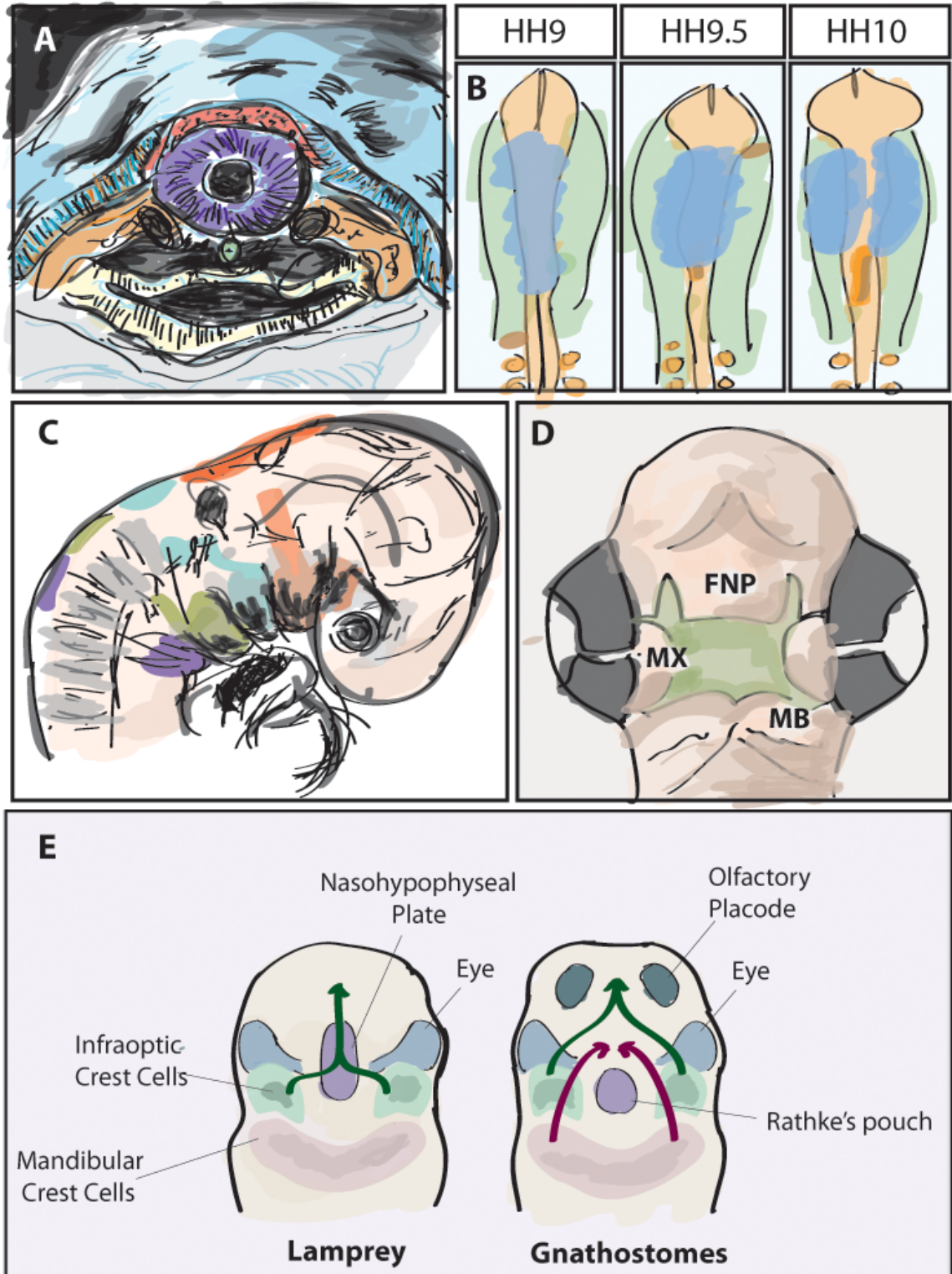
GTG TCC TCT GAG ATT CTT ATT TTT

p27 T3 shRNA 5'

TGG AAG CTT

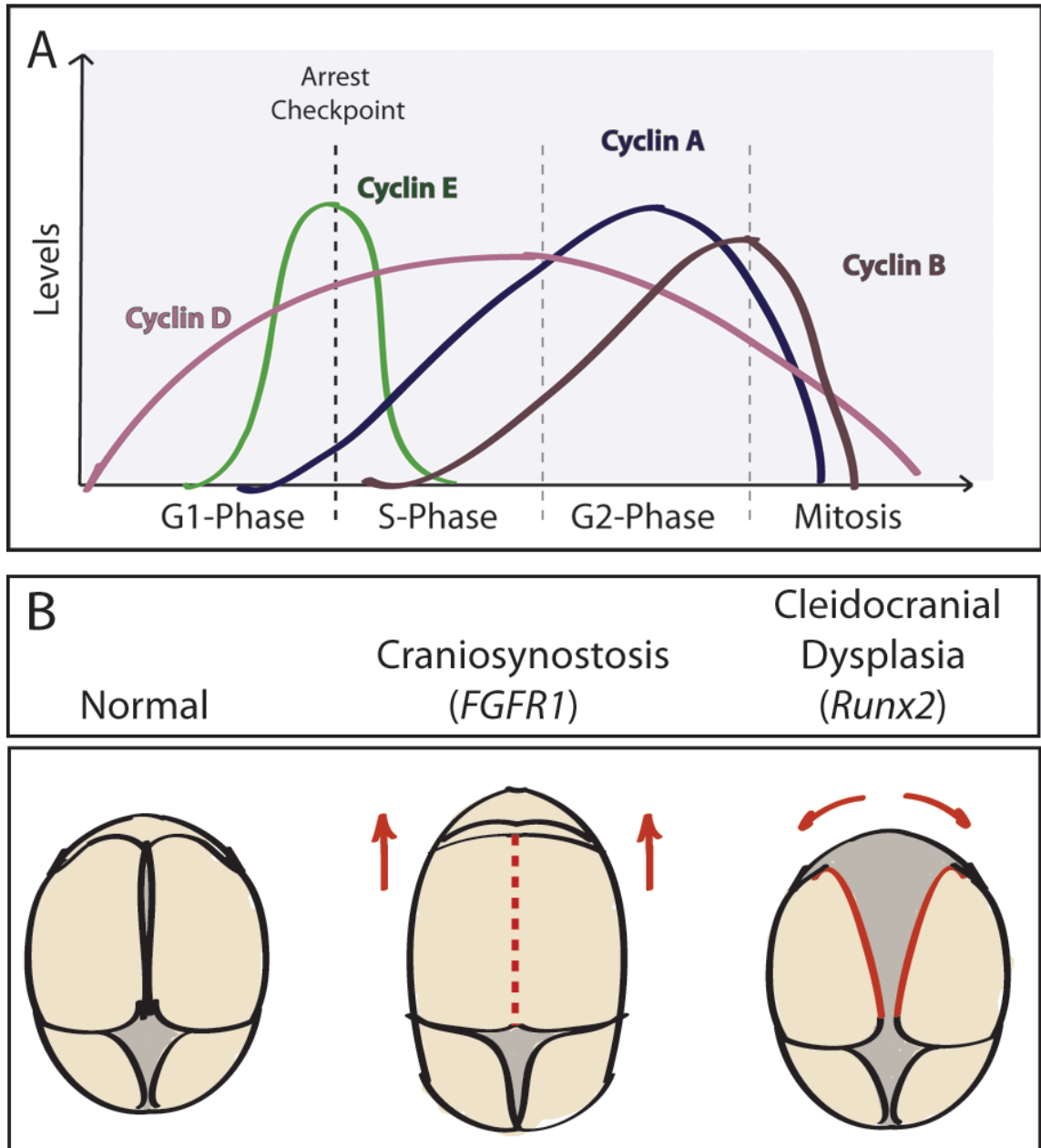
KB

Figure 1. Ontogenetic and Phylogenetic Origins of the Face



(A) Neural crest mesenchyme (pink) arises from the lateral margins of the neural fold (blue), above the neural tube (purple). Mesodermal mesenchyme gives rise to many overlapping cell types (orange). Notochord in green and endoderm in yellow (adapted from Larsen, 1993). **(B)** Dorsal view of neural crest migration medially from anterior neural tube (blue). At this stage, neural crest cells can be easily transplanted or extirpated. In this schematic, the anterior neuropore is at the top, and the somites are at the bottom. **(C)** Streams of neural crest migrate rostrally. Neural crest from the mid-brain and hind-brain region gives rise to mesenchyme of the first arch, highlighted in orange (adapted from Guthrie, 2007). **(D)** The facial primordial in chick, HH23, prior to fusion. Frontonasal process (FNP, including nares) will fuse with the maxilla (mx) to form the upper beak. Mandibular primordial (mb) will fuse at the midline to form the lower beak. **(E)** Neural crest migration in lamprey versus gnathostomes. Formation of an upper jaw is physically restricted by the presence of a nasohypophyseal plate (adapted from Kuratani et al., 2001).

Figure 2. Molecular and Cellular Regulation in Craniofacial Development

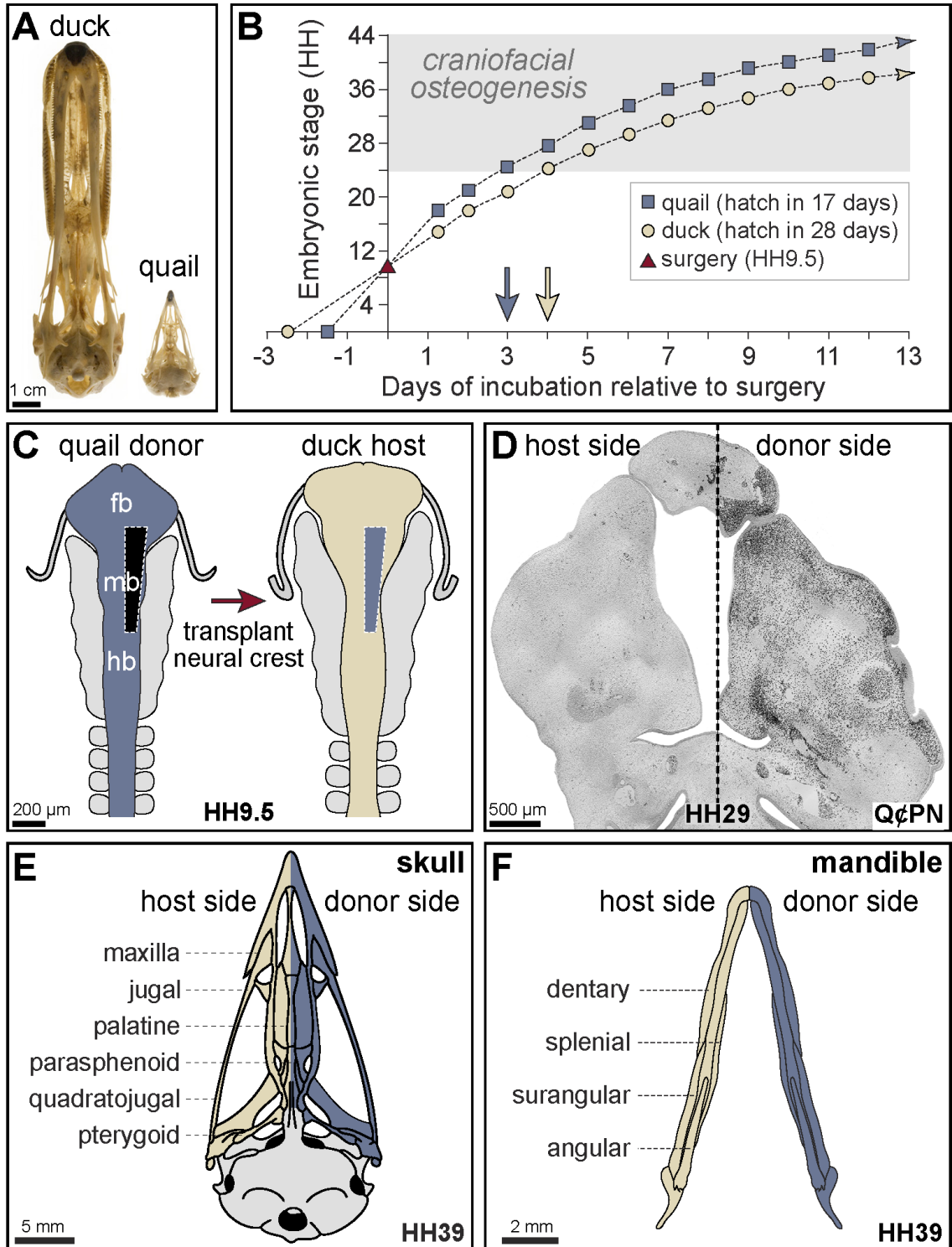


(A) Rising and falling levels of cyclins dictate the progression of the cell cycle.

Cyclin D drives progression for the length of the cycle. **Cyclin E** promotes entry

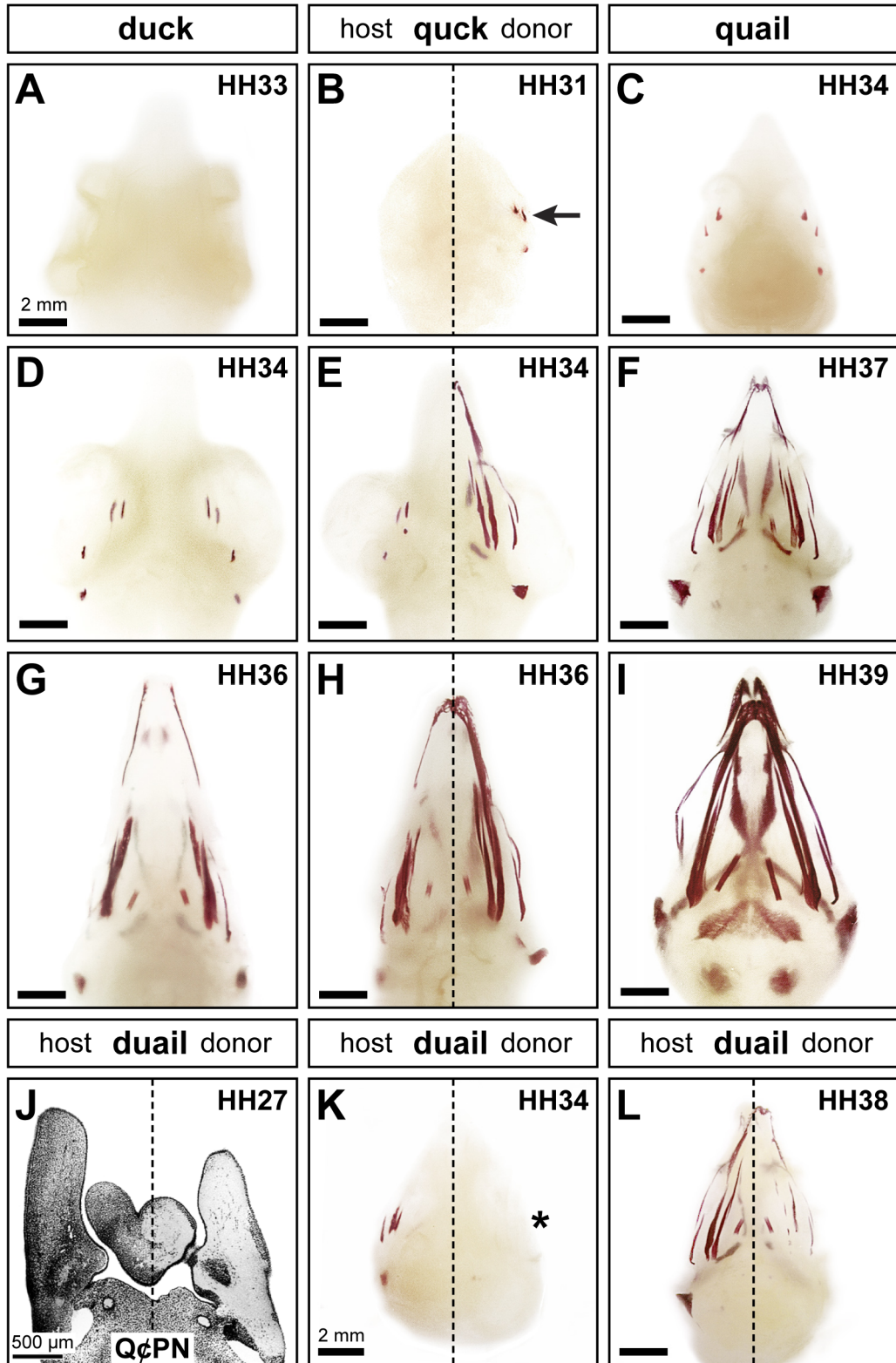
into S-phase, a key checkpoint for cells fated to continue proliferation versus differentiate. **Cyclin B** controls entry into mitosis. **(B)** Skull shape changes due to changes to timing of osteogenesis at sutures in human disease. Red dotted line indicates prematurely fused suture in craniosynostosis, often due to loss-of-function *FGFR1* mutations. Red arrow denotes force causing skull elongation and frontal bossing. Red solid line indicates open sutures in craniosynostosis, often caused by partial *Runx2* deficiency. Red arrows denote expansion of forehead region, which leads to the wide set eyes that are often observed in patients with craniosynostosis.

Figure 3. Avian Chimeric System



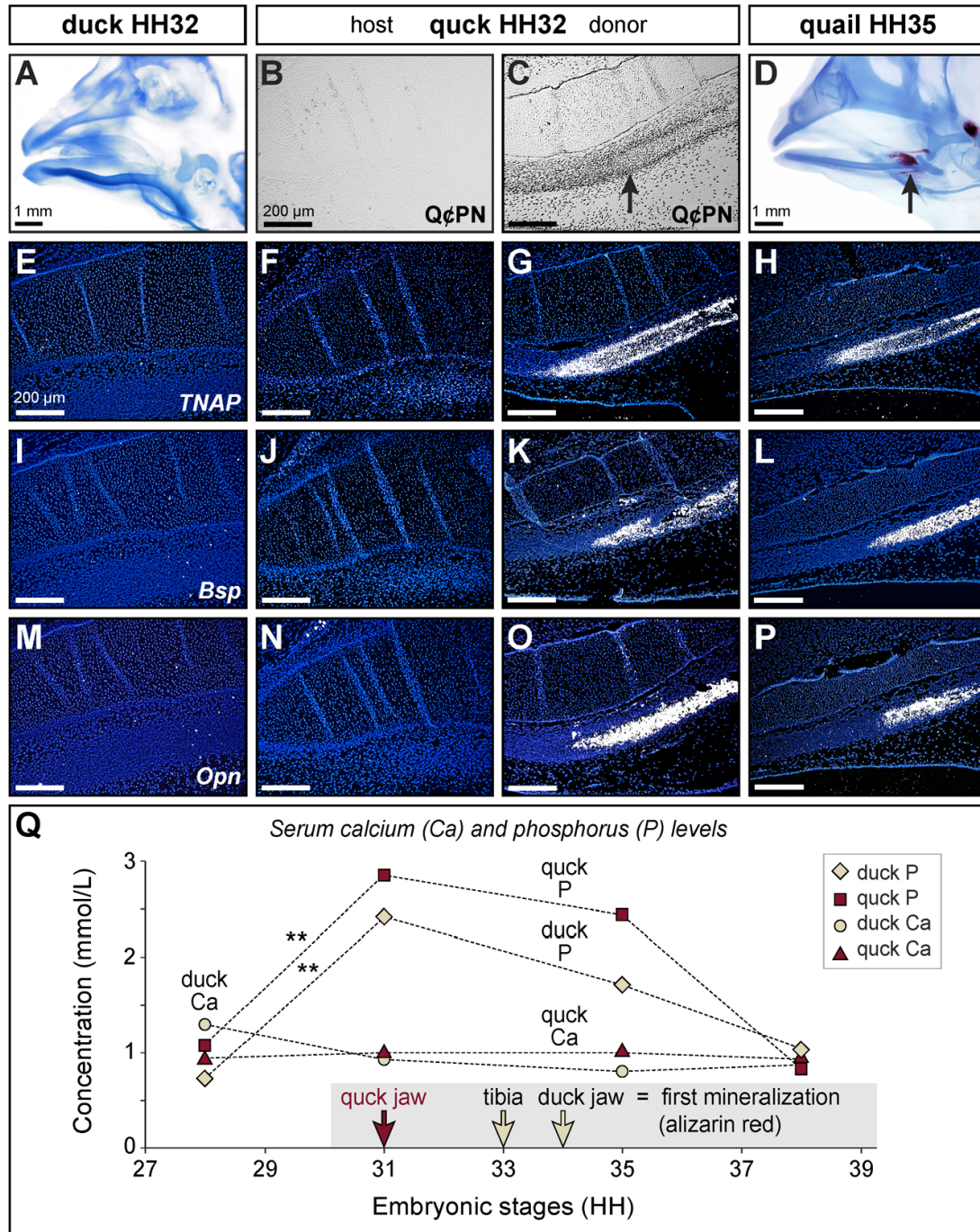
(A) Adult quail skull (left), adult duck skull (right). **(B)** Graph illustrating the distinct developmental trajectories of quail (blue squares) versus duck (tan circles) after being stage-matched at HH9.5 for surgery (red triangle on Y-axis). Approximately three HH stages separate quail and duck embryos within two days following surgery, and this three-stage difference remains relatively constant throughout osteogenesis in the mandibular arch. **(C)** Schematic of rostral neural tube at HH9.5 depicting the levels of NCM grafted unilaterally from quail (blue) to duck (tan). **(D)** Coronal section through the mandibular arch of a HH29 chimeric quack (rostral at top). Quail donor NCM (black) are visualized by the quail-specific antibody Q ϕ PN on the surgical (right) side, while few to no quail cells are observed on the contra-lateral duck host side. **(E)** As shown schematically, quack skulls have a side derived from the duck host as well as a side formed by the donor quail. **(F)** The lower jaw skeleton depicting the contributions of donor and host NCM to cartilage and bone.

Figure 4. NCM Controls Timing of Mineralization



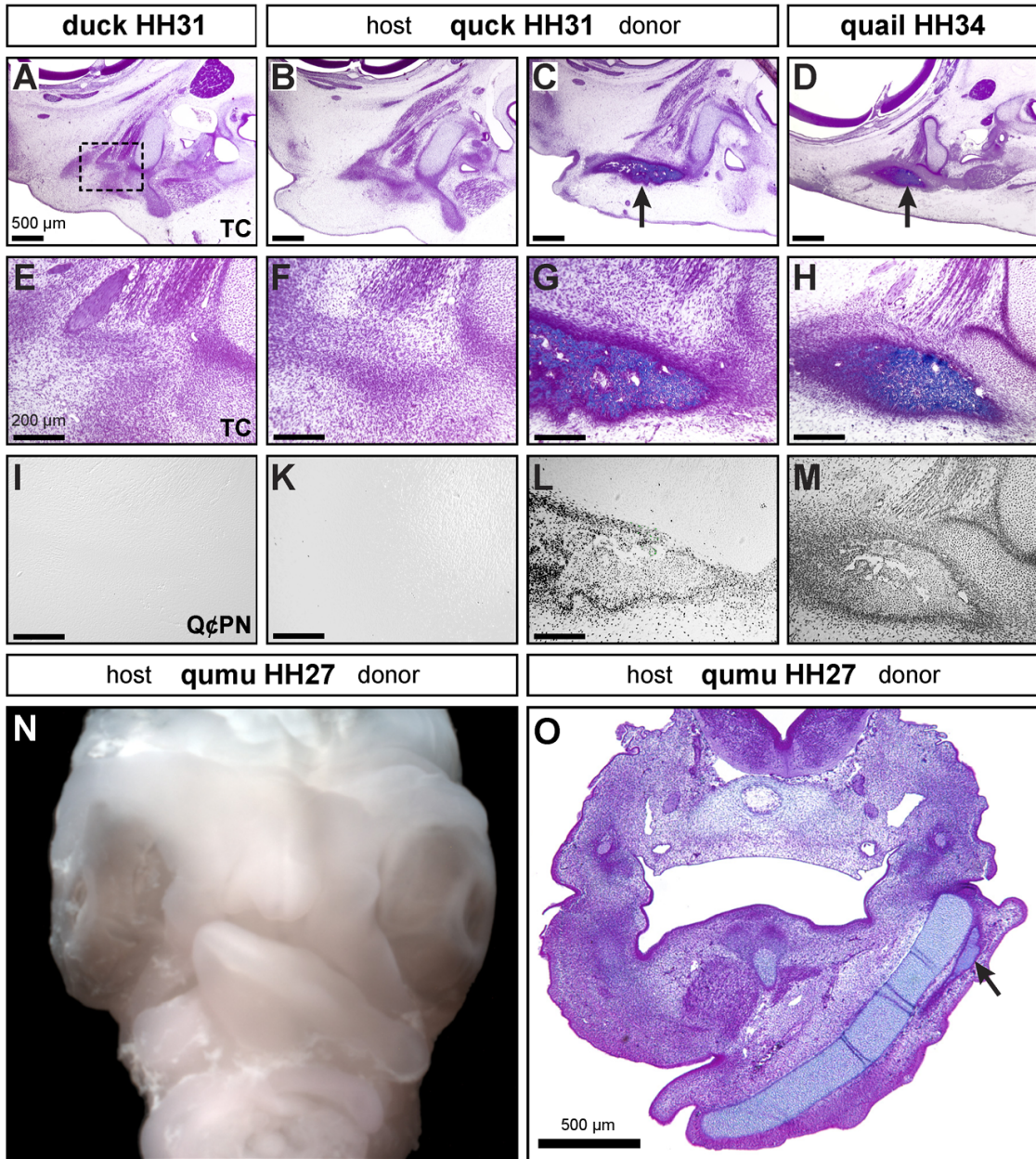
(A-I) Alizarin red staining showing early mineralization (arrow) in quack compared to stage-matched duck (ventral view). **(J-L)** Delayed mineralization (*) in duck donor NCM of duail.

Figure 5. NCM Controls Expression of Mineralization Genes and Levels of Circulating Minerals



(A) Whole mount skeletal preparation of a duck at HH32 reveals that mineralization has yet to occur in the jaw. **(B, C)** Q ϕ PN staining of a duck at HH32 shows abundant quail-derived NCM on the donor side of the embryo. **(D)** By HH35 mineralization can be detected in the angular bone (arrow) of quail (and duck). **(E-P)** Molecular markers of mineralization are not yet expressed in HH32 duck or the host side of quack, whereas expression on the donor side is like that in HH35 quail. **(Q)** Serum phosphorous levels increase significantly by HH31 in both control duck (tan diamond) and quack (red square), preceding the first evidence of mineralization in the jaw by at least three stages. Meanwhile, serum calcium levels remain constant throughout the time points studied (HH28-38) in control duck (tan circle) and quack (red triangle).

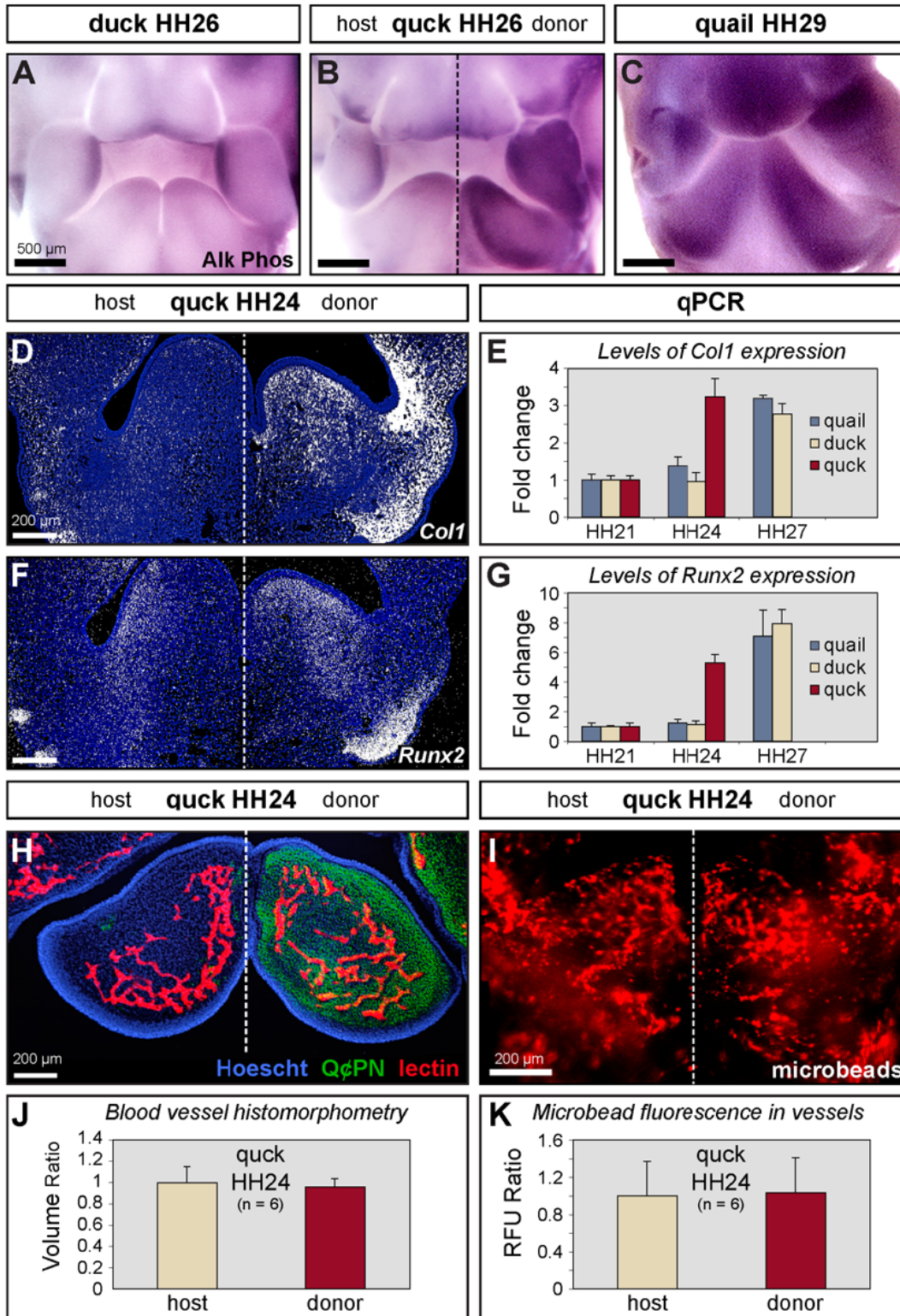
Figure 6. NCM Controls Timing of Osteoid Deposition



(A-H) Trichrome histology of osteoid deposition in quck versus control quail and duck surangular bone **(L-M)** Osteoid is premature coincident with quail donor NCM (QϕPN positive). **(N)** Frontal view of qumu head. **(O)** Trichrome histology

on a coronal section of a quail. Osteoid deposition is apparent on the quail donor side (arrow), though not on the emu host side. **(P-R)** Whole mount detection of alkaline phosphatase activity in quail versus control quail and duck.

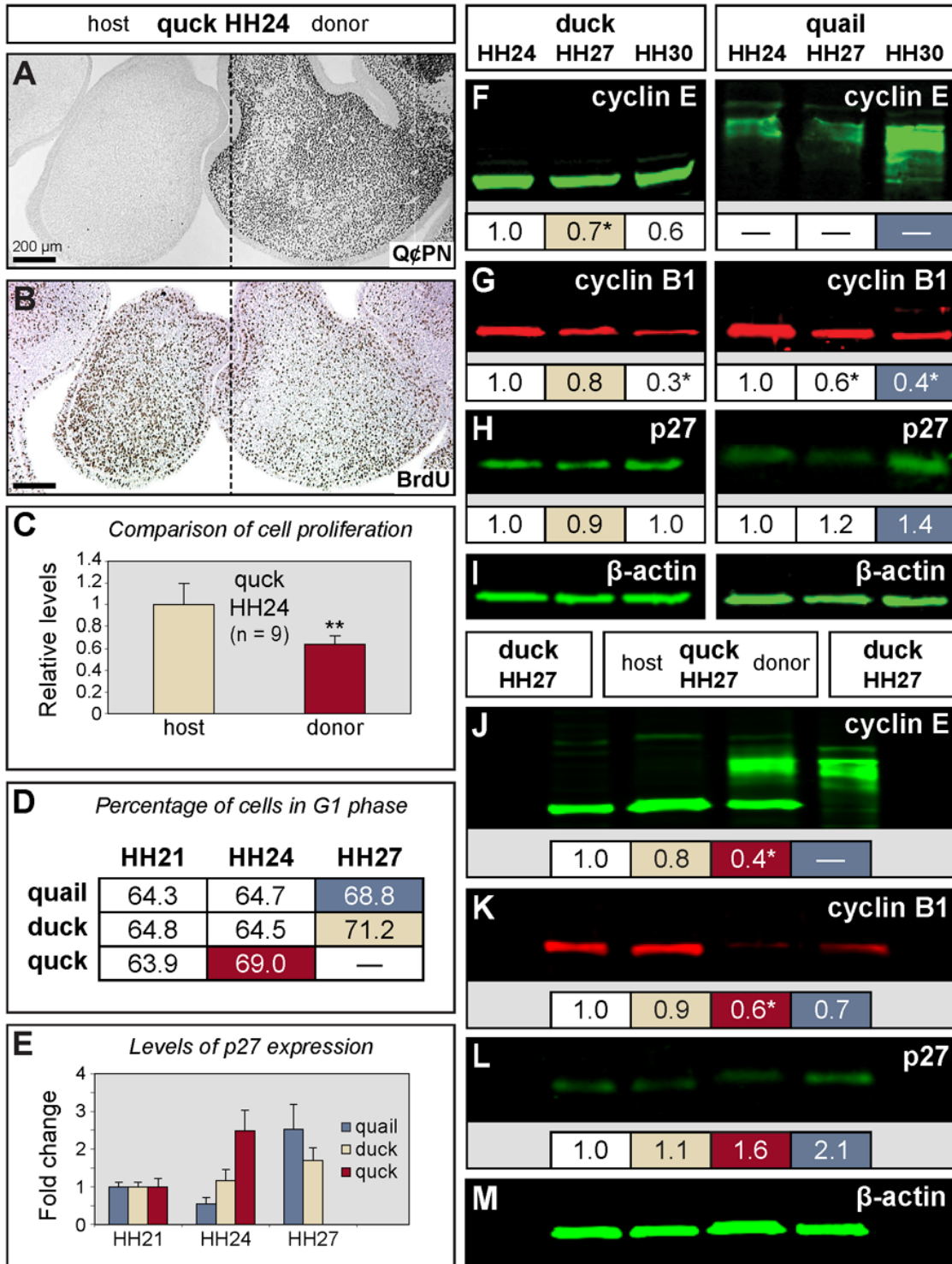
Figure 7. NCM Controls Timing of Osteoblast Differentiation



(A-C) Whole mount detection of alkaline phosphatase activity. Note higher levels on the quail donor side compared to the duck host. **(D,F)** *In situ* hybridization: up-regulation of *Runx2* and *Col1* on the donor side of HH24 quack mandibular section. **(E,G)** qPCR showing *Runx2* and *Col1* mRNA levels in quail, duck, and quack from HH21-HH27. **(H,I)** No difference in vascularization in HH24 donor side of quack mandible versus host control by lectin staining or fluorescent microbead injection. **(J,K)** Quantification of section series and whole mount mandibles for which **H**, and **I** are representative samples.

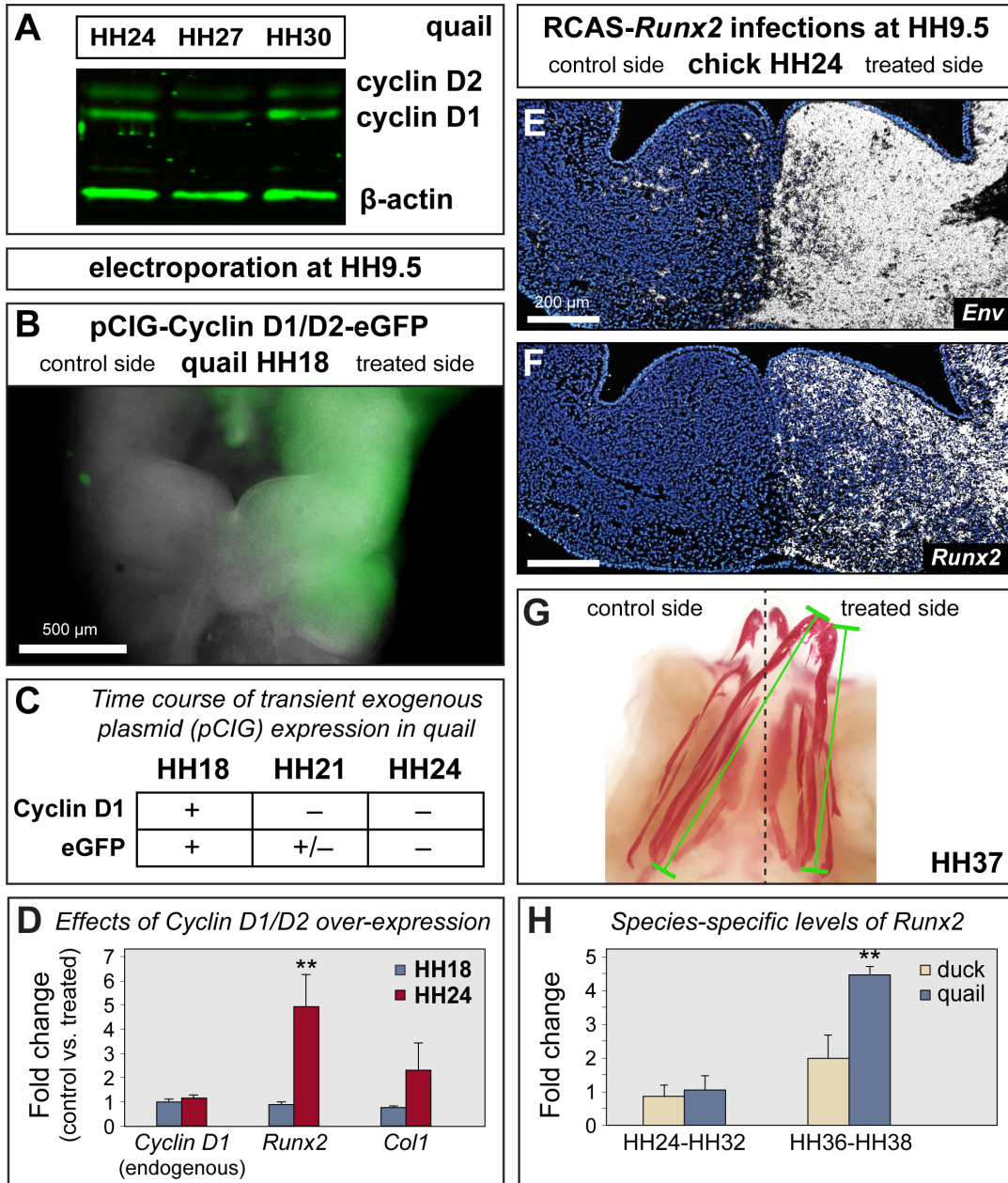
Figure 8. NCM Regulates Stage- and Species-Specific Cell Cycle Progression

Progression



(A) Q ϕ PN staining showing donor cells in chimeric quack mandible section. **(B)** Adjacent section to Fig. 6A showing decrease in number of BrdU-positive cells on the donor side of HH24 quack. **(C)** Quantification of BrdU-positive cells on host versus donor sides of HH24 quack. **(D)** Percentage of cells in G1 arrest versus cells cycling through G2, M and S phase in quail, duck, and quack at from HH21-HH27, as sorted by FACS. **(E)** qPCR showing *p27* mRNA levels in quail, duck, and quack at HH21, HH24, and HH27. **(F-I)** Western blot of cyclin E, cyclin B1, *p27* expression levels in control quail and duck from HH24-HH30, with B-actin as a loading control. Quantifications from multiple blots shown below each panel. **(J-M)** Western blot of host and donor sides of HH27 quack, compared to control HH27 duck and HH30 quail.

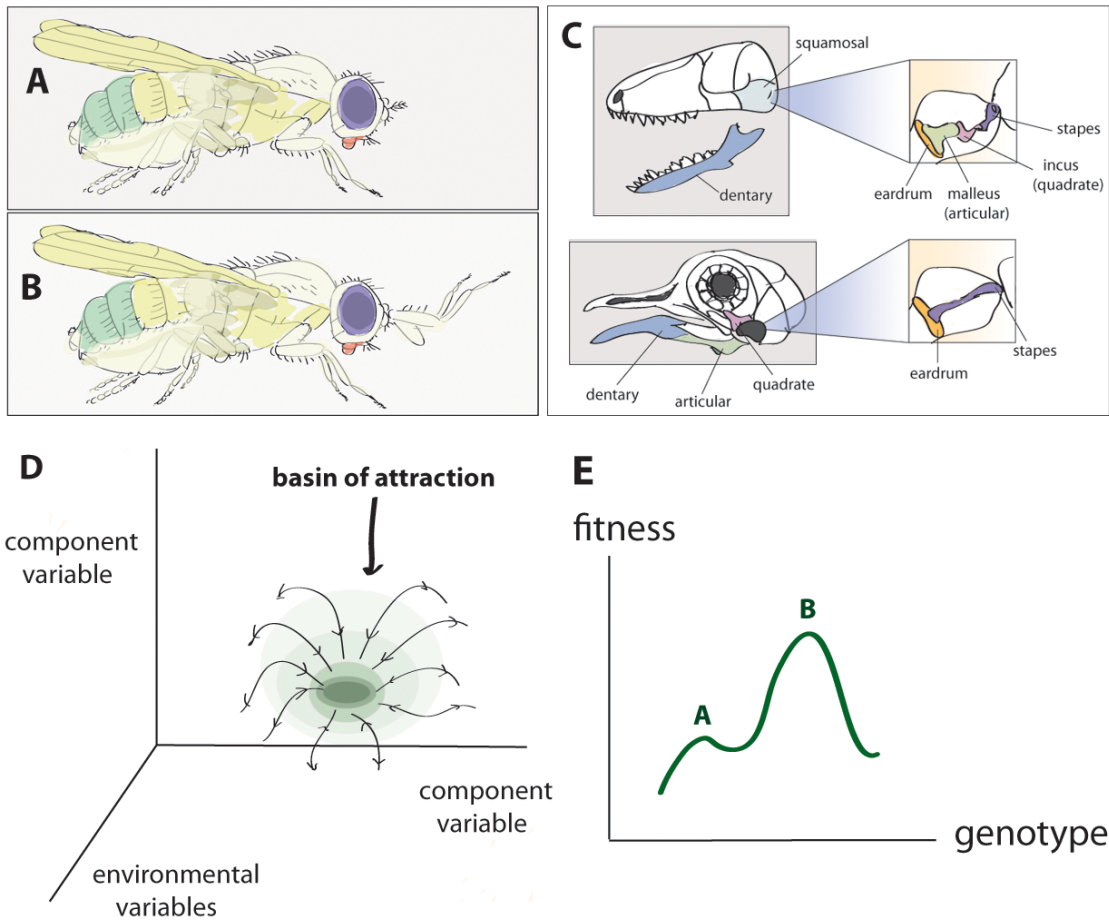
Figure 9. Transient D-type Cyclin and Continuous Runx2 Over-expression Analyses



(A) Endogenous levels of cyclin D1 and cyclin D2 protein in quail HH24-HH30. (B) Unilateral *Cyclin D1/D2* over-expression by electroporation, visualized by eGFP co-expression. (C) Time course of transient exogenous D-type cyclin over-

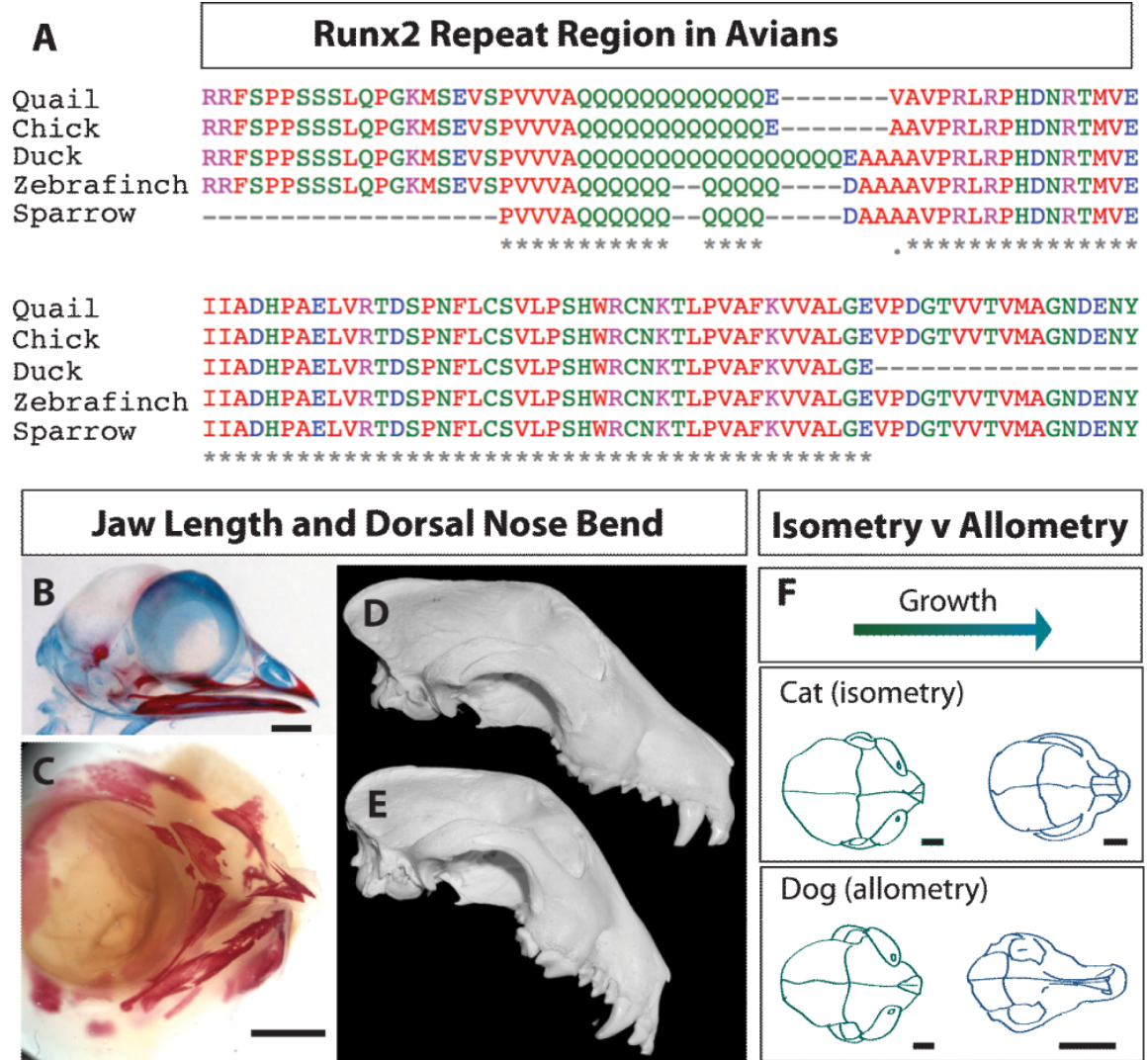
expression in quail. **(D)** Fold change in mRNA expression levels of osteogenic genes D-type cyclin electroporated versus control sides of treated quail mandibles. **(E)** *In situ* hybridization for viral envelope (*env*) and **(F)** *Runx2* transcript showing unilateral RCAS-*Runx2* infection in chick HH24 mandibular sections. **(G)** Skeletal preparation of a representative RCAS-*Runx2* infected embryos with alizarin red, showing shortened jaw on the treated side. **(H)** Species-specific levels of endogenous *Runx2* mRNA.

Figure 10. Laws of Variation



(A) Wild-type *Drosophila* with antenna versus **(B)** *Antennapedia* mutant with second pair of legs in place of antenna (adapted from De Robertis et al., 1990). **(C)** Evolution of the mammalian ear: the malleus and incus arising from the articular and quadrate. The dentary is expanded in mammals to fulfill functions at the jaw joint (adapted from UC Museum of Paleontology, 2012). **(D)** In the geometric model of evolution, a basin of attraction denotes stability of structure and phenotype, while **(E)** fitness peaks are higher for better-optimized structures. The distance between peaks may affect how simple or difficult it would be to reach a change in structure via a change in genotype (adapted from Orr, 1998).

Figure 11. Runx2 Repeats and Facial Shape



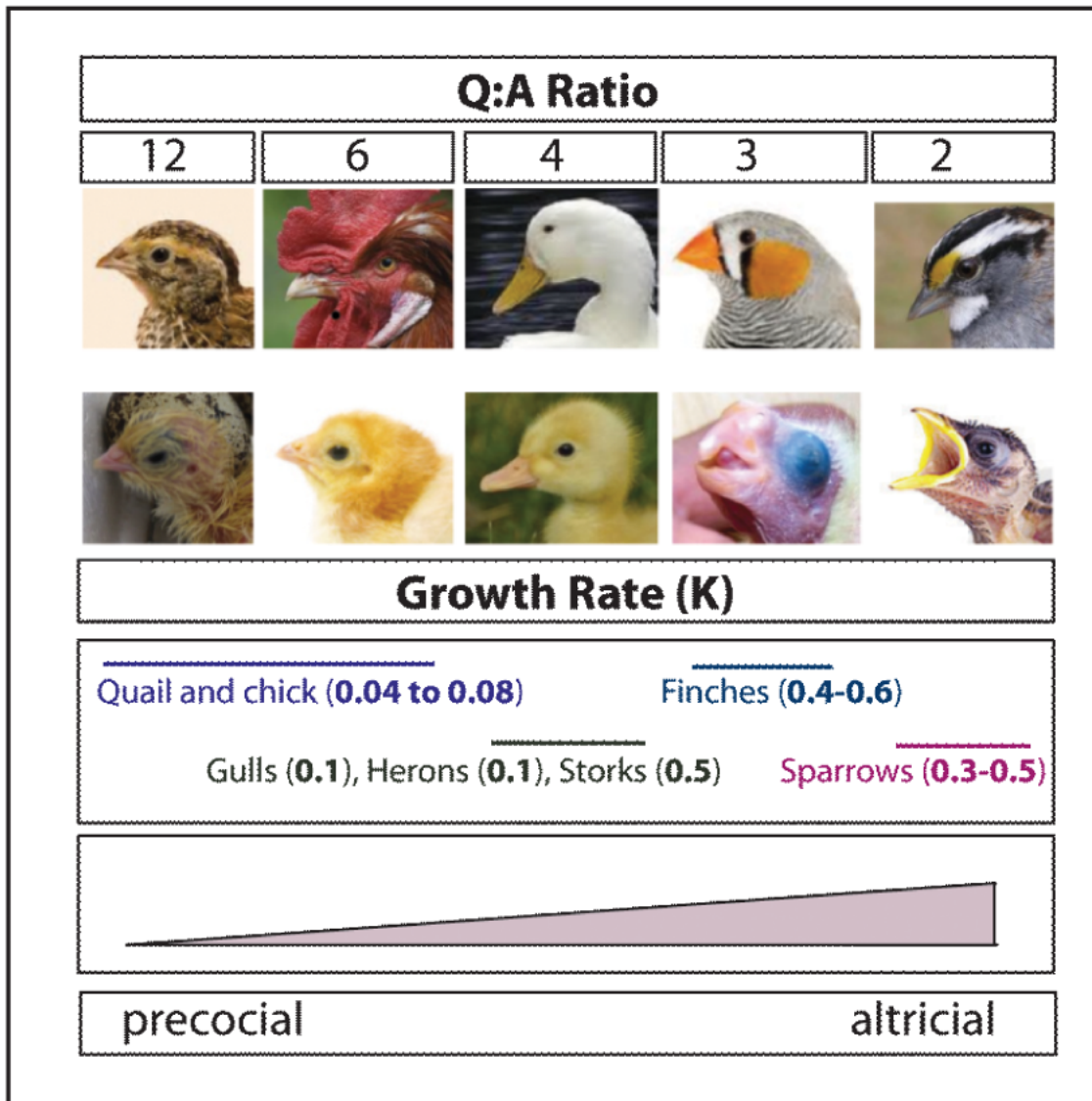
(A) A partial sequence of the 5' end of the *Runx2* sequence in five avians.

Variation is apparent in the tandem repeat region (blanks or dots below amino acid alignments), whereas the rest of the gene is mostly conserved (asterisks).

(B) Long, straight jaw in HH37 control chick skeletal preparation (done with Alcian blue for cartilage and Alizarin red for bone), versus **(C)** Short, curved jaws

in HH37 RCAS-*Runx2* infected embryo (prepared with only Alizarin red). **(D)** Longer, straighter upper jaws in dogs with lower Q:A ratios, versus **(E)** shorter, bent jaws in dogs with higher Q:A ratios (adapted from Fondon and Garner, 2004). **(F)** Isometry versus allometry in neonatal growth of cats and dogs (adapted from Sears et al., 2007).

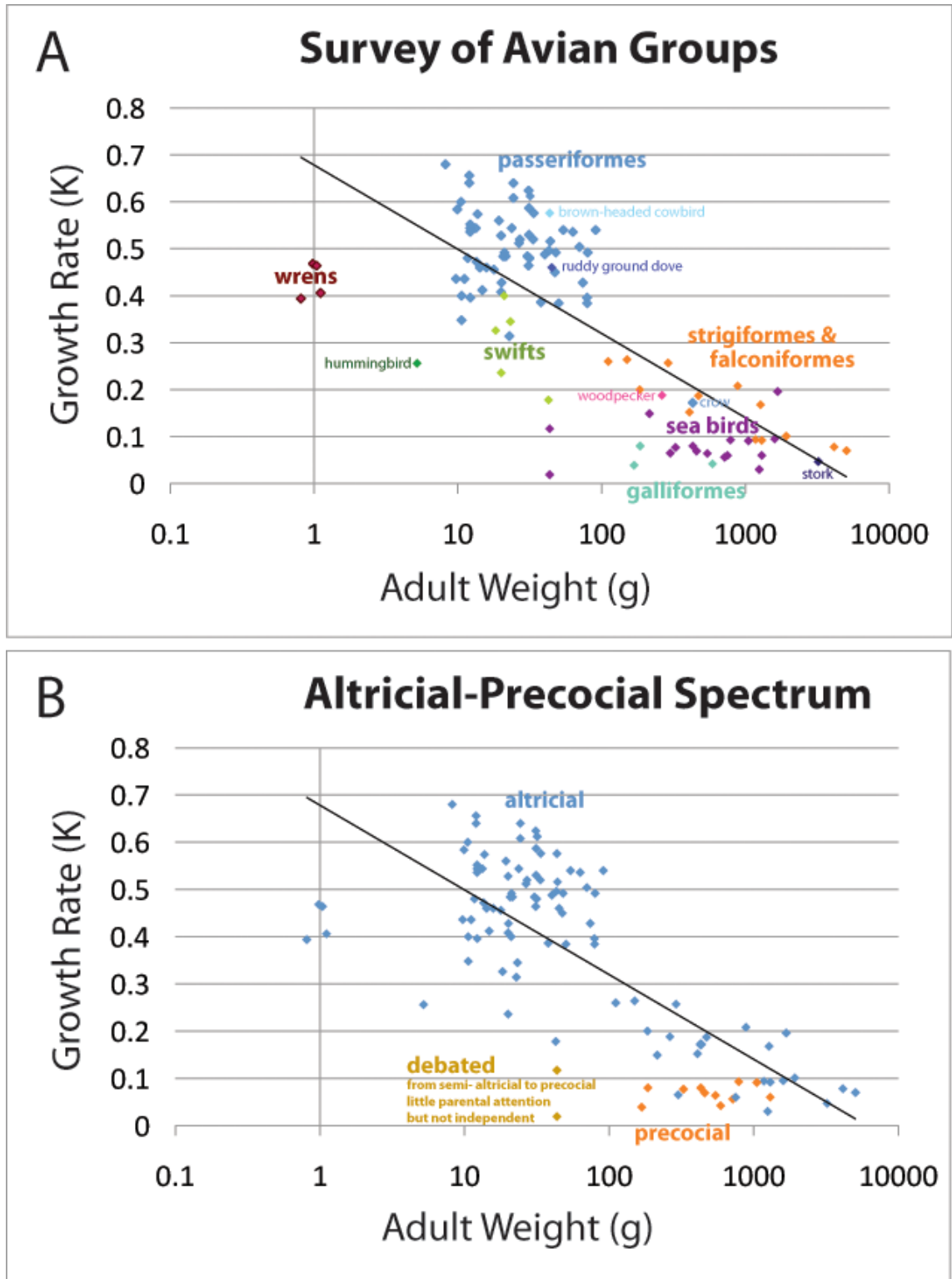
Figure 12. Runx2 Repeats and Rate of Growth



Q:A ratio correlates to growth rate (K, as calculated by Ricklefs, 1968) in a survey of five avian species. Growth rate is tightly linked to avian developmental maturity at hatching, i.e., where it lies on the spectrum of precocial versus

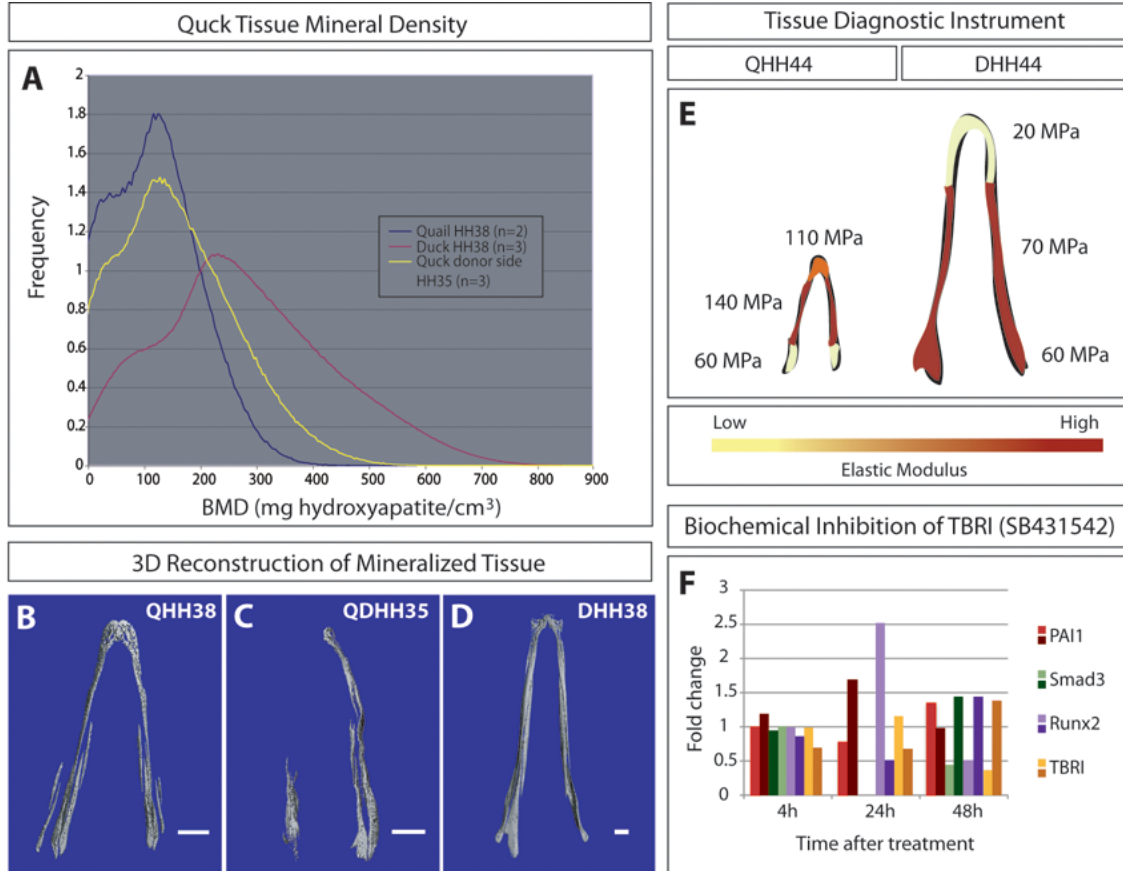
altricial. In turn, these variables are tied to other selective pressures such as predation and nutrient/energy availability.

Figure 13. Relations between Avian Growth Rate and Adult Weight



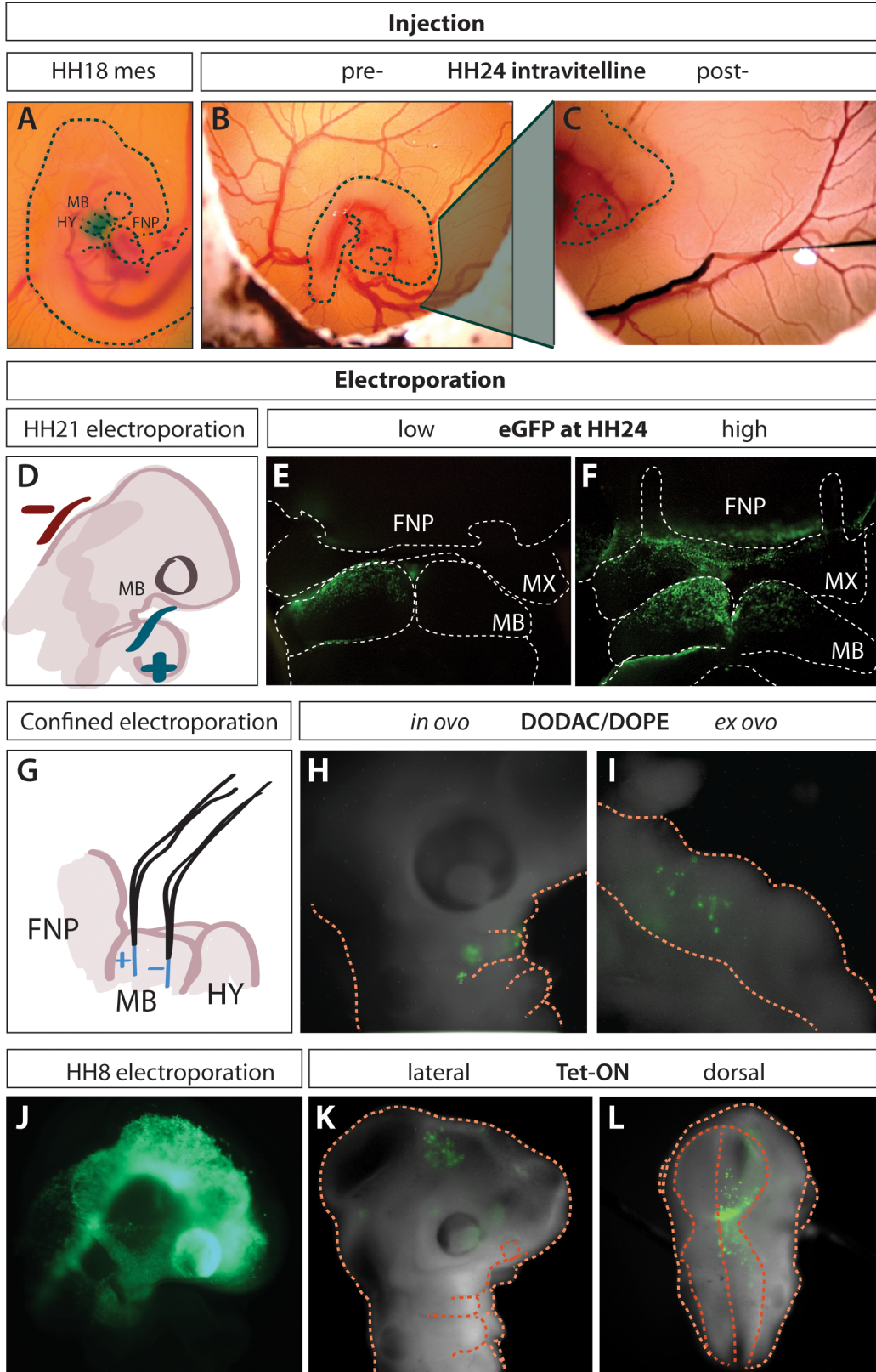
(A) Avian groups sorted by adult weight and growth rate. (B) Maturity at hatching, along the altricial-precocial spectrum, sorted by adult weight and growth rate.

Figure 14. Bone Tissue Properties



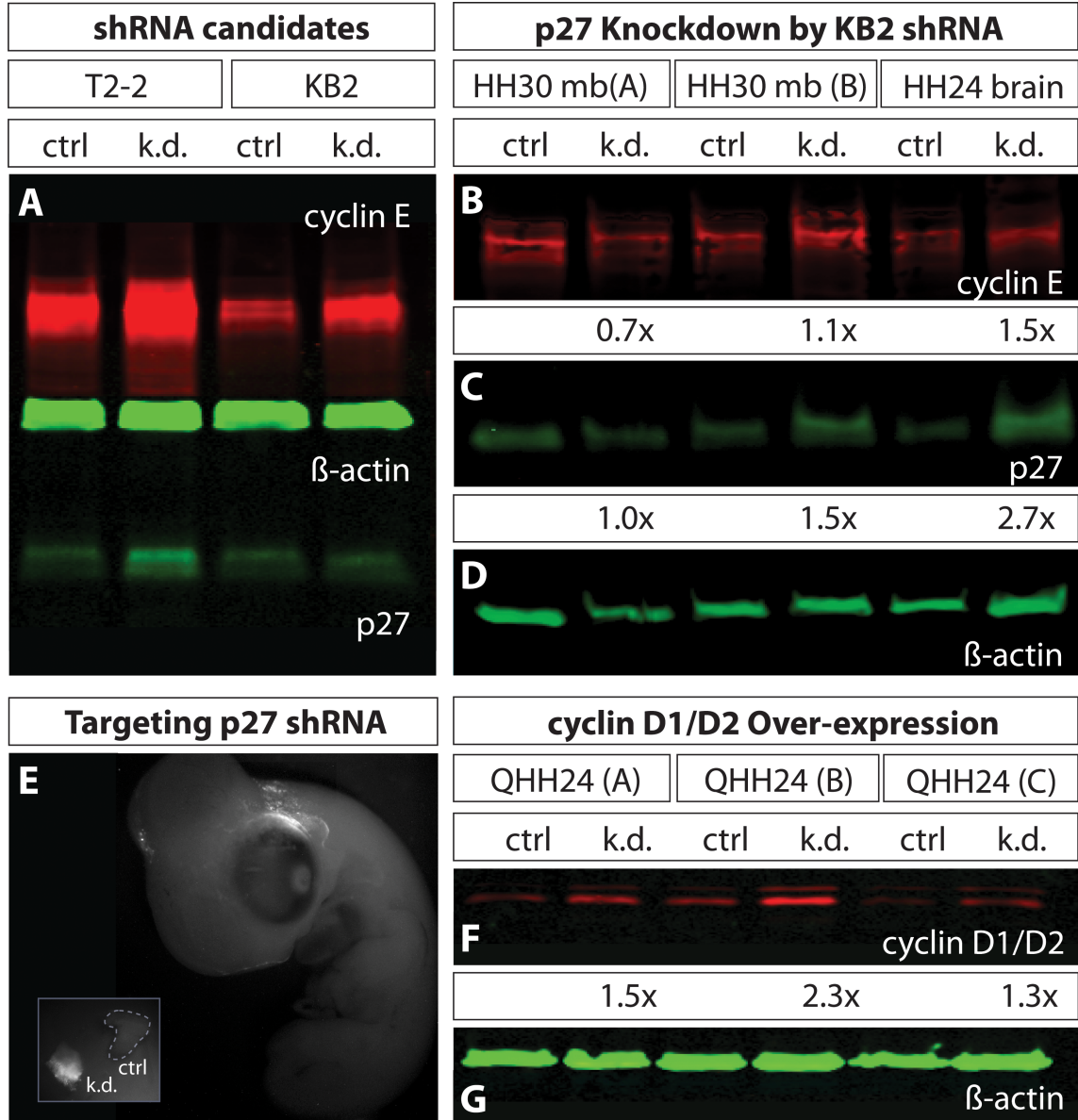
(A) Intensity histogram of tissue mineral density in HH38 quail (blue), donor-side HH35 quack (yellow) and HH38 duck (red) lower jaws, as measured by microCT. At HH38, duck have a higher average TMD than quail. In HH35 quack, the donor-side TMD distribution is similar to that of HH38 quail. **(B-D)** 3-D reconstruction of mineralized bone in lower jaws for representative samples of quail HH38, quack HH35, and duck HH38 by microCT. At HH38, duck mineralized bone has a smoother appearance (characteristic of more mature bone) than HH38 quail. In quack, the maturation on the donor side appears similar to that of HH38 quail.

Figure 15. Gain- and Loss-of-Function Techniques



(A) Injection into mesenchyme of mandible (MB) and hyoid (HY) mesenchyme in HH18 chick (tracer dye in green). **(B)** Quail at HH24 before injection into an intravitelline vein and **(C)** after injection. **(D)** Schematic showing electrode positioning for electroporation of HH18 mandibular mesenchyme (lateral view). **(E)** Following electroporation at HH21, low eGFP expression in mandibular epithelium of HH24 quail and **(F)** high eGFP expression in frontonasal process (FNP), maxillary (MX) and mandibular epithelium (frontal views). **(G)** Schematic showing electrode positioning for confined electroporation. Electrodes in black, exposed (not insulated) sharpened ends are shown in blue. **(H)** eGFP expression 24 hours after DODAC/DOPE-mediated lipofection *in ovo* **(I)** and *ex ovo*. **(J)** eGFP expression in HH18 quail following electroporation of neuroepithelium and neural crest mesenchyme at HH8. **(K)** Spotty, but stable eGFP expression following the electroporation of a Tet-inducible set of constructs and doxycycline injection.

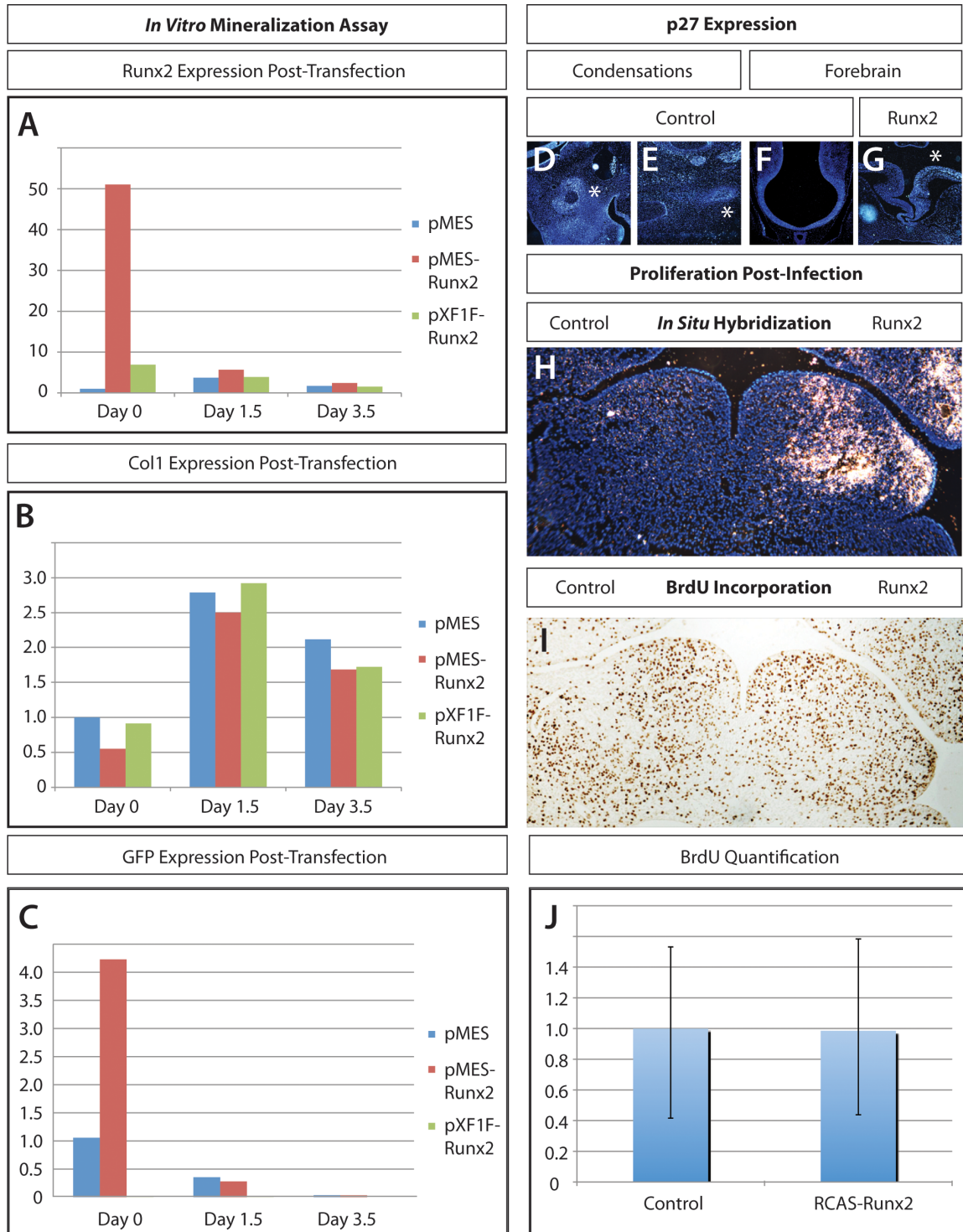
Figure 16. Transient Gain-and Loss-of-Function Analyses



(A) Western blot screening p27 shRNA candidates for ability to knockdown p27 (green) and increase cyclin E (red) protein expression. B-actin (green) is the loading control. T2-2 was tested in mandible and maxilla tissue. KB2 was tested in post-orbital tissue. Protein from control tissue (ctrl) is run next to that of shRNA-treated tissue (k.d.). **(B)** Western blot testing p27 shRNA candidate “KB2” in different embryos and tissue types, including mandible and brain. Cyclin E

expression (red) is not dramatically changed in treated embryos (quantification of fold change in expression is shown below). **(C)** p27 levels seem to slightly increased in treated samples by quantification, and greatly increased by visualization. **(D)** B-actin loading control. **(E)** p27 shRNA was targeted to regions of known high endogenous p27 expression including the brain, FNP, and post-orbital region. Shown here is a side view of a whole-mount embryo under epifluorescence with expression from co-electroporated eGFP construct in the post-orbital region. Inset shows a representative tissue collection of eGFP positive, shRNA-treated tissue alongside control, eGFP-negative tissue from the contra-lateral, untreated side. **(F)** Western blot of proteins from HH24 quail mandible electroporated with cyclin D1/D2 over-expression plasmids. Cyclin D1/D2 shows a slight fold increase in expression in the electroporated tissue versus that of the contra-lateral control side (quantifications below).

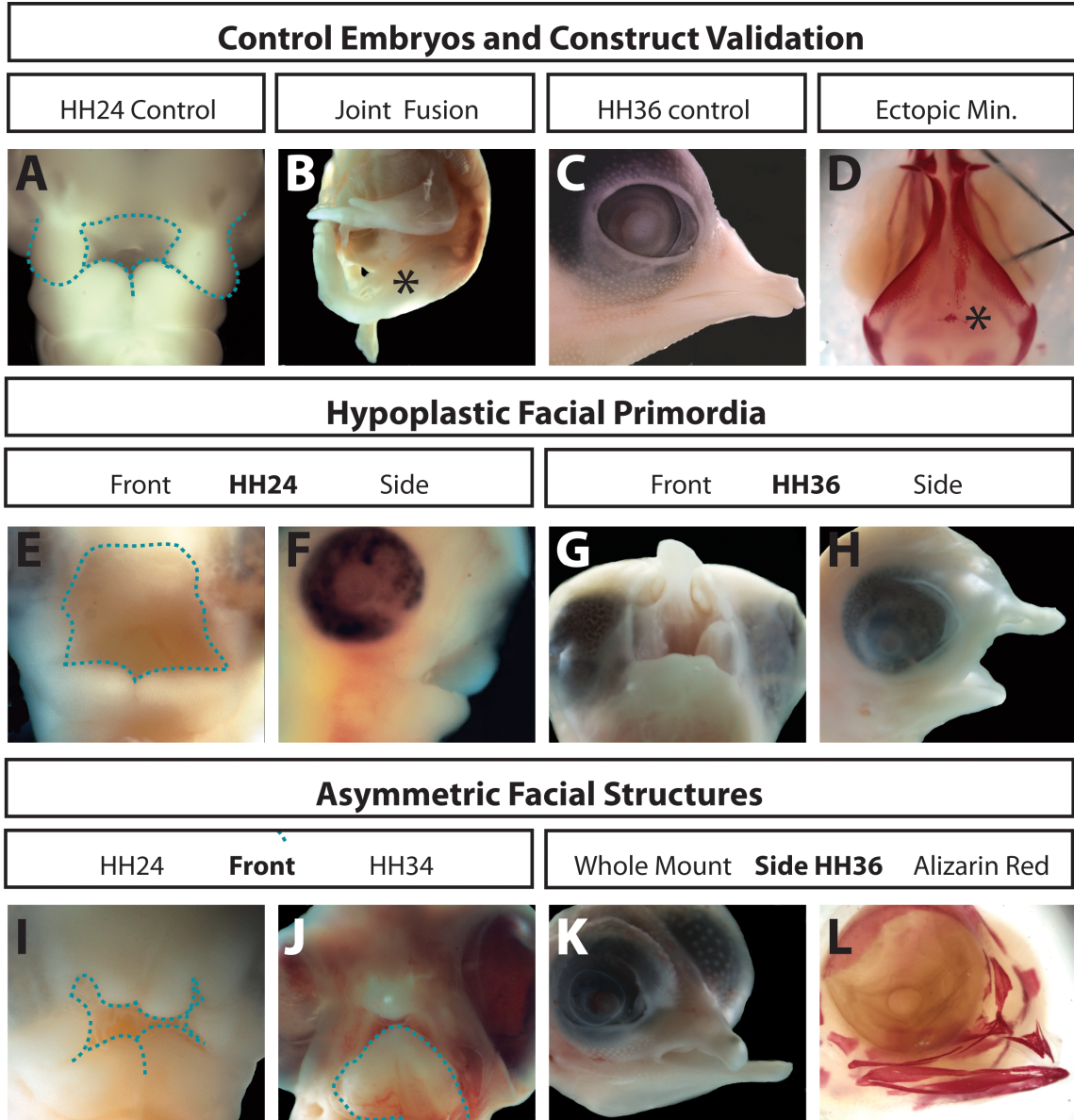
Figure 17. Effects of Runx2 Over-Expression on Proliferation and *In Vitro* Mineralization



The charts in A-C show fold change in mRNA expression levels over the time course of an *in vitro* mineralization assay in DF-1 cells following transfection with pMES (blue), pMES-Runx2 (pink), or pXF1F-Runx2 (green). **(A)** *Runx2* expression decreases to endogenous levels by day 1.5. **(B)** *Col1* expression is similar in treated and control cells throughout the time course. **(C)** *GFP* co-expression in bi-cistronic pMES and pMES-Runx2 decreases to minimal levels by day 3.5.

Panels D-G show *in situ* hybridization for p27 mRNA on sections. **(D)** *p27* expression in myogenic condensation (*) of control HH25 duck. **(E)** *p27* expression localized to osteoid (*) of control HH32 chick. **(F)** Forebrain expressing *p27* in control HH28 duck. **(G)** *p27* up-regulation in the forebrain on the injected side (*) of an HH24 RCAS-Runx2 infected chick embryo.

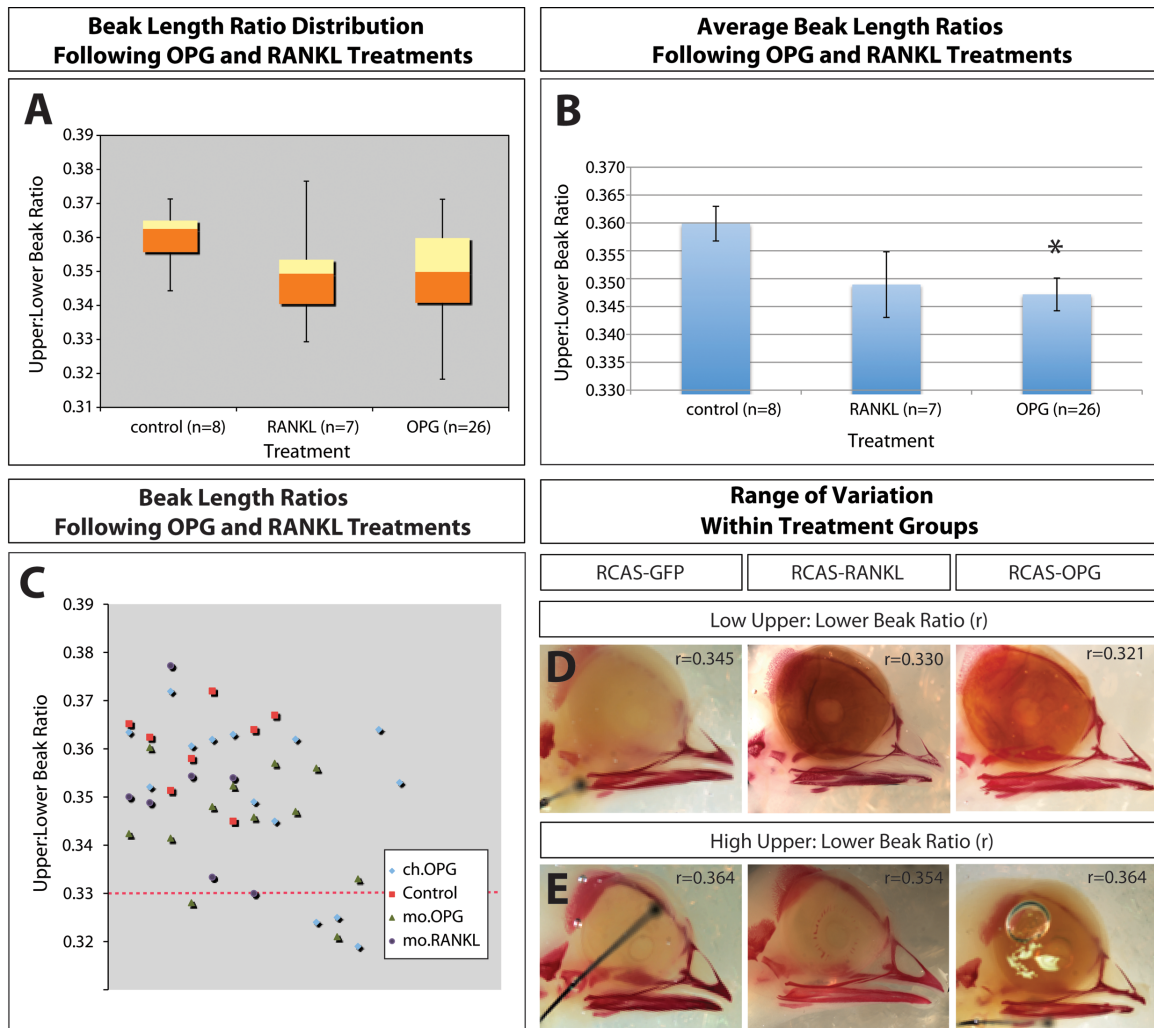
Figure 18. Effects of Runx2 Over-Expression on Morphology



(A) Frontal view of control HH24 chick embryo. **(B)** Validation of RCAS-Runx2 construct testing for the joint fusion (*) phenotype from Stricker et al., 2002, seen in limbs rather than digits of HH35 chick infected at HH15. **(C)** Side view of control HH36 chick embryo. **(D)** Validation of RCAS-Runx2 construct testing for the ectopic mineralization phenotype from Eames et al., 2004. Ectopic mineral (*) seen in calvaria of HH36 chick infected at HH8– top of picture is rostral. **(E)**

Hypoplastic mandible, maxillae, and frontonasal process in an HH8 infected HH24 chick embryo in frontal view and **(F)** side view. **(G)** The severity of hypoplasia in the craniofacial complex continues in development as seen in a frontal view and **(H)** side view of an HH36 chick embryo infected at HH8. **(I)** Asymmetric facial structures indicative of growth dysregulation in frontal views of an HH24 chick embryo infected at HH8 and **(J)** HH34 chick embryo infected at HH8. **(K)** Side view of a cross-beaking phenotype in an HH36 chick embryo infected at HH8, as seen in whole-mount and **(L)** after Alizarin Red staining and clearing.

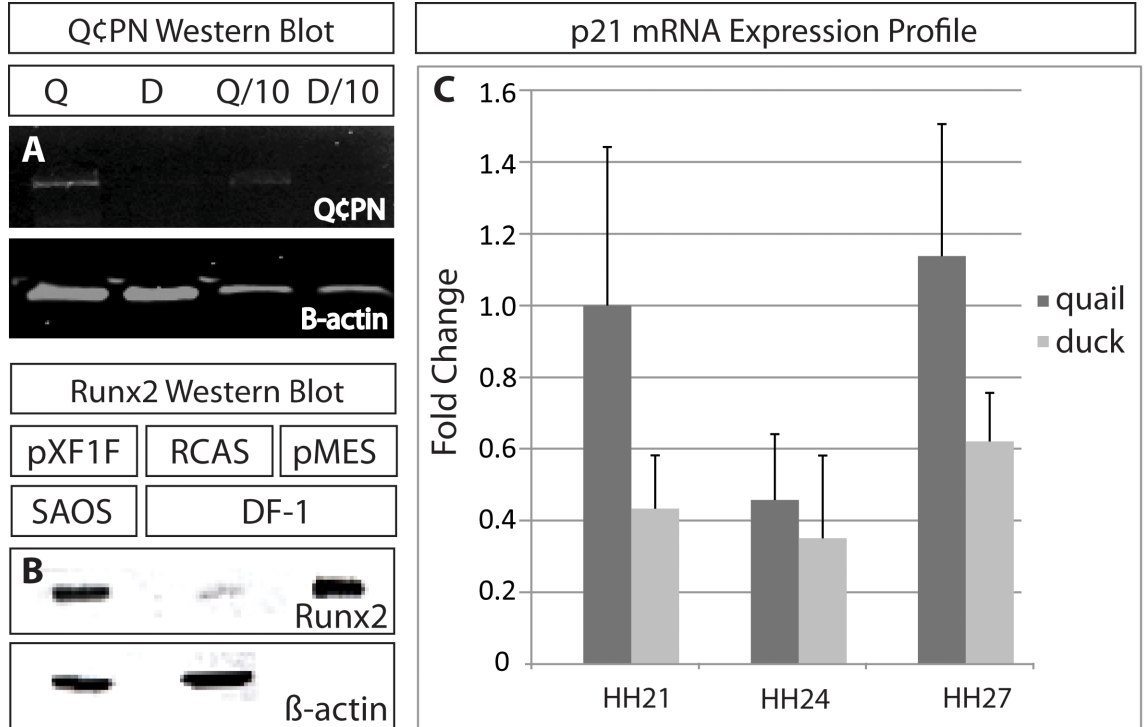
Figure 19. Effects of OPG and RANKL Over-Expression on Beak Length Ratio



(A) Box-and-whisker chart showing distribution of upper:lower beak length ratios following OPG and RANKL treatments. Control group shows tighter data points, while RANKL treated-embryos show the most spread in upper:lower beak ratios. OPG also shows much greater spread in ratios than control embryos. Greater spread may be indicative of dysregulation of upper and lower jaw growth coordination. **(B)** Column graph showing the average beak length ratios following OPG and RANKL treatments. OPG-treated embryos have significantly lower

upper:lower beak ratios. RANKL appears to trend toward this tendency as well, however a greater data spread could preclude a significant difference at this sample size. **(C)** Scatter plot showing all beak length ratio data points of each individual embryo measured. Control embryos (red square) cluster toward the top of the graph, and do not have beak length ratios that drop below the 0.33 mark. Embryos treated with chick OPG (ch.OPG; blue diamond) have a few outliers at the low end of the graph, though the majority cluster with the controls. Embryos treated with mouse OPG (mo.OPG; green triangle) cluster slightly lower than control embryos, again with a few outliers at the low end of the graph. Embryos treated with mouse RANKL (mo.RANKL; purple circle) show even distribution across a large range extending from the top to bottom end of the graph. **(D)** Shows the range of phenotypes correlating to low upper:lower beak ratios (r) and **(E)** high upper:lower beak ratios within RCAS-GFP, RCAS-RANKL, and RCAS-OPG infected treatment groups.

Figure 20. Western Blot and qRT-PCR



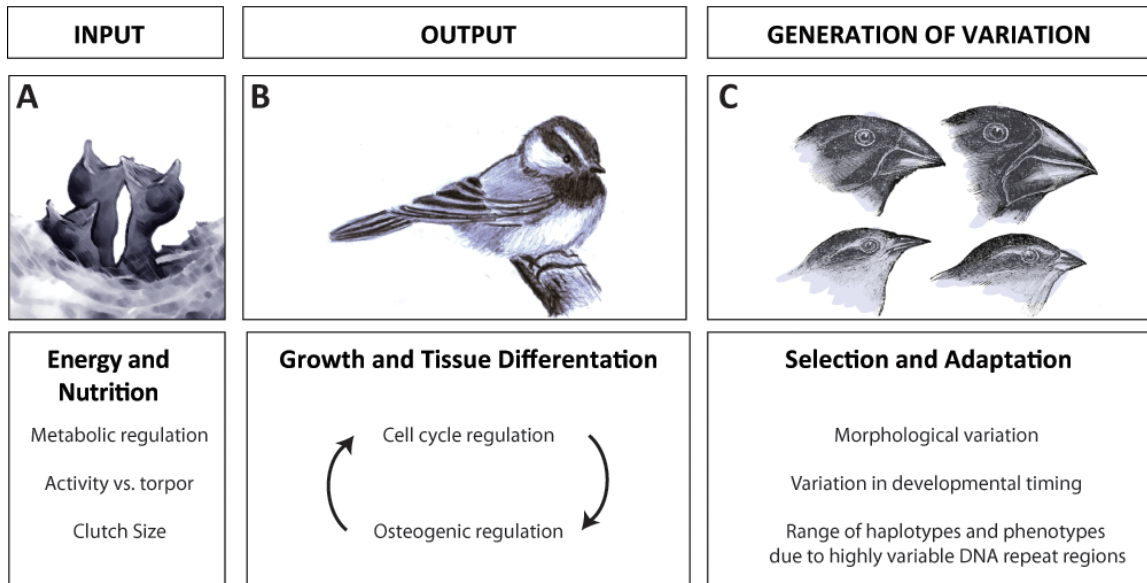
(A) Western blot using QcPN to detect quail tissue. High signal in quail tissue sample (Q), low signal in a 1/10 dilution of the same quail tissue (Q/10), and no signal in duck tissue (D) or 1/10 dilution of duck tissue (D/10). The protein complex detected by QcPN is larger than 250 kDa and has not been identified.

(B) Western blot for Runx2 protein. First lane shows protein from control SAOS cells transfected with pXF1F-Runx2 (from Daniel Nyugen, lab of Tamara Alliston). Second lane shows 80ug of protein from DF-1 cells transfected with RCAS-Runx2, where Runx2 is only faintly detected. Third lane shows protein from a re-sonicated cell pellet from DF-1 cells transfected with pMES-Runx2, where Runx2 is strongly detected, but no β -actin (which would be found in the supernatant of centrifuged cell lysate).

(C) mRNA expression of p21 in the

mandible, as detected by qRT-PCR, is not overtly up- or down-regulated as osteogenesis begins. However, duck may have lower levels of p21 than quail – or this could be an artifact of p21 primers designed against chick which have poor binding with duck mRNA, but recognize quail, a much closer relative.

Figure 21. Model: Roles for Cell Cycle and Osteogenic Regulation in Generation of Variation



(A) Fitness at acquiring food and nutrition is correlated to metabolic regulation and energy budgeting. Examples of energy budgeting include decreased clutch size or entering a state of torpor. *Pictured:* nestlings calling for food (modified from Qatar&Me; Creative Commons License 2.0). **(B)** During development and growth, cell cycle regulation affects timing of osteogenic differentiation and eventual beak size. *Pictured:* mountain chickadee at full adult size. **(C)** Changes to cell cycle regulation generate variation in morphologies and developmental timing at the population level, enabling functional adaptation. In addition, a broad range of haplotypes resulting from highly variable DNA repeat regions allows for genetic selection. *Pictured:* finch beak morphologies (modified from Darwin's Voyage of the Beagle; 1845).

REFERENCES

Adlakha, R.C., Sahasrabudde, C.G., Wright, D.A., and Rao, P.N. (1983). Evidence for the presence of inhibitors of mitotic factors during G1 period in mammalian cells. *J Cell Biol* 97, 1707-1713.

Albrecht, A.N., Kornak, U., Boddrich, A., Suring, K., Robinson, P.N., Stiege, A.C., Lurz, R., Stricker, S., Wanker, E.E., and Mundlos, S. (2004). A molecular pathogenesis for transcription factor associated poly-alanine tract expansions. *Hum Mol Genet* 13, 2351-2359.

Allin, E.F. (1975). Evolution of the mammalian middle ear. *J Morphol* 147, 403-437.

Alliston, T., Choy, L., Ducey, P., Karsenty, G., and Derynck, R. (2001). TGF-beta-induced repression of CBFA1 by Smad3 decreases cbfa1 and osteocalcin expression and inhibits osteoblast differentiation. *EMBO J* 20, 2254-2272.

Anan, K., Yoshida, N., Kataoka, Y., Sato, M., Ichise, H., Nasu, M., and Ueda, S. (2007). Morphological change caused by loss of the taxon-specific polyalanine tract in Hoxd-13. *Mol Biol Evol* 24, 281-287.

Antonopoulou, I., Mavrogiannis, L.A., Wilkie, A.O., and Morriss-Kay, G.M. (2004). Alx4 and Msx2 play phenotypically similar and additive roles in skull vault

differentiation. *J Anat* 204, 487-499.

Aota, S., Nakajima, N., Sakamoto, R., Watanabe, S., Ibaraki, N., and Okazaki, K. (2003). Pax6 autoregulation mediated by direct interaction of Pax6 protein with the head surface ectoderm-specific enhancer of the mouse Pax6 gene. *Dev Biol* 257, 1-13.

Ashley-Koch, A., Yang, Q., and Olney, R.S. (2000). Sickle hemoglobin (HbS) allele and sickle cell disease: a HuGE review. *Am J Epidemiol* 151, 839-845.

Atchley, W.R., and Hall, B.K. (1991). A model for development and evolution of complex morphological structures. *Biol Rev Camb Philos Soc* 66, 101-157.

Aubin, J.E. (1998). Bone stem cells. *J Cell Biochem Suppl* 30-31, 73-82.

Badyaev, A.V. (2010). The beak of the other finch: coevolution of genetic covariance structure and developmental modularity during adaptive evolution. *Philos Trans R Soc Lond B Biol Sci* 365, 1111-1126.

Berthold, P. (1999) Towards a comprehensive theory for the evolution, control and adaptability of avian migration. Adams, N.J. & Slotow, R.H. (Eds) *Proc. 22 Int. Ornithol. Congr., Durban, Ostrich*. 70 (1):1-11.

Bialek, P., Kern, B., Yang, X., Schrock, M., Sobic, D., Hong, N., Wu, H., Yu, K.,

Ornitz, D.M., Olson, E.N., *et al.* (2004). A twist code determines the onset of osteoblast differentiation. *Dev Cell* 6, 423-435.

Boivin, G., and Meunier, P.J. (2002). The degree of mineralization of bone tissue measured by computerized quantitative contact microradiography. *Calcif Tissue Int* 70, 503-511.

Borton, A.J., Frederick, J.P., Datto, M.B., Wang, X.F., and Weinstein, R.S. (2001). The loss of Smad3 results in a lower rate of bone formation and osteopenia through dysregulation of osteoblast differentiation and apoptosis. *J Bone Miner Res* 16, 1754-1764.

Brown, L.Y., and Brown, S.A. (2004). Alanine tracts: the expanding story of human illness and trinucleotide repeats. *Trends Genet* 20, 51-58.

Brown, L.Y., Odent, S., David, V., Blayau, M., Dubourg, C., Apacik, C., Delgado, M.A., Hall, B.D., Reynolds, J.F., Sommer, A., *et al.* (2001). Holoprosencephaly due to mutations in ZIC2: alanine tract expansion mutations may be caused by parental somatic recombination. *Hum Mol Genet* 10, 791-796.

Burr, D.B., Miller, L., Grynblas, M., Li, J., Boyde, A., Mashiba, T., Hirano, T., and Johnston, C.C. (2003). Tissue mineralization is increased following 1-year treatment with high doses of bisphosphonates in dogs. *Bone* 33, 960-969.

Burrows, M., Rogers, S.M., and Ott, S.R. (2011). Epigenetic remodelling of brain, body and behaviour during phase change in locusts. *Neural Syst Circuits* 1, 11.

Cameron, R.D. (1994). Reproductive Pauses by Female Caribou. *Journal of Mammalogy* 75, 10-13.

Cao, X., Pfaff, S.L., and Gage, F.H. (2008). YAP regulates neural progenitor cell number via the TEA domain transcription factor. *Genes Dev* 22, 3320-3334.

Carpenter, F.L. (1974). Torpor in an Andean hummingbird: its ecological significance. *Science*, 193, 545-574.

Carroll, S.B. (1995). Homeotic genes and the evolution of arthropods and chordates. *Nature* 376, 479-485.

Carroll, S.B. (2005). Evolution at two levels: on genes and form. *PLoS Biol* 3, e245.

Chen, C.M., Smith, D.M., Peters, M.A., Samson, M.E., Zitz, J., Tabin, C.J., and Cepko, C.L. (1999). Production and design of more effective avian replication-incompetent retroviral vectors. *Dev Biol* 214, 370-384.

Chesnutt, C., Burrus, L.W., Brown, A.M., and Niswander, L. (2004). Coordinate

regulation of neural tube patterning and proliferation by TGFbeta and WNT activity. *Dev Biol* 274, 334-347.

Chesnutt, C., and Niswander, L. (2004). Plasmid-based short-hairpin RNA interference in the chicken embryo. *Genesis* 39, 73-78.

Chisaka, O., Musci, T.S., and Capecchi, M.R. (1992). Developmental defects of the ear, cranial nerves and hindbrain resulting from targeted disruption of the mouse homeobox gene *Hox-1.6*. *Nature* 355, 516-520.

Coats, S., Flanagan, W.M., Nourse, J., and Roberts, J.M. (1996). Requirement of p27Kip1 for restriction point control of the fibroblast cell cycle. *Science* 272, 877-880.

Condie, B.G., and Capecchi, M.R. (1993). Mice homozygous for a targeted disruption of *Hoxd-3* (*Hox-4.1*) exhibit anterior transformations of the first and second cervical vertebrae, the atlas and the axis. *Development* 119, 579-595.

Conrad, M. (1990). The geometry of evolution. *Biosystems* 24, 61-81.

Couly, G., Creuzet, S., Bennaceur, S., Vincent, C., and Le Douarin, N.M. (2002). Interactions between Hox-negative cephalic neural crest cells and the foregut endoderm in patterning the facial skeleton in the vertebrate head. *Development*

129, 1061-1073.

Creuzet, S., Couly, G., Vincent, C., and Le Douarin, N.M. (2002). Negative effect of Hox gene expression on the development of the neural crest-derived facial skeleton. *Development* 129, 4301-4313.

Croaker, G.D., Shi, E., Simpson, E., Cartmill, T., and Cass, D.T. (1998). Congenital central hypoventilation syndrome and Hirschsprung's disease. *Arch Dis Child* 78, 316-322.

Currey, J.D. (2010). Mechanical properties and adaptations of some less familiar bony tissues. *J Mech Behav Biomed Mater* 3, 357-372.

Czypionka, T., Cheng, J., Pozhitkov, A., and Nolte, A.W. (2012). Transcriptome changes after genome-wide admixture in invasive sculpins (*Cottus*). *Mol Ecol* 21, 4797-4810.

D'Souza, R.N., Aberg, T., Gaikwad, J., Cavender, A., Owen, M., Karsenty, G., and Thesleff, I. (1999). *Cbfa1* is required for epithelial-mesenchymal interactions regulating tooth development in mice. *Development* 126, 2911-2920.

Darwin, C., Colburn, H., Dower, J., J. & C. Walker (Firm) (1845). *Journal of researches into the natural history and geology of the countries visited during the*

voyage of H.M.S. Beagle round the world: under the command of Capt. Fitz Roy.
Henry Colburn, London.

Darwin, C. (1859). On the origin of species by means of natural selection or the preservation of favored races in the struggle for life. Murray, London.

Deckers, M.M., van Bezooijen, R.L., van der Horst, G., Hoogendam, J., van Der Bent, C., Papapoulos, S.E., and Lowik, C.W. (2002). Bone morphogenetic proteins stimulate angiogenesis through osteoblast-derived vascular endothelial growth factor A. *Endocrinology* 143, 1545-1553.

Depew, M.J., Lufkin, T., and Rubenstein, J.L. (2002). Specification of jaw subdivisions by Dlx genes. *Science* 298, 381-385.

Depew, M.J., Simpson, C.A., Morasso, M., and Rubenstein, J.L. (2005). Reassessing the Dlx code: the genetic regulation of branchial arch skeletal pattern and development. *J Anat* 207, 501-561.

De Robertis, E.M., Oliver, G., and Wright, C.V. (1990). Homeobox genes and the vertebrate body plan. *Sci Am* 263, 46-52.

Doronkin, S., Djagaeva, I., and Beckendorf, S.K. (2003). The COP9 signalosome

promotes degradation of Cyclin E during early *Drosophila* oogenesis. *Dev Cell* 4, 699-710.

Downie, S.A., and Newman, S.A. (1995). Different roles for fibronectin in the generation of fore and hind limb precartilaginous condensations. *Dev Biol* 172, 519-530.

Drissi, H., Hushka, D., Aslam, F., Nguyen, Q., Buffone, E., Koff, A., van Wijnen, A., Lian, J.B., Stein, J.L., and Stein, G.S. (1999). The cell cycle regulator p27kip1 contributes to growth and differentiation of osteoblasts. *Cancer Res* 59, 3705-3711.

Ducy, P. (2000). Cbfa1: a molecular switch in osteoblast biology. *Dev Dyn* 219, 461-471.

Ducy, P., Starbuck, M., Priemel, M., Shen, J., Pinero, G., Geoffroy, V., Amling, M., and

Karsenty, G. (1999). A Cbfa1-dependent genetic pathway controls bone formation beyond embryonic development. *Genes Dev* 13, 1025-1036.

Ducy, P., Zhang, R., Geoffroy, V., Ridall, A.L., and Karsenty, G. (1997). *Osf2/Cbfa1*: a transcriptional activator of osteoblast differentiation. *Cell* 89, 747-

754.

Dugger, K.M., Anthony, R.G., and Andrews, L.S. (2011). Transient dynamics of invasive competition: barred owls, spotted owls, habitat, and the demons of competition present. *Ecol Appl* 21, 2459-2468.

Dumont, E.R. (2007). Feeding mechanisms in bats: variation within the constraints of flight. *Integr Comp Biol* 47, 137-146.

Dunlop, L.L., and Hall, B.K. (1995). Relationships between cellular condensation, preosteoblast formation and epithelial-mesenchymal interactions in initiation of osteogenesis. *Int J Dev Biol* 39, 357-371.

Eames, B.F., Sharpe, P.T., and Helms, J.A. (2004). Hierarchy revealed in the specification of three skeletal fates by Sox9 and Runx2. *Dev Biol* 274, 188-200.

Eames, B.F., and Schneider, R.A. (2005). Quail-duck chimeras reveal spatiotemporal plasticity in molecular and histogenic programs of cranial feather development. *Development* 132, 1499-1509.

Eames, B.F., and Schneider, R.A. (2008). The genesis of cartilage size and shape during development and evolution. *Development* 135, 3947-3958.

Ede, D.A., and Kelly, W.A. (1964). Developmental Abnormalities in the Trunk and Limbs of the Talpid3 Mutant of the Fowl. *J Embryol Exp Morphol* 12, 339-356.

Eherlich, P.R., Dobkin, D.S., Wheye, D. (1988) *The Birder's Handbook*. Simon and Shucstster, Inc., New York.

Erlebacher, A., and Derynck, R. (1996). Increased expression of TGF-beta 2 in osteoblasts results in an osteoporosis-like phenotype. *J Cell Biol* 132, 195-210.

Erlebacher, A., Filvaroff, E.H., Gitelman, S.E., and Derynck, R. (1995). Toward a molecular understanding of skeletal development. *Cell* 80, 371-378.

Ettinger, L., and Doljanski, F. (1992). On the generation of form by the continuous interactions between cells and their extracellular matrix. *Biol Rev Camb Philos Soc* 67, 459-489.

Faibish, D., Ott, S.M., and Boskey, A.L. (2006). Mineral changes in osteoporosis: a review. *Clin Orthop Relat Res* 443, 28-38.

Farner, D.S., and King, J.R., Eds. (1974) *Thermal and caloric relations of birds*. *Avian Biology*, Vol.4. Academic Press, New York.

Fish, J.L., Villmoare, B., Kobernick, K., Compagnucci, C., Britanova, O., Tarabykin, V., and Depew, M.J. (2011). *Satb2*, modularity, and the evolvability of the vertebrate jaw. *Evol Dev* 13, 549-564.

Fisher, R.A. (1930) *The Genetical Theory of Natural Selection*. Clarendon, Oxford.

Fondon, J.W., 3rd, and Garner, H.R. (2004). Molecular origins of rapid and continuous morphological evolution. *Proc Natl Acad Sci U S A* 101, 18058-18063.

Fondon, J.W., 3rd, and Garner, H.R. (2007). Detection of length-dependent effects of tandem repeat alleles by 3-D geometric decomposition of craniofacial variation. *Dev Genes Evol* 217, 79-85.

Foppiano, S., Hu, D., and Marcucio, R.S. (2007). Signaling by bone morphogenetic proteins directs formation of an ectodermal signaling center that regulates craniofacial development. *Dev Biol* 312, 103-114.

Friedman, H. and Kiff, L.F. (1985). The parasitic cowbirds and their hosts. *Proceedings of the Western Foundation of Vertebrate Zoology* 2, 225-304.

Frost, H.M. (1963) *Bone remodeling dynamics*. Thomas, Springfield.

Galindo, M., Pratap, J., Young, D.W., Hovhannisyan, H., Im, H.J., Choi, J.Y., Lian, J.B., Stein, J.L., Stein, G.S., and van Wijnen, A.J. (2005). The bone-specific expression of Runx2 oscillates during the cell cycle to support a G1-related antiproliferative function in osteoblasts. *J Biol Chem* 280, 20274-20285.

Geetha-Loganathan, P., Nimmagadda, S., Hafez, I., Fu, K., Cullis, P.R., and Richman, J.M. (2011). Development of high-concentration lipoplexes for in vivo gene function studies in vertebrate embryos. *Dev Dyn* 240, 2108-2119.

Gendron-Maguire, M., Mallo, M., Zhang, M., and Gridley, T. (1993). Hoxa-2 mutant mice exhibit homeotic transformation of skeletal elements derived from cranial neural crest. *Cell* 75, 1317-1331.

Gerber, H.P., Seipel, K., Georgiev, O., Hofferer, M., Hug, M., Rusconi, S., and Schaffner, W. (1994). Transcriptional activation modulated by homopolymeric glutamine and proline stretches. *Science* 263, 808-811.

Gil, D., Bulmer, E., Celis, P., and Lopez-Rull, I. (2008). Adaptive developmental plasticity in growing nestlings: sibling competition induces differential gape growth. *Proc Biol Sci* 275, 549-554.

Gjorevski, N., Boghaert, E., and Nelson, C.M. (2012). Regulation of Epithelial-Mesenchymal Transition by Transmission of Mechanical Stress through Epithelial

Tissues. *Cancer Microenviron* 5, 29-38.

Grande, C., and Patel, N.H. (2009). Nodal signalling is involved in left-right asymmetry in snails. *Nature* 457, 1007-1011.

Guilak, F., Cohen, D.M., Estes, B.T., Gimble, J.M., Liedtke, W., and Chen, C.S. (2009). Control of stem cell fate by physical interactions with the extracellular matrix. *Cell Stem Cell* 5, 17-26.

Guthrie, S. (2007). Patterning and axon guidance of cranial motor neurons. *Nat Rev Neurosci* 8, 859-871.

Haldane, J.B.S. (1927). A mathematical theory of natural and artificial selection, part V: Selection and mutation. *Math Proc Camb Philos Soc* 23, 838-844.

Hall, B.K. (2000). The neural crest as a fourth germ layer and vertebrates as quadroblastic not triploblastic. *Evol Dev* 2, 3-5.

Hall, B.K. (2000). Epithelial-mesenchymal interactions. *Methods Mol Biol* 137, 235-243.

Hall, B.K., and Miyake, T. (2000). All for one and one for all: condensations and the initiation of skeletal development. *Bioessays* 22, 138-147.

Hallgrímsson, B., Jamniczky, H., Young, N.M., Rolian, C., Parsons, T.E., Boughner, J.C., and Marcucio, R.S. (2009). Deciphering the palimpsest: studying the relationship between morphological integration and phenotypic covariation. *Evolutionary Biology* 36, 355-376.

Hamburger, V., and Hamilton, H.L. (1992). A series of normal stages in the development of the chick embryo. 1951. *Dev Dyn* 195, 231-272.

Han, J., Ishii, M., Bringas, P., Jr., Maas, R.L., Maxson, R.E., Jr., and Chai, Y. (2007). Concerted action of Msx1 and Msx2 in regulating cranial neural crest cell differentiation during frontal bone development. *Mech Dev* 124, 729-745.

Hassan, M.Q., Gordon, J.A., Beloti, M.M., Croce, C.M., van Wijnen, A.J., Stein, J.L., Stein, G.S., and Lian, J.B. (2010). A network connecting Runx2, SATB2, and the miR-23a~27a~24-2 cluster regulates the osteoblast differentiation program. *Proc Natl Acad Sci U S A* 107, 19879-19884.

Hehr, U., Pineda-Alvarez, D.E., Uyanik, G., Hu, P., Zhou, N., Hehr, A., Schell-Apacik, C., Altus, C., Daumer-Haas, C., Meiner, A., *et al.* (2010). Heterozygous mutations in SIX3 and SHH are associated with schizencephaly and further expand the clinical spectrum of holoprosencephaly. *Hum Genet* 127, 555-561.

Hernandez, C.J. (2008). How can bone turnover modify bone strength

independent of bone mass? *Bone* 42, 1014-1020.

Hesse, E., Saito, H., Kiviranta, R., Correa, D., Yamana, K., Neff, L., Toben, D., Duda, G., Atfi, A., Geoffroy, V., *et al.* (2010). Zfp521 controls bone mass by HDAC3-dependent attenuation of Runx2 activity. *J Cell Biol* 191, 1271-1283.

Hill-Harfe, K.L., Kaplan, L., Stalker, H.J., Zori, R.T., Pop, R., Scherer, G., and Wallace, M.R. (2005). Fine mapping of chromosome 17 translocation breakpoints > or = 900 Kb upstream of SOX9 in acampomelic campomelic dysplasia and a mild, familial skeletal dysplasia. *Am J Hum Genet* 76, 663-671.

Hirano, K., Hirano, M., Zeng, Y., Nishimura, J., Hara, K., Muta, K., Nawata, H., and Kanaide, H. (2001). Cloning and functional expression of a degradation-resistant novel isoform of p27Kip1. *Biochem J* 353, 51-57.

Hu, D., and Marcucio, R.S. (2009). A SHH-responsive signaling center in the forebrain regulates craniofacial morphogenesis via the facial ectoderm. *Development* 136, 107-116.

Hu, D., and Marcucio, R.S. (2012). Neural crest cells pattern the surface cephalic ectoderm during FEZ formation. *Dev Dyn* 241, 732-740.

Hu, D., Marcucio, R.S., and Helms, J.A. (2003). A zone of frontonasal ectoderm

regulates patterning and growth in the face. *Development* 130, 1749-1758.

Hu, W.Y., Myers, C.P., Kilzer, J.M., Pfaff, S.L., and Bushman, F.D. (2002). Inhibition of retroviral pathogenesis by RNA interference. *Curr Biol* 12, 1301-1311.

Huang, J., Zhao, L., Xing, L., and Chen, D. (2010). MicroRNA-204 regulates Runx2 protein expression and mesenchymal progenitor cell differentiation. *Stem Cells* 28, 357-364.

Hughes, S.H., Greenhouse, J.J., Petropoulos, C.J., and Suttrave, P. (1987). Adaptor plasmids simplify the insertion of foreign DNA into helper-independent retroviral vectors. *J Virol* 61, 3004-3012.

Ishii, K., Nielsen, I.L., and Vargervik, K. (1998). Characteristics of jaw growth in cleidocranial dysplasia. *Cleft Palate Craniofac J* 35, 161-166.

Janody, F., Sturny, R., Schaeffer, V., Azou, Y., and Dostatni, N. (2001). Two distinct domains of Bicoid mediate its transcriptional downregulation by the Torso pathway. *Development* 128, 2281-2290.

Jeon, E.J., Lee, K.Y., Choi, N.S., Lee, M.H., Kim, H.N., Jin, Y.H., Ryoo, H.M., Choi, J.Y., Yoshida, M., Nishino, N., *et al.* (2006). Bone morphogenetic protein-2

stimulates Runx2 acetylation. *J Biol Chem* 281, 16502-16511.

Jeong, Y., Leskow, F.C., El-Jaick, K., Roessler, E., Muenke, M., Yocum, A., Dubourg, C., Li, X., Geng, X., Oliver, G., *et al.* (2008). Regulation of a remote Shh forebrain enhancer by the Six3 homeoprotein. *Nat Genet* 40, 1348-1353.

Ji, C., Casinghino, S., Chang, D.J., Chen, Y., Javed, A., Ito, Y., Hiebert, S.W., Lian, J.B., Stein, G.S., McCarthy, T.L., *et al.* (1998). CBFa(AML/PEBP2)-related elements in the TGF-beta type I receptor promoter and expression with osteoblast differentiation. *J Cell Biochem* 69, 353-363.

Jones, F.C., Grabherr, M.G., Chan, Y.F., Russell, P., Mauceli, E., Johnson, J., Swofford, R., Pirun, M., Zody, M.C., White, S., *et al.* (2012). The genomic basis of adaptive evolution in threespine sticklebacks. *Nature* 484, 55-61.

Kang, J.S., Alliston, T., Delston, R., and Derynck, R. (2005). Repression of Runx2 function by TGF-beta through recruitment of class II histone deacetylases by Smad3. *EMBO J* 24, 2543-2555.

Kashi, Y., and King, D.G. (2006). Simple sequence repeats as advantageous mutators in evolution. *Trends Genet* 22, 253-259.

Kaufmann, S.A. (1993) *The Origins of order: Self-organization and selection in*

evolution. Oxford University Press, Oxford.

Kawakami, Y., Esteban, C.R., Matsui, T., Rodriguez-Leon, J., Kato, S., and Izpisua Belmonte, J.C. (2004). Sp8 and Sp9, two closely related buttonhead-like transcription factors, regulate Fgf8 expression and limb outgrowth in vertebrate embryos. *Development* 131, 4763-4774.

Kimmel, C.B., DeLaurier, A., Ullmann, B., Dowd, J., and McFadden, M. (2010). Modes of developmental outgrowth and shaping of a craniofacial bone in zebrafish. *PLoS One* 5, e9475.

Kimura, M. (1968). Evolutionary rate at the molecular level. *Nature* 217, 624-626.

Kirschner, M., and Gerhart, J. (1998). Evolvability. *Proc Natl Acad Sci U S A* 95, 8420-8427.

Kleinjan, D.A., and van Heyningen, V. (2005). Long-range control of gene expression: emerging mechanisms and disruption in disease. *Am J Hum Genet* 76, 8-32.

Kobayashi, H., Gao, Y., Ueta, C., Yamaguchi, A., and Komori, T. (2000). Multilineage differentiation of Cbfa1-deficient calvarial cells in vitro. *Biochem Biophys Res Commun* 273, 630-636.

Komori, T., Yagi, H., Nomura, S., Yamaguchi, A., Sasaki, K., Deguchi, K., Shimizu, Y., Bronson, R.T., Gao, Y.H., Inada, M., *et al.* (1997). Targeted disruption of *Cbfa1* results in a complete lack of bone formation owing to maturational arrest of osteoblasts. *Cell* 89, 755-764.

Kress, W., Schropp, C., Lieb, G., Petersen, B., Busse-Ratzka, M., Kunz, J., Reinhart, E., Schafer, W.D., Sold, J., Hoppe, F., *et al.* (2006). Saethre-Chotzen syndrome caused by *TWIST 1* gene mutations: functional differentiation from Muenke coronal synostosis syndrome. *Eur J Hum Genet* 14, 39-48.

Krull, C.E., Lansford, R., Gale, N.W., Collazo, A., Marcelle, C., Yancopoulos, G.D., Fraser, S.E., and Bronner-Fraser, M. (1997). Interactions of Eph-related receptors and ligands confer rostrocaudal pattern to trunk neural crest migration. *Curr Biol* 7, 571-580.

Krull, C.E. (2004). A primer on using *in ovo* electroporation to analyze gene function. *Dev Dyn* 229, 433-439.

Kuratani, S. (2004). Evolution of the vertebrate jaw: comparative embryology and molecular developmental biology reveal the factors behind evolutionary novelty. *J Anat* 205, 335-347.

Kuratani, S. (2005). Developmental studies on the vertebrate head evolution.

Zoolog Sci 22, 1361-1366.

Kuratani, S. (2005). Cephalic neural crest cells and the evolution of craniofacial structures in vertebrates: morphological and embryological significance of the premandibular-mandibular boundary. *Zoology (Jena)* 108, 13-25.

Kuratani, S. (2005). Developmental studies of the lamprey and hierarchical evolutionary steps towards the acquisition of the jaw. *J Anat* 207, 489-499.

Kuratani, S. (2012). Evolution of the vertebrate jaw from developmental perspectives. *Evol Dev* 14, 76-92.

Kuratani, S., Nobusada, Y., Horigome, N., and Shigetani, Y. (2001). Embryology of the lamprey and evolution of the vertebrate jaw: insights from molecular and developmental perspectives. *Philos Trans R Soc Lond B Biol Sci* 356, 1615-1632.

Lack, D. (1948). THE SIGNIFICANCE OF CLUTCH-SIZE. Part III.—Some Interspecific Comparisons. *Ibis* 90, 25-45.

Laidlaw, J., Gelfand, Y., Ng, K.W., Garner, H.R., Ranganathan, R., Benson, G., and Fondon, J.W., 3rd (2007). Elevated basal slippage mutation rates among the Canidae. *J Hered* 98, 452-460.

Lan, Y., and Jiang, R. (2009). Sonic hedgehog signaling regulates reciprocal epithelial-mesenchymal interactions controlling palatal outgrowth. *Development* 136, 1387-1396.

Larsen, W.J. (1993). *Human embryology* (New York, Churchill Livingstone).

Lee, K., Chen, Q.K., Lui, C., Cichon, M.A., Radisky, D.C., and Nelson, C.M. (2012). Matrix compliance regulates Rac1b localization, NADPH oxidase assembly, and epithelial-mesenchymal transition. *Mol Biol Cell* 23, 4097-4108.

Lehmann, O.J., Ebenezer, N.D., Jordan, T., Fox, M., Ocaka, L., Payne, A., Leroy, B.P., Clark, B.J., Hitchings, R.A., Povey, S., *et al.* (2000). Chromosomal duplication involving the forkhead transcription factor gene FOXC1 causes iris hypoplasia and glaucoma. *Am J Hum Genet* 67, 1129-1135.

Leung, A.K., and Sharp, P.A. (2010). MicroRNA functions in stress responses. *Mol Cell* 40, 205-215.

Li, S.F., Wang, R.Z., Meng, Q.H., Li, G.L., Hu, G.J., Dou, W.C., Li, Z.J., and Zhang, Z.X. (2006). Intra-ventricular infusion of rAAV1-EGFP resulted in transduction in multiple regions of adult rat brain: a comparative study with rAAV2 and rAAV5 vectors. *Brain Res* 1122, 1-9.

Lobjois, V., Bel-Vialar, S., Trousse, F., and Pituello, F. (2008). Forcing neural progenitor cells to cycle is insufficient to alter cell-fate decision and timing of neuronal differentiation in the spinal cord. *Neural Dev* 3, 4.

Lobjois, V., Benazeraf, B., Bertrand, N., Medevielle, F., and Pituello, F. (2004). Specific regulation of cyclins D1 and D2 by FGF and Shh signaling coordinates cell cycle progression, patterning, and differentiation during early steps of spinal cord development. *Dev Biol* 273, 195-209.

Lopes, F.L., Desmarais, J.A., and Murphy, B.D. (2004). Embryonic diapause and its regulation. *Reproduction* 128, 669-678.

Lou, Y., Javed, A., Hussain, S., Colby, J., Frederick, D., Pratap, J., Xie, R., Gaur, T., van Wijnen, A.J., Jones, S.N., *et al.* (2009). A Runx2 threshold for the cleidocranial dysplasia phenotype. *Hum Mol Genet* 18, 556-568.

Love, A.C., and Raff, R.A. (2003). Knowing your ancestors: themes in the history of evo-devo. *Evol Dev* 5, 327-330.

MacKenzie, R.B. (1868) *The Darwinian Theory of the Transmutation of Species Examined*. Nisbet & Co., London.

McIntyre, G.J., and Fanning, G.C. (2006). Design and cloning strategies for

constructing shRNA expression vectors. *BMC Biotechnol* 6, 1.

Maeno, T., Moriishi, T., Yoshida, C.A., Komori, H., Kanatani, N., Izumi, S., Takaoka, K., and Komori, T. (2011). Early onset of Runx2 expression caused craniosynostosis, ectopic bone formation, and limb defects. *Bone* 49, 673-682.

Martinez-Abadias, N., Percival, C., Aldridge, K., Hill, C.A., Ryan, T., Sirivunnabood, S., Wang, Y., Jabs, E.W., and Richtsmeier, J.T. (2010). Beyond the closed suture in apert syndrome mouse models: evidence of primary effects of FGFR2 signaling on facial shape at birth. *Dev Dyn* 239, 3058-3071.

Mayr, E. (1942) *Systematics and the origin of species, from the viewpoint of a zoologist*. Harvard University Press, Cambridge.

McHale, P., Mizutani, C.M., Kosman, D., MacKay, D.L., Belu, M., Hermann, A., McGinnis, W., Bier, E., and Hwa, T. (2011). Gene length may contribute to graded transcriptional responses in the *Drosophila* embryo. *Dev Biol* 360, 230-240.

Meguro, T., Yoshida, Y., Hayashi, M., Toyota, K., Otagiri, T., Mochizuki, N., Kishikawa, Y., Sasaki, A., and Hayasaka, K. (2012). Inheritance of polyalanine expansion mutation of PHOX2B in congenital central hypoventilation syndrome. *J Hum Genet* 57, 335-337.

Merrill, A.E., Eames, B.F., Weston, S.J., Heath, T., and Schneider, R.A. (2008). Mesenchyme-dependent BMP signaling directs the timing of mandibular osteogenesis. *Development* 135, 1223-1234.

Morales, A.E., Perez-Jimenez, A., Hidalgo, M.C., Abellan, E., and Cardenete, G. (2004). Oxidative stress and antioxidant defenses after prolonged starvation in *Dentex dentex* liver. *Comp Biochem Physiol C Toxicol Pharmacol* 139, 153-161.

Morgan, B.A., and Fekete, D.M. (1996). Manipulating gene expression with replication-competent retroviruses. *Methods Cell Biol* 51, 185-218.

Mulder, L., Koolstra, J.H., den Toonder, J.M., and van Eijden, T.M. (2007). Intratrabecular distribution of tissue stiffness and mineralization in developing trabecular bone. *Bone* 41, 256-265.

Noden, D.M. (1983). The role of the neural crest in patterning of avian cranial skeletal, connective, and muscle tissues. *Dev Biol* 96, 144-165.

Noden, D.M., and Schneider, R.A. (2006). Neural crest cells and the community of plan for craniofacial development: historical debates and current perspectives. *Adv Exp Med Biol* 589, 1-23.

Oberdoerffer, P., Michan, S., McVay, M., Mostoslavsky, R., Vann, J., Park, S.K.,

Hartlerode, A., Stegmuller, J., Hafner, A., Loerch, P., *et al.* (2008). SIRT1 redistribution on chromatin promotes genomic stability but alters gene expression during aging. *Cell* 135, 907-918.

Orr, H.A. (1998). The population genetics of adaptation: The distribution of factors fixed during adaptive evolution. *Evolution* 52, 935-949.

Ott, C.E., Hein, H., Lohan, S., Hoogeboom, J., Foulds, N., Grunhagen, J., Stricker, S.,

Villavicencio-Lorini, P., Klopocki, E., and Mundlos, S. (2012). Microduplications upstream of MSX2 are associated with a phenocopy of cleidocranial dysplasia. *J Med Genet* 49, 437-441.

Otto, F., Kanegane, H., and Mundlos, S. (2002). Mutations in the RUNX2 gene in patients with cleidocranial dysplasia. *Hum Mutat* 19, 209-216.

Otto, F., Thornell, A.P., Crompton, T., Denzel, A., Gilmour, K.C., Rosewell, I.R., Stamp, G.W., Beddington, R.S., Mundlos, S., Olsen, B.R., *et al.* (1997). *Cbfa1*, a candidate gene for cleidocranial dysplasia syndrome, is essential for osteoblast differentiation and bone development. *Cell* 89, 765-771.

Padilla, P.A., and Ladage, M.L. (2012). Suspended animation, diapause and quiescence: arresting the cell cycle in *C. elegans*. *Cell Cycle* 11, 1672-1679.

Parker, S.E., Mai, C.T., Canfield, M.A., Rickard, R., Wang, Y., Meyer, R.E., Anderson, P., Mason, C.A., Collins, J.S., Kirby, R.S., *et al.* (2010). Updated National Birth Prevalence estimates for selected birth defects in the United States, 2004-2006. *Birth Defects Res A Clin Mol Teratol* **88**, 1008-1016.

Pavlopoulos, A., Kontarakis, Z., Liubicich, D.M., Serano, J.M., Akam, M., Patel, N.H., and Averof, M. (2009). Probing the evolution of appendage specialization by Hox gene misexpression in an emerging model crustacean. *Proc Natl Acad Sci U S A* **106**, 13897-13902.

Pfeiffer, R.A. (1964). [Dominant Hereditary Acrocephalosyndactylia]. *Z Kinderheilkd* **90**, 301-320.

Pigliucci, M. (2007). Finding the way in phenotypic space: the origin and maintenance of constraints on organismal form. *Ann Bot* **100**, 433-438.

Pointer, M.A., Kamilar, J.M., Warmuth, V., Chester, S.G., Delsuc, F., Mundy, N.I., Asher, R.J., and Bradley, B.J. (2012). RUNX2 tandem repeats and the evolution of facial length in placental mammals. *BMC Evol Biol* **12**, 103.

Polyak, K., Kato, J.Y., Solomon, M.J., Sherr, C.J., Massague, J., Roberts, J.M., and Koff, A. (1994). p27Kip1, a cyclin-Cdk inhibitor, links transforming growth factor-beta and contact inhibition to cell cycle arrest. *Genes Dev* **8**, 9-22.

Polyak, K., Lee, M.H., Erdjument-Bromage, H., Koff, A., Roberts, J.M., Tempst, P., and Massague, J. (1994). Cloning of p27Kip1, a cyclin-dependent kinase inhibitor and a potential mediator of extracellular antimitogenic signals. *Cell* 78, 59-66.

Powder, K.E., Ku, Y.C., Brugmann, S.A., Veile, R.A., Renaud, N.A., Helms, J.A., and Lovett, M. (2012). A cross-species analysis of microRNAs in the developing avian face. *PLoS One* 7, e35111.

Pratap, J., Galindo, M., Zaidi, S.K., Vradii, D., Bhat, B.M., Robinson, J.A., Choi, J.Y., Komori, T., Stein, J.L., Lian, J.B., *et al.* (2003). Cell growth regulatory role of Runx2 during proliferative expansion of preosteoblasts. *Cancer Res* 63, 5357-5362.

Qiao, M., Shapiro, P., Fosbrink, M., Rus, H., Kumar, R., and Passaniti, A. (2006). Cell cycle-dependent phosphorylation of the RUNX2 transcription factor by cdc2 regulates endothelial cell proliferation. *J Biol Chem* 281, 7118-7128.

Qiu, M., Bulfone, A., Ghattas, I., Meneses, J.J., Christensen, L., Sharpe, P.T., Presley, R., Pedersen, R.A., and Rubenstein, J.L. (1997). Role of the Dlx homeobox genes in proximodistal patterning of the branchial arches: mutations of Dlx-1, Dlx-2, and Dlx-1 and -2 alter morphogenesis of proximal skeletal and soft tissue structures derived from the first and second arches. *Dev Biol* 185,

165-184.

Qiu, M., Bulfone, A., Martinez, S., Meneses, J.J., Shimamura, K., Pedersen, R.A., and Rubenstein, J.L. (1995). Null mutation of *Dlx-2* results in abnormal morphogenesis of proximal first and second branchial arch derivatives and abnormal differentiation in the forebrain. *Genes Dev* 9, 2523-2538.

Rabie, A.B., Leung, F.Y., Chayanupatkul, A., and Hagg, U. (2002). The correlation between neovascularization and bone formation in the condyle during forward mandibular positioning. *Angle Orthod* 72, 431-438.

Rabie, A.B., Shum, L., and Chayanupatkul, A. (2002). VEGF and bone formation in the glenoid fossa during forward mandibular positioning. *Am J Orthod Dentofacial Orthop* 122, 202-209.

Remes, V. (2006). Growth strategies of passerine birds are related to brood parasitism by the brown-headed cowbird (*Molothrus ater*). *Evolution* 60, 1692-1700.

Richman, J., and Mitchell, P.J. (1996). Craniofacial development: knockout mice take one on the chin. *Curr Biol* 6, 364-367.

Ricklefs, R.E. (1968). Patterns of Growth in Birds. *The Ibis* 110.

Rieseberg, L.H., Raymond, O., Rosenthal, D.M., Lai, Z., Livingstone, K., Nakazato, T., Durphy, J.L., Schwarzbach, A.E., Donovan, L.A., and Lexer, C. (2003). Major ecological transitions in wild sunflowers facilitated by hybridization. *Science* 301, 1211-1216.

Rijli, F.M., Mark, M., Lakkaraju, S., Dierich, A., Dolle, P., and Chambon, P. (1993). A homeotic transformation is generated in the rostral branchial region of the head by disruption of *Hoxa-2*, which acts as a selector gene. *Cell* 75, 1333-1349.

Robin, N.H., Falk, M.J., and Haldeman-Englert, C.R. (1993). FGFR-Related Craniosynostosis Syndromes.

Roybal, P.G., Wu, N.L., Sun, J., Ting, M.C., Schafer, C.A., and Maxson, R.E. (2010). Inactivation of *Msx1* and *Msx2* in neural crest reveals an unexpected role in suppressing heterotopic bone formation in the head. *Dev Biol* 343, 28-39.

Sankar, U., Patel, K., Rosol, T.J., and Ostrowski, M.C. (2004). RANKL coordinates cell cycle withdrawal and differentiation in osteoclasts through the cyclin-dependent kinase inhibitors p27KIP1 and p21CIP1. *J Bone Miner Res* 19, 1339-1348.

Santiago, A., and Erickson, C.A. (2002). Ephrin-B ligands play a dual role in the

control of neural crest cell migration. *Development* 129, 3621-3632.

Schmalhausen, I.I. (1949). *Factors of evolution: the theory of stabilization selection*. University of Chicago Press, Chicago.

Schneider, R.A., and Helms, J.A. (2003). The cellular and molecular origins of beak morphology. *Science* 299, 565-568.

Schneider, R.A. (2005). Developmental mechanisms facilitating the evolution of bills and quills. *J Anat* 207, 563-573.

Schroeder, T.M., Kahler, R.A., Li, X., and Westendorf, J.J. (2004). Histone deacetylase 3 interacts with runx2 to repress the osteocalcin promoter and regulate osteoblast differentiation. *J Biol Chem* 279, 41998-42007.

Sears, K.E., Behringer, R.R., Rasweiler, J.J.t., and Niswander, L.A. (2006). Development of bat flight: morphologic and molecular evolution of bat wing digits. *Proc Natl Acad Sci U S A* 103, 6581-6586.

Sears, K.E., Goswami, A., Flynn, J.J., and Niswander, L.A. (2007). The correlated evolution of Runx2 tandem repeats, transcriptional activity, and facial length in carnivora. *Evol Dev* 9, 555-565.

Semina, E.V., Murray, J.C., Reiter, R., Hrstka, R.F., and Graw, J. (2000). Deletion in the promoter region and altered expression of Pitx3 homeobox gene in aphakia mice. *Hum Mol Genet* 9, 1575-1585.

Shen, R., Wang, X., Drissi, H., Liu, F., O'Keefe, R.J., and Chen, D. (2006). Cyclin D1-cdk4 induce runx2 ubiquitination and degradation. *J Biol Chem* 281, 16347-16353.

Shigetani, Y., Sugahara, F., Kawakami, Y., Murakami, Y., Hirano, S., and Kuratani, S. (2002). Heterotopic shift of epithelial-mesenchymal interactions in vertebrate jaw evolution. *Science* 296, 1316-1319.

Shipman, C.M., and Croucher, P.I. (2003). Osteoprotegerin is a soluble decoy receptor for tumor necrosis factor-related apoptosis-inducing ligand/Apo2 ligand and can function as a paracrine survival factor for human myeloma cells. *Cancer Res* 63, 912-916.

Siegemund, F., and Eimert, K. (1995). Electroporation of Brassica. *Methods Mol Biol* 55, 109-120.

Smith, E., Frenkel, B., MacLachlan, T.K., Giordano, A., Stein, J.L., Lian, J.B., and Stein, G.S. (1997). Post-proliferative cyclin E-associated kinase activity in differentiated osteoblasts: inhibition by proliferating osteoblasts and

osteosarcoma cells. *J Cell Biochem* 66, 141-152.

Smith, E., Frenkel, B., Schlegel, R., Giordano, A., Lian, J.B., Stein, J.L., and Stein, G.S. (1995). Expression of cell cycle regulatory factors in differentiating osteoblasts: postproliferative up-regulation of cyclins B and E. *Cancer Res* 55, 5019-5024.

Smith, K.K., and Schneider, R.A. (1998). Have gene knockouts caused evolutionary reversals in the mammalian first arch? *Bioessays* 20, 245-255.

Smith, M.M., and Hall, B.K. (1990). Development and evolutionary origins of vertebrate skeletogenic and odontogenic tissues. *Biol Rev Camb Philos Soc* 65, 277-373.

Solem, R.C., Eames, B.F., Tokita, M., and Schneider, R.A. (2011). Mesenchymal and mechanical mechanisms of secondary cartilage induction. *Dev Biol* 356, 28-39.

Soler, J.J., and Aviles, J.M. (2010). Sibling competition and conspicuousness of nestling gapes in altricial birds: a comparative study. *PLoS One* 5, e10509.

Starck, J.M., and Ricklefs, R.E. (1998). *Avian growth and development : evolution within the altricial-precocial spectrum* (New York, Oxford University

Press).

Stein, G.S., Lian, J.B., Stein, J.L., Van Wijnen, A.J., and Montecino, M. (1996). Transcriptional control of osteoblast growth and differentiation. *Physiol Rev* 76, 593-629.

Stock, M., and Otto, F. (2005). Control of RUNX2 isoform expression: the role of promoters and enhancers. *J Cell Biochem* 95, 506-517.

Stricker, S., Fundele, R., Vortkamp, A., and Mundlos, S. (2002). Role of Runx genes in chondrocyte differentiation. *Dev Biol* 245, 95-108.

Stuart, A.J., and Smith, D.A. (1992). Use of the fluorochromes xylenol orange, calcein green, and tetracycline to document bone deposition and remodeling in healing fractures in chickens. *Avian Dis* 36, 447-449.

Swartz, M., Eberhart, J., Mastick, G.S., and Krull, C.E. (2001). Sparking new frontiers: using in vivo electroporation for genetic manipulations. *Dev Biol* 233, 13-21.

Takahashi, Y., Watanabe, T., Nakagawa, S., Kawakami, K., and Sato, Y. (2008). Transposon-mediated stable integration and tetracycline-inducible expression of electroporated transgenes in chicken embryos. *Methods Cell Biol* 87, 271-280.

Takechi, M., and Kuratani, S. (2010). History of studies on mammalian middle ear evolution: a comparative morphological and developmental biology perspective. *J Exp Zool B Mol Dev Evol* 314, 417-433.

Thirunavukkarasu, K., Mahajan, M., McLarren, K.W., Stifani, S., and Karsenty, G. (1998). Two domains unique to osteoblast-specific transcription factor *Osf2/Cbfa1* contribute to its transactivation function and its inability to heterodimerize with *Cbfbeta*. *Mol Cell Biol* 18, 4197-4208.

Thomas, D.M., Johnson, S.A., Sims, N.A., Trivett, M.K., Slavin, J.L., Rubin, B.P., Waring, P., McArthur, G.A., Walkley, C.R., Holloway, A.J., *et al.* (2004). Terminal osteoblast differentiation, mediated by *runx2* and *p27KIP1*, is disrupted in osteosarcoma. *J Cell Biol* 167, 925-934.

Thomas, T., Kurihara, H., Yamagishi, H., Kurihara, Y., Yazaki, Y., Olson, E.N., and Srivastava, D. (1998). A signaling cascade involving endothelin-1, *dHAND* and *msx1* regulates development of neural-crest-derived branchial arch mesenchyme. *Development* 125, 3005-3014.

Tokita, M., and Schneider, R.A. (2009). Developmental origins of species-specific muscle pattern. *Dev Biol* 331, 311-325.

Trainor, P.A. (2003). Making headway: the roles of Hox genes and neural crest

cells in craniofacial development. *ScientificWorldJournal* 3, 240-264.

Trainor, P.A., Ariza-McNaughton, L., and Krumlauf, R. (2002). Role of the isthmus and FGFs in resolving the paradox of neural crest plasticity and pre-patterning. *Science* 295, 1288-1291.

Trainor, P.A., and Krumlauf, R. (2000). Patterning the cranial neural crest: hindbrain segmentation and Hox gene plasticity. *Nat Rev Neurosci* 1, 116-124.

Trainor, P.A., Melton, K.R., and Manzanares, M. (2003). Origins and plasticity of neural crest cells and their roles in jaw and craniofacial evolution. *Int J Dev Biol* 47, 541-553.

University of California Museum of Paleontology. (2012). Understanding Evolution. <<http://evolution.berkeley.edu/>> .

von Baer, K.E. (1828) *Entwicklungsgeschichte der Thiere: Beobachtung und Reflexion*. Königsberg, Bornträger.

vonHoldt, B.M., Pollinger, J.P., Earl, D.A., Knowles, J.C., Boyko, A.R., Parker, H., Geffen, E., Pilot, M., Jedrzejewski, W., Jedrzejewska, B., *et al.* (2011). A genome-wide perspective on the evolutionary history of enigmatic wolf-like canids. *Genome Res* 21, 1294-1305.

Wagner, G.P., and Altenberg, L. (1996) Perspective: Complex adaptations and the evolution of evolvability. *Evolution* 50(3):967-976.

Wagner, A. (2008). Neutralism and selectionism: a network-based reconciliation. *Nat Rev Genet* 9, 965-974.

Wang, T., Hung, C.C., and Randall, D.J. (2006). The comparative physiology of food deprivation: from feast to famine. *Annu Rev Physiol* 68, 223-251.

Wang, W.D., Melville, D.B., Montero-Balaguer, M., Hatzopoulos, A.K., and Knapik, E.W. (2011). *Tfap2a* and *Foxd3* regulate early steps in the development of the neural crest progenitor population. *Dev Biol* 360, 173-185.

Wassersug, R.J. (1976). A procedure for differential staining of cartilage and bone in whole formalin-fixed vertebrates. *Stain Technol* 51, 131-134.

Weiner, S., and Traub, W. (1986). Organization of hydroxyapatite crystals within collagen fibrils. *FEBS Lett* 206, 262-266.

Weiner, S., Traub, W., and Wagner, H.D. (1999). Lamellar bone: structure-function relations. *J Struct Biol* 126, 241-255.

Westendorf, J.J., Zaidi, S.K., Cascino, J.E., Kahler, R., van Wijnen, A.J., Lian, J.B., Yoshida, M., Stein, G.S., and Li, X. (2002). *Runx2* (*Cbfa1*, *AML-3*) interacts

with histone deacetylase 6 and represses the p21(CIP1/WAF1) promoter. *Mol Cell Biol* 22, 7982-7992.

Winograd, J., Reilly, M.P., Roe, R., Lutz, J., Laughner, E., Xu, X., Hu, L., Asakura, T., vander Kolk, C., Strandberg, J.D., *et al.* (1997). Perinatal lethality and multiple craniofacial malformations in MSX2 transgenic mice. *Hum Mol Genet* 6, 369-379.

Wright, S. (1932) The roles of mutation, inbreeding, crossbreeding, and selection in evolution. *Proceedings of the Sixth International Congress on Genetics*, 355-366.

Wu, M., Hesse, E., Morvan, F., Zhang, J.P., Correa, D., Rowe, G.C., Kiviranta, R., Neff, L., Philbrick, W.M., Horne, W.C., *et al.* (2009). Zfp521 antagonizes Runx2, delays osteoblast differentiation in vitro, and promotes bone formation in vivo. *Bone* 44, 528-536.

Xiao, Z.S., Hjelmeland, A.B., and Quarles, L.D. (2004). Selective deficiency of the "bone-related" Runx2-II unexpectedly preserves osteoblast-mediated skeletogenesis. *J Biol Chem* 279, 20307-20313.

Yamada, G., Mansouri, A., Torres, M., Stuart, E.T., Blum, M., Schultz, M., De

Robertis, E.M., and Gruss, P. (1995). Targeted mutation of the murine goosecoid gene results in craniofacial defects and neonatal death. *Development* 121, 2917-2922.

Yang, Y.Q., Tan, Y.Y., Wong, R., Wenden, A., Zhang, L.K., and Rabie, A.B. (2012). The role of vascular endothelial growth factor in ossification. *Int J Oral Sci* 4.

Yeung, K., Kim, S., and Reinberg, D. (1997). Functional dissection of a human Dr1-DRAP1 repressor complex. *Mol Cell Biol* 17, 36-45.

Yokota, Y., Saito, D., Tadokoro, R., and Takahashi, Y. (2011). Genomically integrated transgenes are stably and conditionally expressed in neural crest cell-specific lineages. *Dev Biol* 353, 382-395.

Young, D.W., Hassan, M.Q., Pratap, J., Galindo, M., Zaidi, S.K., Lee, S.H., Yang, X., Xie, R., Javed, A., Underwood, J.M., *et al.* (2007). Mitotic occupancy and lineage-specific transcriptional control of rRNA genes by Runx2. *Nature* 445, 442-446.

Young, N.M., Chong, H.J., Hu, D., Hallgrimsson, B., and Marcucio, R.S. (2010). Quantitative analyses link modulation of sonic hedgehog signaling to continuous variation in facial growth and shape. *Development* 137, 3405-3409.

Yuan, B., Latek, R., Hossbach, M., Tuschl, T., and Lewitter, F. (2004). siRNA Selection Server: an automated siRNA oligonucleotide prediction server. *Nucleic Acids Res* 32, W130-134.

Zarbalis, K., Siegenthaler, J.A., Choe, Y., May, S.R., Peterson, A.S., and Pleasure, S.J. (2007). Cortical dysplasia and skull defects in mice with a *Foxc1* allele reveal the role of meningeal differentiation in regulating cortical development. *Proc Natl Acad Sci U S A* 104, 14002-14007.

Zavitz, K.H., and Zipursky, S.L. (1997). Controlling cell proliferation in differentiating tissues: genetic analysis of negative regulators of G1-->S-phase progression. *Curr Opin Cell Biol* 9, 773-781.

Zhang, W., Bergamaschi, D., Jin, B., and Lu, X. (2005). Posttranslational modifications of p27kip1 determine its binding specificity to different cyclins and cyclin-dependent kinases in vivo. *Blood* 105, 3691-3698.

Zhong, X., Zan, L.S., Wang, H.B., and Liu, Y.F. (2010). Polymorphic CA microsatellites in the third exon of the bovine *BMP4* gene. *Genet Mol Res* 9, 868-874.

Zhou, Y.X., Xu, X., Chen, L., Li, C., Brodie, S.G., and Deng, C.X. (2000). A Pro250Arg substitution in mouse *Fgfr1* causes increased expression of *Cbfa1*

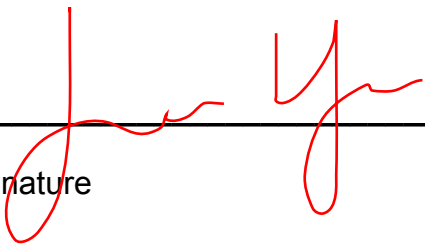
and premature fusion of calvarial sutures. *Hum Mol Genet* 9, 2001-2008.

Zilinski, C.A., Shah, R., Lane, M.E., and Jamrich, M. (2005). Modulation of zebrafish *pitx3* expression in the primordia of the pituitary, lens, olfactory epithelium and cranial ganglia by hedgehog and nodal signaling. *Genesis* 41, 33-40.

Publishing Agreement

It is the policy of the University to encourage the distribution of all theses, dissertations, and manuscripts. Copies of all UCSF theses, dissertations, and manuscripts will be routed to the library via the Graduate Division. The library will make all theses, dissertations, and manuscripts accessible to the public and will preserve these to the best of their abilities, in perpetuity.

I hereby grant permission to the Graduate Division of the University of California, San Francisco to release copies of my thesis, dissertation, or manuscript to the Campus Library to provide access and preservation, in whole or in part, in perpetuity.



Author Signature

12-8-2012

Date